INVESTIGATION OF WET PAPER VISCOELASTIC STRUCTURAL PROPERTIES

A Thesis
Presented to
The Academic Faculty

by

Tyler L. Smith

In Partial Fulfillment
of the Requirements for the
Master's Degree in the
School of Mechanical Engineering

Georgia Institute of Technology

May, 2006

INVESTIGATION OF WET PAPER VISCOELASTIC STRUCTURAL PROPERTIES

Approved by:

Dr. Timothy Patterson
School of Mechanical Engineering
Georgia Institute of Technology

Dr. Frederick W. Ahrens
School of Mechanical Engineering
Georgia Institute of Technology

Dr. Preet M. Singh
School of Materials Science and Engineering
Georgia Institute of Technology

Date Approved:

Friday December 2, 2005

ACKNOWLEDGEMENTS

I wish to thank Dr. Timothy Patterson for all of the thought, assistance and guidance that he has given to this thesis topic and me. Especially thanks for allowing the project to naturally run its own course in determining what needs to be researched. In doing so, I think the research may have taken a little longer than initially anticipated, but the end result is more informative. In addition I would also like to thank my fiancée Kristen Parks for all of the moral and physical support she has given me throughout my graduate education. Without her never-ending motivation I would not be where I am today in education or life.

TABLE OF CONTENTS

Page

LIST OF FIGURES

LIST OF SYMBOLS

F	Force applied to fibers or sheet
γ	Surface tension
L	Length of fiber-air-water interface
ΔP	Compacting pressure between fibers
x	Thickness of film
t	Tensile strength of sheet
Z	Zero-span tensile strength of sheet
A	Fiber cross-sectional area
ρ	Density of fiber wall
g	Acceleration due to gravity
b	Bond shear strength per unit area
P	Perimeter of fiber cross-section
l	Fiber length
RBA	Relative bonded area
W	Work of removing a sheet from a flat surface
m	Mass of sheet measured per unit area
V	Velocity of split propagation
T	Tension on the splitting sheet
Φ	Peel angle between sheet and surface
W_T	Total work of removing a sheet from a flat surface
ε	Strain in sheet

W_S	Work associated with separation
W_E	Work associated with extension
W_M	Work associated moment of inertia
$h_{Initial}$	Initial height of sheet prior to testing
$h_{Ins\tan t}$	Height of sheet relative to datum
Splitting	Energy needed to split sheet
Friciton	Energy of losses while sheet is splitting
Splitting _ Energy	Energy measured during splitting of the sheet

SUMMARY

Dry cellulose fibers as well as dried sheets of paper can be thought of as stiff materials. The material properties of these dried fibers and sheets have been extensively researched through theoretical and experimental methods. The amount of research on dried sheets and fibers is logical considering they represent the majority of the end use products. However, for a large part of the paper manufacturing process the sheet's moisture content differs greatly from the finished product. This higher water content during production allows the viscoelastic properties of the paper to dominate. These viscoelastic properties allow the paper when subject to loading to elastically stretch and plastically deform and dissipate energy. It is this plastic deformation and elastic stretching in areas such as open draws on a paper machine that limit the overall production speed.

This thesis introduces a new testing apparatus designed specifically for measuring the energy required to split sheets of paper with varying moisture contents and sheet additives. Because this device is new to the paper industry many tests are conducted to determine the magnitude and sources of errors within the experimental results. The results from this testing apparatus in combination with results from standard tensile and z-direction tests are combined to describe the transformation of internal sheet properties during the transition from the wet end of the paper mill to the finished state. In addition to moisture content the effect on the sheet strength caused by bonder and debonder additives is also determined.

CHAPTER 1 – INTRODUCTION

While being manufactured, paper progresses from a sheet high in water content to a sheet low in water content. As would be expected, the paper properties also change dramatically during this transition. In addition to water content, temperature, sheet pressing, and additives affect the way bonding occurs throughout the production process. All of these conditions are altered on the paper-manufacturing machine to produce a final product with a desired set of characteristics. In addition to affecting the final product these variables also determine the ability to manufacture the paper during the production process.

In this thesis the underlying properties surrounding the formation of strength within a sheet are looked at through experimental testing and computer modeling of the system. It is thought that there are two primary internal sources of strength present within a sheet of paper. The first source of strength is hydrogen-bonding occurring between individual fibers and the second is a frictional resistance that is caused by the increase in normal forces between fibers due to surface tension. This can also be thought of as "entanglement". The degrees to which bonding and entanglement occur within a sheet are highly dependent on moisture content. This thesis examines the internal strength of paper at the full range of moisture contents that would occur during paper production. In addition to varying moisture contents an attempt is made to isolate the effects of bonding and fiber entanglement through the addition of sheet additives.

To measure the internal strength of a sheet a paper splitting device was designed and constructed for this thesis. The paper splitting device does not rely on adhesives to hold the test sample while splitting. Because of this, the results obtained in this thesis are unique from other experimental paper splitting results because of the wide range of moisture contents that are tested. In addition to the experimental work the rheological finite element model is the first known example of finite element modeling of a splitting sheet of paper.

In chapter two of this thesis a review of literature regarding the strength of paper in both the wet and dry stages is discussed. Chapter three presents the paper splitting apparatus and the associated testing procedures that were used in the experiment. This chapter also discusses the formation of the test sheets and the tensile and z-direction testing apparatuses. Chapter four of this thesis describes a number of experiments that were conducted to determine the amount of error present within the paper splitting device results. Chapter five follows the evolution of the finite element model program from a simple mass-spring-damper system to the advanced multinode model of the splitting sheet. Chapter six presents and discusses the results from the experimental and theoretical testing of the sheet splitting. In addition, the results for both the tensile tester and z-direction tester are also presented and discussed. Chapter seven gives an overview of the results that were found and discusses how well they achieved the initial goals set for the research. Chapter eight outlines downfalls of the existing system, how they can be fixed, and future research that could be conducted using the paper splitting apparatus.

CHAPTER 2 – LITERATURE REVIEW

A great deal of theoretical and experimental work has been done in the field of web separation from surfaces. In most of the research the surfaces are other objects like the exterior of a drying can, but in the case of web splitting, the surface is another web. Interest in this research is primarily due to the direct relationship that can be formed between the degree of surface adhesion and the overall runability of a paper machine.

If the total amount of tension used to remove a wet-web from a press section can be reduced then the machine speed can be increased, resulting in increased production and a lower product cost (27). However, as stated by Mardon, (9) with an increase in web tension an increase in the number of breaks occurring in the open draws and other high tension areas in the machine is seen. This failure is due to the lack of strength of the wet-web in the early production stages.

The velocity on paper machines has been steadily increasing to increase mill production. This increase in production speed has not been accomplished by increasing the wet-web strength but primarily by decreasing many of the problematic areas of the machine. The open draws have been reduced in length or eliminated and the use of vacuum pick-ups have lowered the sheet's early stage water content.

In addition to catastrophic web breakage, the strength of the wet-web is also a large factor in the final sheet quality. Small sections or individual fibers sticking to the

exterior surface of a drying or pressing roll can result in poor heat transfer in drying sections or poor quality paper with dimples or holes punched into the surface (1).

Both catastrophic tensile failure and localized tensile failure in picking of fibers from a sheet occur as a result of the failure in bonds or the bonding mechanisms present. The degree of fiber bonding within paper is perhaps also one of the most important sheet properties because it accounts for almost all of the final sheet strength. However, the amount of bonding varies at different moisture contents and thus at different places within the paper manufacturing process.

For the ease of understanding the difference between the extreme ends of the manufacturing process and the experimental tests, the existing research on paper properties is divided into research on wet and dry paper. However it has to be stated that there is not a hard line between wet and dry paper, it is more of a gradual transition from one to the other. In addition to the research that has been performed on paper properties, developments on the splitting of sheets are also discussed.

Wet Paper

The strength of a sheet of paper, especially when wet, is a result of two properties: the amount of inter-fiber bonding and the degree of fiber entanglement. At a low solids level fiber entanglement and the associated surface tension are the primary source of sheet strength. Throughout dewatering the solids content and the bonding begin to increase until bonding alone accounts for almost all of the strength within the dried sheet.

During this transition period when a sheet is drying there is not a definite point where fiber entanglement ends and fiber bonding begins and both are highly dependent on pulp preparation and external factors associated with the sheet. It is because of this gradual transition that the shift from wet paper to dry paper is difficult to define.

Both Lyne and Gallay (8) and Robertson (24) stated that the transition through the wet web phase of dying occurs in a number of different stages. The first stage takes place when the water content in the sheet is around 88%. At this point all of the free inter fiber water has been removed and the internal surface tension and fiber entanglement is at a maximum. The web is held together by the surface tension occurring from the menisci formed as the water layer retreats into the fibrous structure. This is shown in Figure 2.1a below. The surface tension force pulling the fibers together in this stage is approximately $F = \gamma L$ where γ is the surface tension in dynes per centimeter, and L is the length of the line contact between the air, water, and fiber.

The start of the second stage of drying is shown to occur when air intrusion starts to take place within the sheet. Inter-fiber capillary water is replaced with air leaving an envelope of water around each fiber and contact point. When the capillary water is removed there is a reduction in surface tension allowing the web to relax resulting in an increase in the sheet caliper. At this stage, two menisci form between adjacent fibers (Figure 2.1b) resulting in a compacting force approximated by $F = 2 \gamma L$.

This second stage of the drying process ends when the critical solids content is approached (around 20-25% solids). At this point most of the inter-fiber water that was being held in by capillary action has been replaced with air. It is also here that inter-fiber bonding starts occurring at a rapid rate resulting in the swift increase of the sheet strength. The total surface tension force decreases very rapidly and the remaining liquid water films are sporadic across the surface of a fiber, see Figure 2.1c. The forces exerted by the surface tension becomes more of a function of the distance between the two fibers then the length of the fiber-air-water interface. This force can be approximated by $\Delta P = 2\gamma/x$ where x is the thickness of the film, γ is the surface tension and ΔP is the compacting pressure. Due to the inverse relationship between compacting pressure and the film thickness the compacting pressure can reach incredibly high values in the order of 100-200 atmospheres as the sheet is dried further.

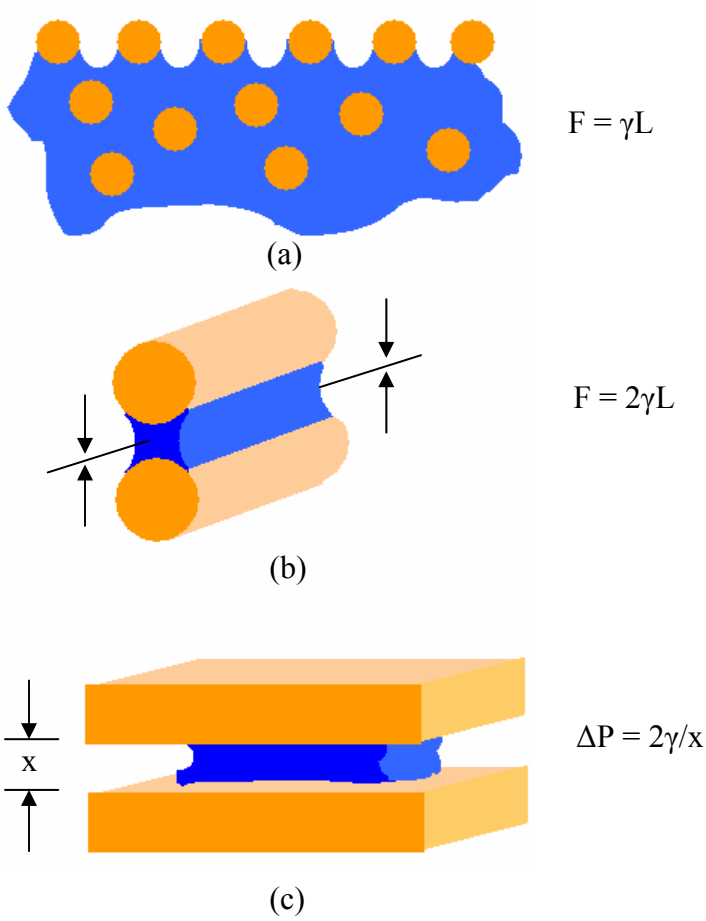

Figure 2.1 – Diagrams for Action of Surface Tension Forces During Drying of Paper (2).

This high compacting pressure is thought by Campbell (3) to provide the force that pushes the fibers close enough together for molecular bonding to occur during drying. This effect is amplified even further if any beating is done on the pulp. This is due to the increase in surface area of the fibers that are heavily fibrillated.

In an effort to isolate fiber entanglement and surface tension from inter-fiber bonding Lyne and Gallay (8) constructed handsheets composed of glass fibers as an

alternative to cellulose. The glass fibers were used because they would not chemically bond to one another and any sheet strength would be a result of fiber entanglement. It was found that these glass fiber sheets reached a maximum strength at about 20 to 25 percent solids then decreased rapidly to a low value with in increase in solids content. In addition to the strength becoming a maximum, the sheet density also maximized (thickness minimized) supporting the fact that surface tension is a major factor in fiber entanglement. The effect of wet pressing on the strength of the glass fiber sheets was also looked at because of its importance in the paper making process. The glass fiber sheets that had undergone wet pressing had a reduced strength from those that had just air dried. This was thought to occur because unlike cellulose fibers that bend and deform when pressed the glass fibers do not deform and just break under the pressing load.

Dry Paper

Once the critical solids content in the drying process is reached bonding becomes the primary source of sheet strength. As the paper is dried the tensile strength of the sheet depends upon the strength of the fibers and the strength of the fiber-to-fiber bonds. The fiber-to-fiber bonds then depend on the bonded area between the fibers as well as the shear strength of the bonds per unit area.

Most of the research that is conducted on dried paper utilizes the equation developed by Page (14) that relates the tensile strength of a sheet to the sheet's physical properties see equation 2.1 below.

$$\frac{1}{t} = \frac{9}{8 \cdot Z} + \frac{12 \cdot A \cdot \rho \cdot g}{b \cdot P \cdot l \cdot RBA} \qquad \text{eqn. 2.1}$$

where

t = Tensile strength of sheet.

Z = Zero-span tensile strength of sheet.

A = Fiber cross-sectional area.

ρ = Density of fiber wall.

g = Acceleration due to gravity.

b = Bond shear strength per unit area.

P = Perimeter of the fiber cross-section.

l = Fiber length.

RBA = Relative bonded area of the sheet.

For this equation it is assumed that all of the fibers are straight and free from kinks and that the sheet has good formation. Page's equation seems to work well under most circumstances however it does break down for sheets that are poorly bonded such as mechanically pulped sheets. Research into poorly bonded mechanical pulp sheets proved that very few fibers are broken and the sheet strength can be explained with two independent factors; fiber length and bonding (7).

The hardest values to determine that are needed for Page's equation are the relative bonded area and the bond shear strength. There have been many researchers that have measured and attempted to measure these properties within a dried sheet of paper.

Nordman (10, 11) defined a “bond strength value” as the energy dissipated in breaking bonds divided by the change in scattering coefficient when bonds were broken. The energy dissipated was measured by taking the area under the stress strain curve and the change in scattering coefficient was taken as the difference between the scattering coefficients measured before and after the sample was split.

Another method was developed by Smith and Graminski (25). In their method very thin test sheets were created and pulled apart in a well-calibrated sensitive tensile tester. The resulting stress strain curves had jagged lines in the places where bonds were breaking. The size and number of these jagged results enabled them to calculate the number of bonds breaking as well as the associated energy required to break the bonds.

Several other methods (6, 18, 19, 26) have been developed to determine the amount of bonded area within a paper sample. However, the most widely used of those methods is that of Parsons (19) who employed light scattering to measure the unbonded area within a sheet. The bonded area was then determined as the difference between the unbonded area and the total area obtained from an extrapolated value or from an independent measurement of the unbonded fibers. The results from such a test depend greatly on the basis weight, moisture content and furnish of the sample sheet, making it impractical in most cases to compare results between tests.

In addition to calculating the number of bonds measuring the forces that are present during inter-fiber bonding can also be very difficult. When a single bond is

isolated in a lab environment the stresses and forces present within the fiber do not truly represent any fiber within the sheet. This is due to the lack of shrinking-related forces present in the sample. For example, a fiber with multiple bonds would be subject to a much more complex loading upon drying then that with just a single bond.

The number of inter fiber bonds in a sheet can be increased through pulping methods, mechanical treatment of pulp, chemical additives, or fines additives (22, 23). A wood fiber is comprised of multiple spiral wrapped layers of cellulose held together with a mixture of lignin and small amounts of hemicellulose (20). Bonding within a sheet of paper will occur between two cellulose fibers; therefore in the chemical pulping process where the lignin is removed and many individual fibers or fibrils branch off the surface, the amount of bonding is greater then in mechanical pulping. This removal of the lignin also makes the fiber much more flexible which when present in a wet-web allows for greater entanglement and thus strength. The mechanical treatment or refining of the fibers also results in an increase of fibrils and small particles of loose fibers or fines. Both mechanical and chemical created pulps can be refined but the chemical pulp will break down faster due to the lower amounts of lignin present in the fiber (15). This refining will increase the number of fibrils increasing the wet-web strength due to greater entanglement and increasing the final paper strength due to more bonding surface area. When over-refined the fibers will breakdown to create many loose fibrils or extremely branched fibers that will mechanically bond while still suspended in the pulp and cause the annoyance known as flocks. The cellulose fines created during refining (or added) do

not affect much in the wet-web stage due to their short length but can help increase the final strength of the paper by increasing the amount of cross linking between fibrils.

A dried sheet of paper that is subject to loading displays both the papers elastic and plastic deformation properties. For small strains the sheet behaves as an elastic material. This elastic behavior of the paper is a very important mechanical property in many end-use products. Most of the work on the elastic behavior of paper is based on the work done by Cox (4) who considered paper as a two-dimensional network of randomly oriented, long, straight, linearly inelastic fibers. He assumed that when subject to loading the strain of every fiber was equal to the local strain of the sheet in the fiber direction. From an analysis of the strains and resulting stresses in the fibers Cox concluded that elastic modulus of the paper is equal to one third of the elastic modulus of its component fibers. This simple equation was later broadened by Page and Seth (17) to include the inefficiency of stress distribution within the sheet, and the slackness of the structure caused by curl, micro-compressions, crimps, and kinks.

Unlike the elastic portion of the stress strain graph there has been multiple fields of thought on what is taking place within the sheet during plastic deformation. The first idea, originally proposed by Rance (21) is that every fiber is perfectly elastic and it is the breakage of fiber-to-fiber bonds that causes the viscoelastic behavior. The second idea proposed by Ebeling (16) is that significant irreversible intra-fiber deformation of the cell wall structure creates the plastic deformation. Work done by Page (14) proves that the plastic deformation is most likely due to a combination of the two fields of thought.

Peeling and Splitting

Most current work dealing with peeling and splitting has focused on the force needed to remove a paper sheet from a surface such as a dryer can rather than the force needed to split paper from itself. Work done by Ahrens, et al (1) included the mathematical modeling of sheet separation from a surface as well as experimental results from removing wet sheets from a surface with varying amounts of surface adhesion. Although the conditions for removing paper from itself versus removing paper from a surface may seem relatively different many of the equations that have been developed can be used for both.

The current mathematical theories describing the peeling of webs from surfaces come primarily from J. Mardon (9). In his work, the energy used to remove a sheet of paper from a flat surface is derived as a function of the mass per unit area (m), velocity of separation (V), web tension (T) and the peel angle (Φ), shown below in equation 2.2 and Figure 2.2.

$$W = (T - mV^2)(1 - \cos\Phi) \qquad \text{eqn. 2.2}$$

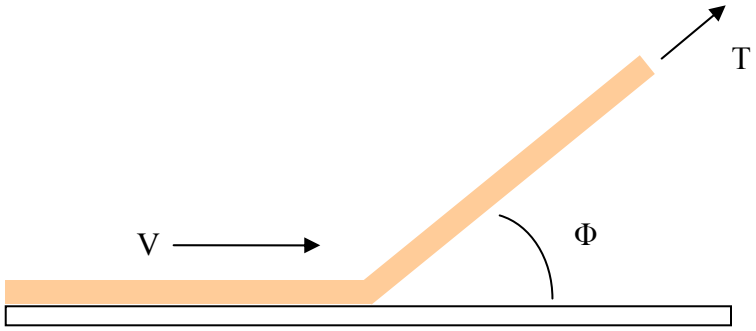

Figure 2.2 - Variables for inextensible web.

This equation represents the work energy needed to change a sheet from lying flat along a surface to traveling at an angle (Φ) to the surface. However, in the paper splitting experiment there are additional factors taking place at the point of splitting that are not accounted for in this simplified equation. The first of those is the fact that the web tested in the experiment will have a degree of straining occurring due to the tensile forces present at the split. This taken into account adds additional terms to the above equation that represent the amount of energy that went into straining the sheet of paper. The modified equation representing the total work done on the sample was derived by Osterberg (12) and is shown below with the strain term (ε) included.

$$W_T = (T - mV^2)(1 - \cos\Phi) + T\varepsilon + mV^2\varepsilon\cos\Phi \qquad \text{eqn. 2.3}$$

The above equation of total work done on the paper test sample is made up of three parts: The work of separating the two surfaces (W_S), the work of the extension of the web (W_E eqn. 2.5), and the work associated with the moment of inertia (W_M eqn. 2.6). In the paper splitting experiment the total work done on the sheet of paper is measured,

but of greater importance is the work of separation of the two surfaces. The relationship between all four terms is given in equation 2.4.

$$W_S = W_T - W_E - W_M \qquad \text{eqn. 2.4}$$

$$W_E = \int_0^{\varepsilon} T d\varepsilon \approx \frac{T\varepsilon}{2} \qquad \text{eqn. 2.5}$$

$$W_M = \frac{m}{2}(V^2(1+\varepsilon)^2 - V^2) = mV^2(\varepsilon + \frac{\varepsilon^2}{2}) \qquad \text{eqn. 2.6}$$

$$W_s = (T - mV^2)(1 - \cos\Phi) + T\varepsilon - mV^2\varepsilon(1 - \cos\Phi + \frac{\varepsilon}{2}) - \frac{T\varepsilon}{2} \qquad \text{eqn. 2.7}$$

In the web splitting work presented in this thesis web peel angle in the splitting tests is 90˚. This is assumed by the observation of previous tests performed with the web splitting apparatus. Substituting cosΦ = 90˚ yields the final relationship between the testing variables and the web splitting energy which is given by equation 2.8.

$$W_s = (T - mV^2) - mV^2\varepsilon(1 + \frac{\varepsilon}{2}) + \frac{T\varepsilon}{2} \qquad \text{eqn. 2.8}$$

The work of separation from the above equation is used as a comparison with the data that is obtained during the paper splitting experiment, see Figure 2.3. To make use of this equation, during the experiment the velocity of crack propagation which is the speed at which both sides split away from the point of separation, work of separation, and the tension of the web are measured. The only part of equation 2.8 that cannot be measured

in the experiment is the strain of the sample. This however can be calculated using Osterberg's modified equation for the work of separation shown in equation 2.9.

$$W_S = \left(T - mV^2\right) - T\varepsilon \qquad \text{eqn. 2.9}$$

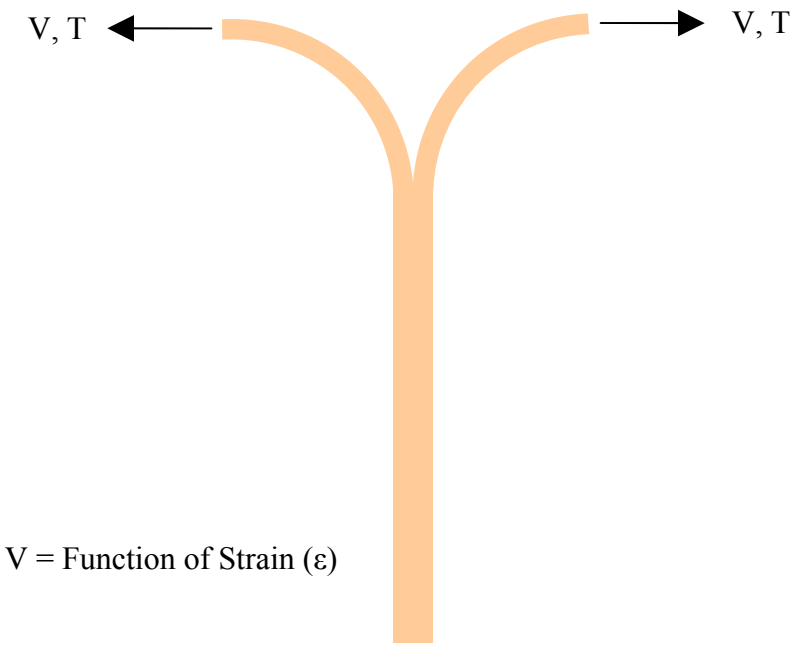

Figure 2.3 - Variables for Extendable Web in the Paper Splitting Device.

CHAPTER 3 – EXPERIMENTAL APPARATUSES AND PROCEDURES

This chapter outlines all of the experimental apparatuses and procedures that were used in the manipulation of experimental data for this thesis. The primary experimental tool that was designed and constructed for this thesis was the paper splitting apparatus. In addition to the paper splitting apparatus a z-direction tester and an Instron tensile tester were used to provide additional complementary data.

Paper Splitter

The paper splitter is a unique testing apparatus that was designed and constructed specifically for this thesis. The paper splitter is the primary focus of this thesis and is used to determine the amount of energy needed to overcome the bonding and frictional cohesion within a sheet. The advantage of the paper splitting apparatus over other bond measuring devices is its distinctive ability to test sheets with the full range of moisture contents that are present within the paper production process.

In the paper splitting apparatus, falling weights are used to split sheets of paper with varying moisture contents and sheet additives. The velocity of the weights is recorded using rotation sensors and the real-time energy needed to split the paper is calculated by determining the difference the kinetic energy and the potential energy of the weights. This data gives an idea of the energy needed as a function of the crack

propagation speed and distance. In addition to this relationship, the moisture contents and chemical additives within the sheet are altered in the experiment to allow the data to be interpreted correctly for varying machine and sheet conditions. The paper splitting apparatus is shown below in Figure 3.1 and is followed by a description of the primary components.

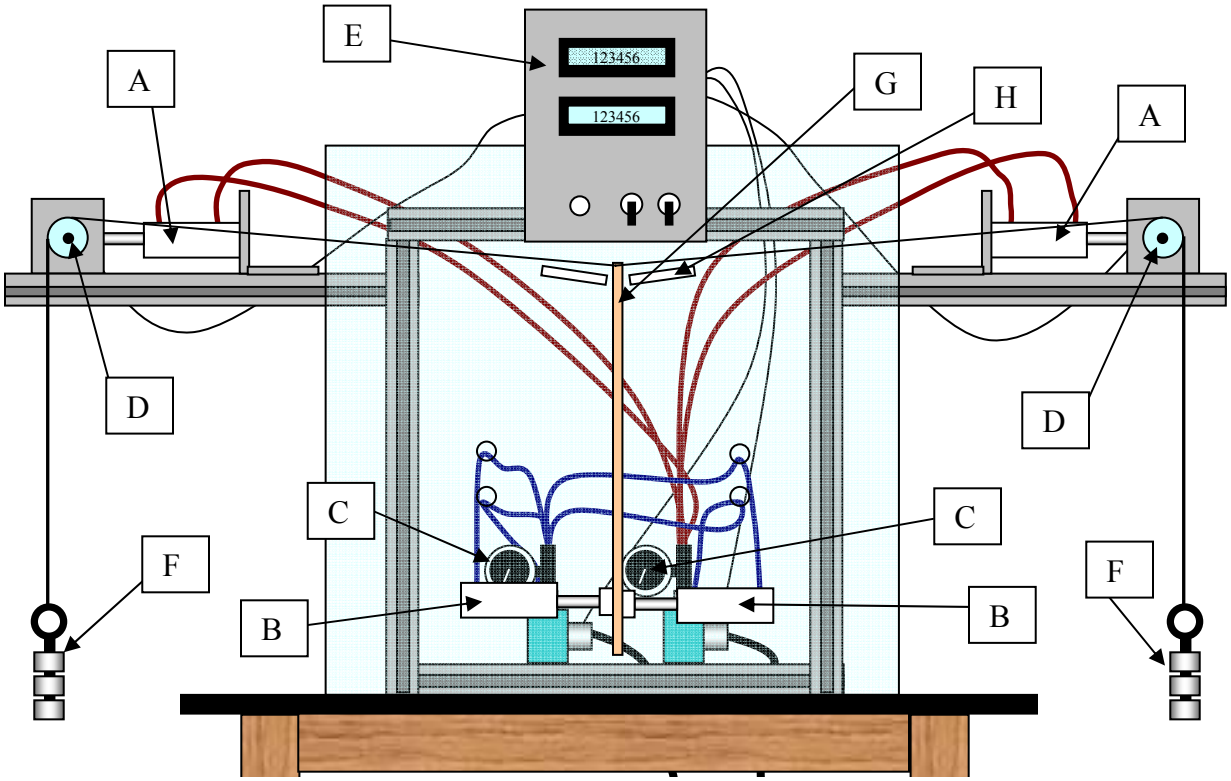

Figure 3.1 – Diagram Showing the Paper Splitting Apparatus.

Paper Splitter Description

The paper splitter shown above in Figure 3.1 is comprised of the following components.

A. Pneumatic Brake Actuators – These pneumatic pistons allow the weights to be released precisely at the same time the paper test sample is released.

B. Pneumatic Sheet Actuators - These pneumatic pistons release the paper test sample from the starting orientation.

C. Pressure Regulators – Used to provide a differential pressure to the brake and sheet actuators. These were installed to reduce the pressure on the shaft of the rotation sensor during braking and also to reduce the stress on the experiment frame by over compressing the paper test sample prior to release.

D. Rotation Sensors – The rotation sensors are used to record the rate and position of the sheet as the test progresses. Both of the rotation sensors are 1000 pulse and send their information to the associated display panel (E) and to the data acquisition system connected to the test apparatus.

E. Display Panel – The display panel has two LED screens displaying the rate sensors data in RPM's. In addition to the screens, the main power switch, run switch and fuse box are located on the outside of the panel. Within the display panel are the relays and associated circuitry used to drive the experiment.

F. Weights – The weights are used in the experiment to split the paper test sample.

G. Paper Test Sample – The paper test sample is what is split during the test. Prior to running the test the paper is conditioned to the appropriate condition (pressing, water content, and temperature) and then is pre-split and inserted into the machine.

H. Ramps – These ramps are used to support the weight of the clips during the setup of the experiment. It was found in high moisture content sheets that the weight of the clips and the associated lines would have the ability to start the split prior to the release of the brakes.

For this thesis, sheets with a variety of moisture contents and sheet additives were created and tested. In the sections below the methods used for producing all of the sample sheets is discussed. A large number of sheets were formed for this experiment, because of this, great care was taken in the sheet formation process to try and eliminate any individual sheet uniqueness. The sample sheets created are tested to determine the degree of fiber bonding and sheet cohesion present for varying moisture contents and additives in the paper splitter machine, the tensile tester, and the z-direction tester.

Pulp Preparation

A bleached southern softwood pulp was used to create all sample sheets tested in this experiment. The softwood pulp was obtained in dried sheet form. This pulp underwent disintegration and refining in a 5lb valley beater using the method outlined in Tappi T-200. The valley beater was run with no weight for 10 minutes on the base plates for disintegration and was then run for an additional 15 minutes with 7kg of weight on the base plates for refining. The pulp created using this process has approximately three percent solids content. The desired freeness value of the pulp following refining is 670ml using the Canadian standard method outlined in Tappi T-227. Once created, the pulp was stored in a refrigerator for no more than one week prior to test sheet formation.

Sheet Formation and Preparation

All of the sheets tested in the splitting apparatus were created in the Formette Dynamique machine using standard operating procedures. The Formette Dynamique was used because of its ability to produce oriented sheets with MD and CD properties closely simulating those made in commercial production. Care has to be taken in sheet construction due to the large amounts of pulp needed to produce the desired 300 g/m^2 basis weight. The first step taken to avoid any difficulties with the heavy sheet basis weight was to run sequentially three separate lower concentration batches of pulp through the machine. Once a sheet has been formed it is pressed between two 3 ft dry blotter papers under a nip pressure of approximately 21.5 lbs/in and placed in a fully sealed plastic bag (with blotters removed). If a greater water content is desired in the test sheets the sheets are sprayed with distilled water and rebaged which allows the sheet to develop a uniform moisture content. If a further reduction in water content is needed it is achieved by allowing the sheets to air dry under moderate pressure to maintain a flat surface. Once the desired water content is achieved the samples are again bagged to stop any further moisture from escaping.

Due to the high basis weight of the sheets as well as the high water content some of the samples were ribbed when they were pressed. This ribbing is undesirable in the experiment because it makes the thickness, and density of the sheet change. In some of the extreme cases of ribbing almost all of the pulp from one section was moved leaving a hole in the finished sheet. This ribbing is due to the shearing of the pulp mat from the

blotter papers during pressing. This was noticed very early on with the first sample sheet that was produced, and because of this early detection a corrective measure was devised. This corrective measure involves speeding up the Formette Dynamique screen from the normal formation speed of 900 m/min to 1500 m/min during the dewatering stage to remove more water from the sheet. This increase in screen speed does not affected the ratio of machine direction to cross direction strength because it is increased only for the dewatering not for the forming stage of production. With the lower water content the sheet was less likely to shear while being pressed. While this worked for the sheet with no additives and the sheet with debonder, the sheet in which the bonder was added was still plagued with the ribbing problem.

The sheets produced from the Formette Dynamique are approximately 48 inches long and 15 inches wide (shown in grey in Figure 3.2). These rough dimensions were then trimmed by hand on a paper cutter to 12 strips 2 inches wide by 22 inches long (shown in orange). Ten of the sheets are tested on the paper splitting experiment while the other two sheets (from opposite corners of sheet shown in light green) are cut down and used to determine the exact water content, sheet basis weight, and to create the test strips (shown in light and dark red) used in both the wet and dry tensile tests. The dried sheets used for the calculation of the basis weight and moisture content are cut down and used for the z-direction test strips (shown in dark green). The overall sheet use is shown below in Figure 3.2.

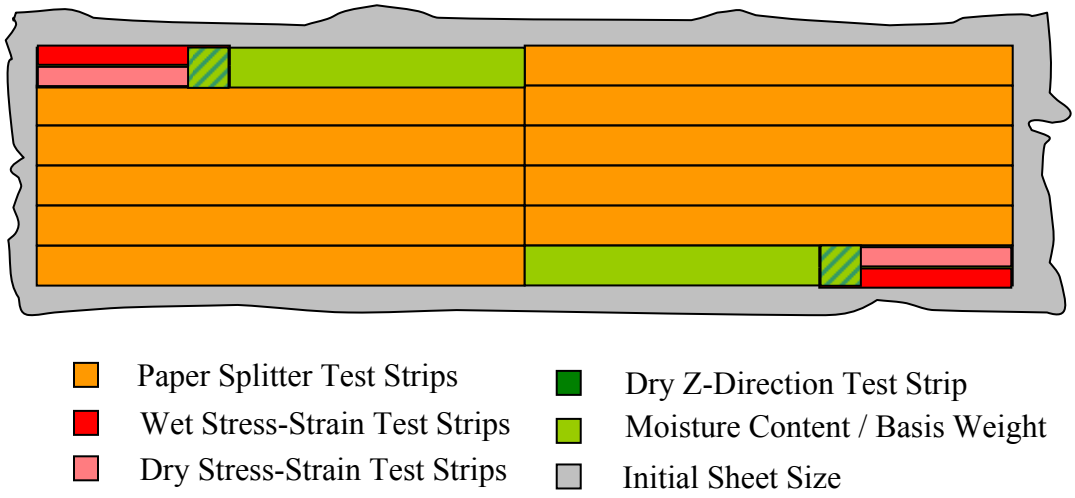

Figure 3.2 – Layout of the test strips on the sheet made in the Formette Dynamique.

In an attempt to closely model the conditions found when a sheet of paper is formed on a paper machine a wide range of sheet moisture contents were tested. In addition to altering the moisture content, additives of bond promoter and bond inhibiter were added when forming the sheets in an attempt to isolate bonding or fiber entanglement as the primary inter-fiber force within sheet.

The bond inhibiter used in the experiment was a liquid washing soap surfactant. The liquid soap is added through a syringe to the Formatte Dynamique holding tank until a 1% concentration is reached. This is repeated for each batch of the pulp that is added to the holding tank during sheet formation. When the surfactant is added to the holding tank the surface of the holding tank foams up, this foaming is minimized with a light DI water mist to the surface.

The bond promoter that was used in the experiment was locust bean gum. This gum comes in a powered form that is difficult to dissolve in water. For this reason, a solution of 1% gum in water was created as an additive. This 1% solution is added to the Formatte Dynamique holding tank until a concentration of 2% is reached. Like the surfactant, this is repeated for each batch of the pulp that is added to the holding tank during sheet formation.

Once the sample sheet is produced with the desired additives and moisture content, all of the test strips are cut to size and are tested on the paper splitting apparatus. The procedure for preparing the sheets for the paper splitter as well as the operation of the paper splitting apparatus is discussed below.

Testing Procedure

The steps for testing a sample on the paper splitting apparatus are outlined below:

1. Connect the computer used for data acquisition to the system.
2. Make sure that the experimental setup (including data acquisition system) has both power and air supplies connected.
3. Turn on power to the experimental setup by activating the power switch on the panel.
4. Make sure that all of the settings of the DT-5TX digital panel mount tachometers are recorded and are set to the appropriate values shown below.

Parameter	Description	Display	Meaning
1	Pulses per revolution	1000	1000 ppr
2	Sensing RPM	01800	1,800 RPM
3	Display units	1800	1,800
4	Update time	0.2	1 second
5	Display “hold” after signal ceases	006.0	6 seconds
6	Input filter	30	30kHz

5. Record the size of the paper splitting weights, and add or take away weight as needed.
6. Place the belts that connect the weights to the paper sample over the clear part of the rotation sensors and clip to the ramps.
7. Form sample sheets by the methods described above and by cutting into 2 inch by 24 inch sample strips.
8. Split approximately the first inch of the sample using the score and peel method shown and described below.

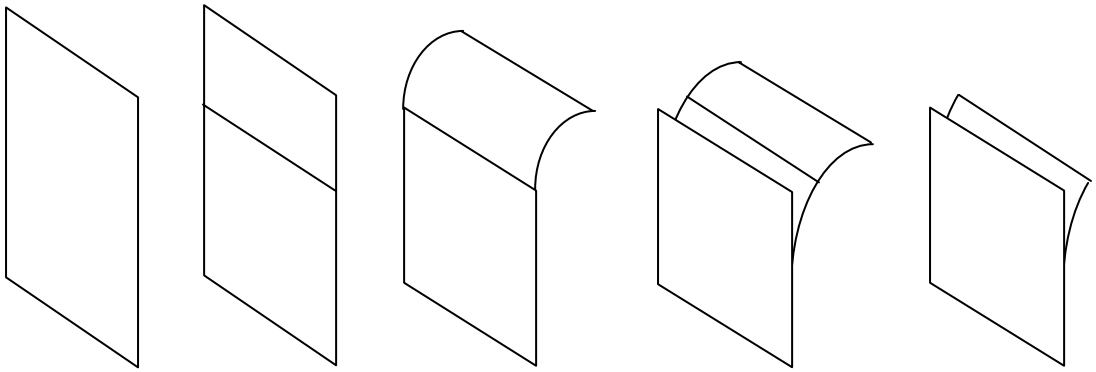

A **B** **C** **D** **E**

A. Start with the initial sheet 22 inches long by 2 inches wide.

B. Score half way though the sheet with a razorblade approximately ½ inch from end of sheet. If while attempting step C the score seems too shallow then the sample can be rescored.

C. Bend the top of the sheet away from the scored side allowing splitting to occur at the score location.

D. Once splitting has started to occur then continue pulling apart the two split halves for one inch in length from the score location.

E. Trim off the longer of the two split sides so that they are both the same length.

9. Set the experiment to the run position to release the brakes on the rotation sensors as well as the sample holder in the center of the apparatus.
10. Insert the test sample with the original screen side edge facing to the right and protruding from the pneumatic clamps approximately 1.5 inches.
11. While holding the sample sheet in place set the experiment to the stop position. This should clamp down on the sample so it no long has to be held in place.
12. Connect both of the clips fully to the split tops of the test sheet.
13. Slide the line connecting the split sheet from the clear part of the pulley to the geared central section making sure there is no slack in the line.
14. Set the data acquisition system to start recording when a high signal is seen on the run switch.
15. Switch the experiment to the run position to run the experiment and start recording data.

Data Recording and Analysis

A data acquisition program collects the voltage value output from the paper splitting apparatus. Three voltage values are recorded, two measure the RPM's of the left and right rotation sensors and one measures the trigger line used to initiate splitting. Data recording is set to initiate when the trigger line (actuated manually) reaches a rising value of 3.3 volts. Once triggered the program records the RPM and trigger values for a period of one second prior to and 10 seconds past the trigger at 100^{th} of a second intervals. Once the data in a single trigger is written to the file the data acquisition program automatically rearms the system for the next test. The use of the automatic rearm allows all ten of the samples to be split in approximately 5 minutes. Once split, the sample thickness at all four of the top and bottom locations is recorded. The samples are then numbered to match the corresponding data file and bagged.

Once entered into the computer the two rotation sensor voltage values are converted to a rotational velocity using the presets of the digital readout contained within the paper splitting apparatus display panel. This rotational velocity along with the hub diameter of the rotation sensor allows for the calculation of the tangential surface velocity of the rotation sensor. Because the sample sheet being split is directly coupled with the rotation sensor then this tangential surface velocity also represents the speed at which crack propagation is occurring in the sheet and the speed at which the splitting weights are falling.

All of the data at this analysis point needs to be scrutinized to determine where actually the splitting starts and truncate all data that occurs before then. When sample sheets are loaded into the splitting apparatus there is a certain amount of play caused by the fact that it is difficult to pretension every sample sheet to the same degree. This play causes a small transition period where the tension within the sheet is increased to a point where splitting starts to occur.

The energy balance within the system is what we are truly interested in because it gives us a value for the amount of force per unit length needed to split the sheet. This force is a combination of both inter-fiber bonding and fiber entanglement. Looking at the paper splitting system as a whole, the only energy stored in the system to begin with are the two splitting weights gravitational potential from the floor. When the experiment is run the energy contained by the weights is transferred primarily to two different sources. The first source is the kinetic energy of the weights and the second is the splitting of the sheet of paper. There is also an error source that has to be accounted for and contains all of the other energy robbing events of the system. Of the two sources to which energy is transferred only one can be measured directly, and that is the kinetic energy of the weights. The amount of energy that goes into splitting the sheet has to be calculated using the initial potential energy of the system, the kinetic energy of the weights as well as the amount of energy lost to error.

Instron Tester

The Instron tensile tester data is used to complement the results obtained through the paper splitting apparatus. For every full sheet that was produced in the Formatte

Dynamique four one inch by seven inch samples were cut from opposite ends, see Figure 3.2. Two of these samples (one from each end) remained at the moisture content of the sheet for testing while the other two were fully dried on a steam drum dryer prior to testing. The data obtained from the tensile test is the stress-strain relationship of the wet and dry paper test sample. Values for the maximum load, percent strain, and modulus of elasticity are computed from the stress-strain relationship curve for a particular sample.

The Instron tester is a closed-loop electro-hydraulic testing machine, which can apply static or slow cyclic loads in tension or compression. In our experiment the tester is used in tension with a defined constant rate of strain. A load-cell is used to measure the tensile force resulting from the defined strain. A linear variable differential transducer (LVDT) is used in the strain measurement of the sample. In Figure 3.3 is a diagram outlining the overall experimental setup as well as a description of individual parts of the tensile tester.

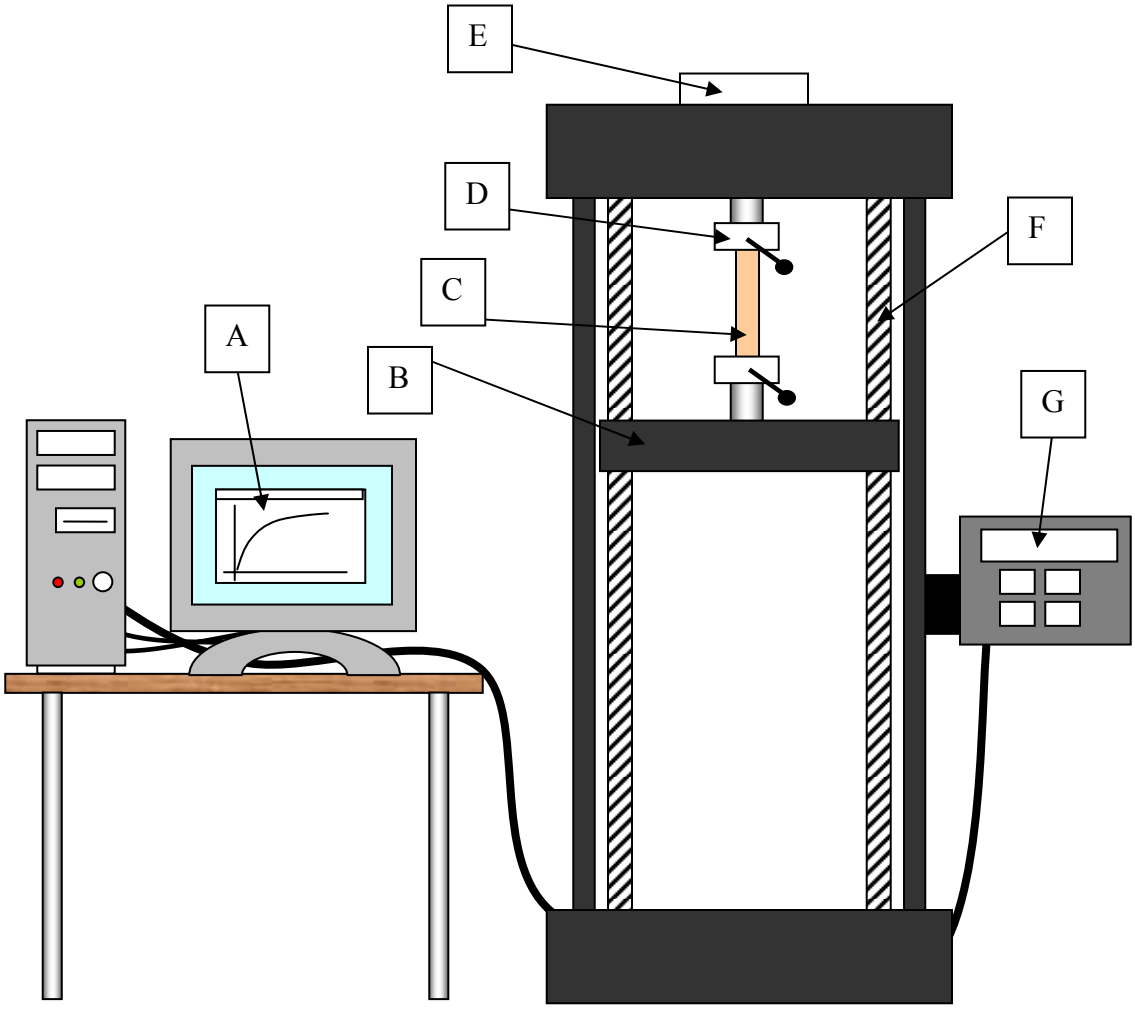

Figure 3.3 – Diagram Showing the Instron Tester.

Instron Tester Description

The Instron Tester shown above in Figure 3.3 is comprised of the following components.

A. Series IX Program – This is the program that is used to record and graphically analyze the data obtained from the tester.

B. Tester Crosshead – This part of the testing apparatus moves along two screw tracks and provides either the tensile or compressive force needed to destructively test a sample.
C. Paper Sample – The paper sample with a width of 1 inch and a length of 7 inches is used to span the 5-inch testing area between the holding clamps.
D. Sample Holding Clamps – These clamps are used to hold the sheet being tested in the Instron. They consist of two plates that screw together each with a rubberized clamping surface.
E. Load Cell – A removable load cell is used to determine the stress on the sample.
F. Feed Screws – These screws are what transfer the applied strain to the crosshead. The screws are driven from motors located in the base of the tester.
G. Instron Tester Control Panel – Computer to control the characteristics of the Instron tester. This computer is mainly used to calibrate the stress and strain prior to testing of a sample.

Z-Direction Tester

The z-direction tester is similar to the tensile tester but acts in the direction perpendicular instead of inline to the plane of formation. Because of this direction the results from this test correlate directly to the results that are obtained through the paper splitting apparatus. Only dried paper can be used in this experiment because of the adhesive used in attaching the sample. It is because of this that the results can only be used to compare to the fully dried samples experimentally tested on the splitting apparatus.

The z-direction test was performed following Tappi T-541 testing methods. To perform this test, double-sided adhesive is attached to both sides of a 2-inch square sample that has been fully dried on a steam drum. The sample is then placed between two plates that first press the sample together to achieve uniform adhesion between the paper and the double sided tape then the apparatus pulls apart the sample while measuring the energy needed to do so. The output of the test is a pressure that represents the maximum force per unit area needed to split the sheet in the z-direction. The data from this test aids in the evaluation of the samples in two different ways. The first is a simple evaluation of how effective the bonding additives were on the overall sheet strength in the z-direction. The second use of the data is that it can be used to evaluate the results from the paper splitting experiment at the driest levels used in the experiment.

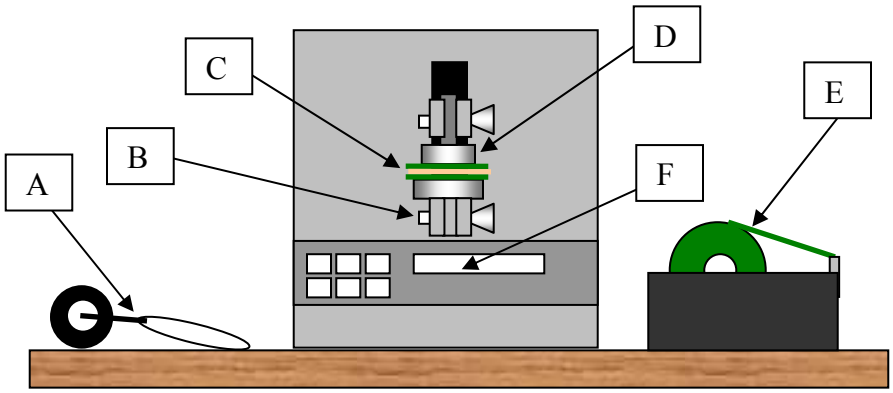

Figure 3.4 – Diagram Showing the Z-Direction Tester.

Z-Direction Tester Description

The Z-Direction Tester shown above in Figure 3.4 is comprised of the following components.

A. Roller – The roller is used to affix the double-sided tape to the paper sample being tested.
B. Plate Locking Pins – These pins connect the two-separation plates to the machine. They are removed for easy application of the test sample as well as easy removal of the sample once the test has been run.
C. Test Sample – 2-inch square sample with double sided adhesive on both sides to attach the sample to the separation plates.
D. Separation plates – The plates are what pull on the double-sided tape splitting the test sample.
E. Double-Sided Tape – This tape is applied to both sides of the test sample and attaches the sample to the two separation plates.
F. Z-direction Tester Computer – This computer runs the z-direction test allowing multiple user defined inputs. This is also the screen that outputs the result from the experiment.

CHAPTER 4 – ERROR ANALYSIS

Measuring Error in the Split Test

There are multiple sources of error that occur with the splitting apparatus during testing. All of these error sources remove energy from the system and if not accounted for will result in a high calculation for the amount of energy that is needed to split the sheet.

The first source of error in the system is the mechanical design of the splitting apparatus. There are frictional and inertial properties of the mechanism that rob the system of some of its initial potential energy. To measure this energy loss the paper splitting apparatus was set up with unequal splitting weights on each side. The two clamps that are usually used for splitting the sheet were attached to each other. A test was then run as though a sheet was being split. This test was then repeated for multiple cases with different weights. It was found that there is a linear relationship between the energy difference and the distance split in all of the cases. However, as can be seen in Figure 4.1, the changes in the line slopes are primarily dependent on the weight difference rather than total weight.

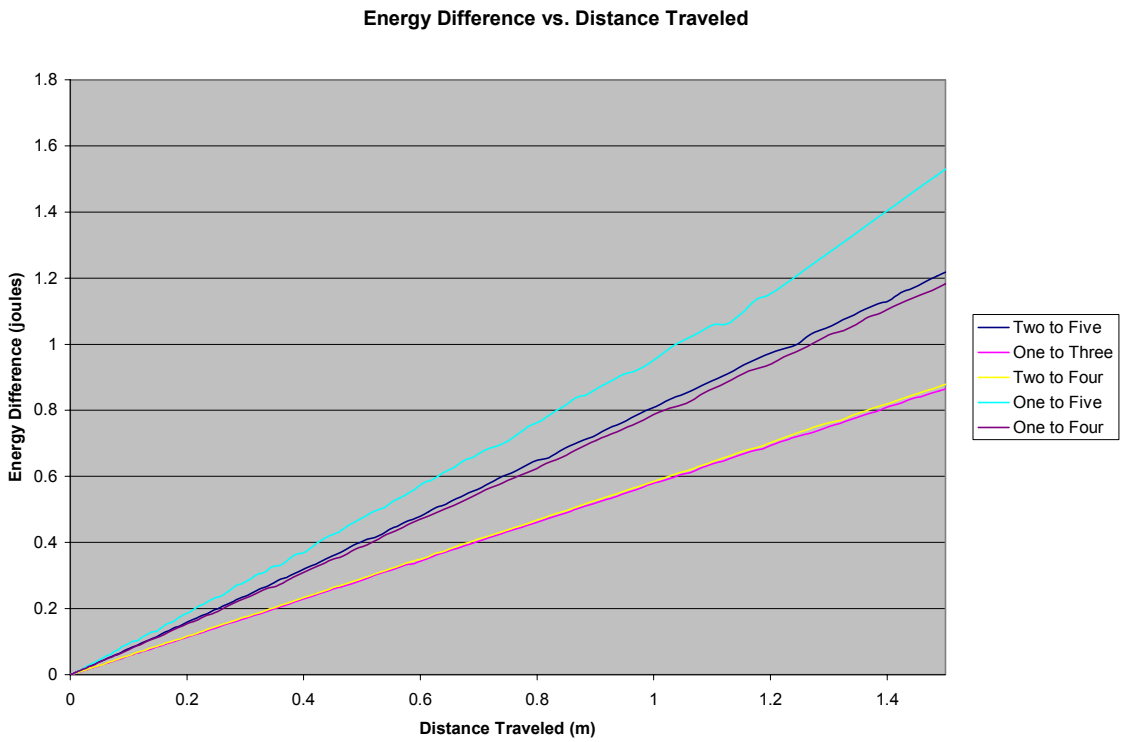

Figure 4.1 – Energy Difference versus Distance Traveled for the Frictional System Loss.

The first thought when looking at this graph would lead one to think that the slope is likely a function of the velocity. However, that is not true because of the high linearity of the graph. The fact that the slope is primarily a function of the weight difference is good in our case because in actual testing both of the weights have the same mass. Using the slopes of the lines in the graph above, along with the total weight on the machine, a new graph was created, and can be seen in Figure 4.2 below.

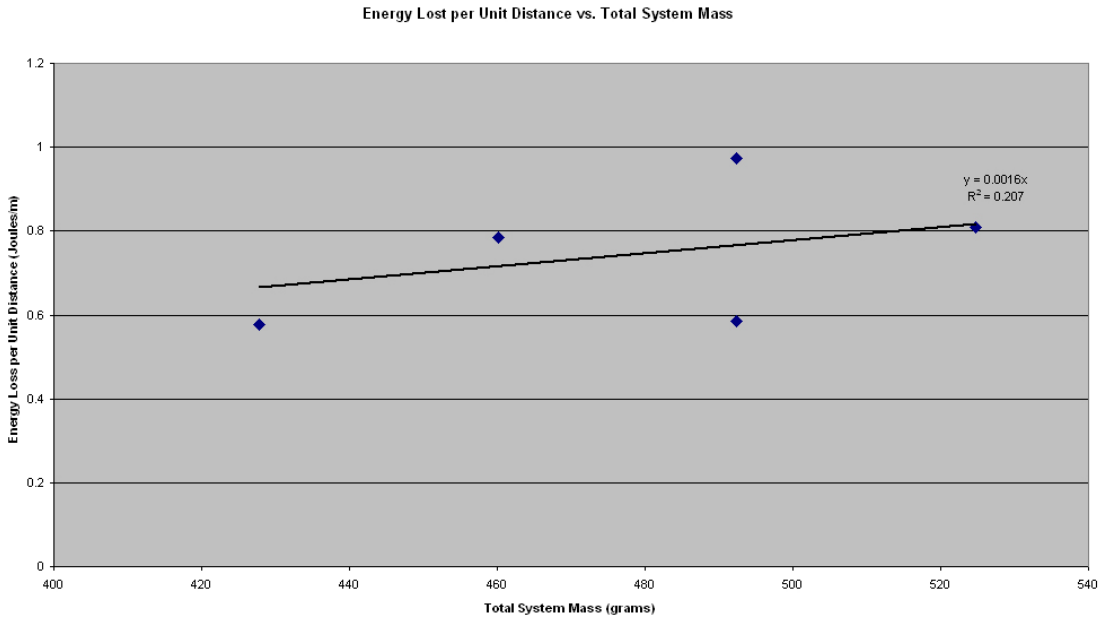

Figure 4.2 – Energy Lost per Unit Distance versus the Total System Mass.

The linear relationship in the above graph can then be used to determine the amount of energy lost from frictional and inertial forces within the test.

$$\text{Total System Mass} = 2 \times 254.15g = 508.3g \qquad \text{eqn. 4.1}$$

$$\text{Energy Lost per Unit Distance} = 508.3g \times 0.0016 \frac{J/m}{g} = 0.81328 J/m$$

This error factor means that a great deal of what is being measured during the experiment is energy that was lost by the system and not used for splitting.

The second primary perceived error in the experiment is the bending of the sheets while being split. At low basis weights there is very little effect, but in the paper splitting

experiment most sheets have a basis weight close to 300 g/m^2 to allow splitting to occur the full length.

In this experiment sheets with similar moisture contents but with varying basis weights were produced. These sheets were then split using the standard method used for all of the samples. The results show that bending energy does play a factor in the energy measured in the experiment. The results in Figure 4.3 show that there is a relationship between the energy required to bend the paper test sample and the basis weights.

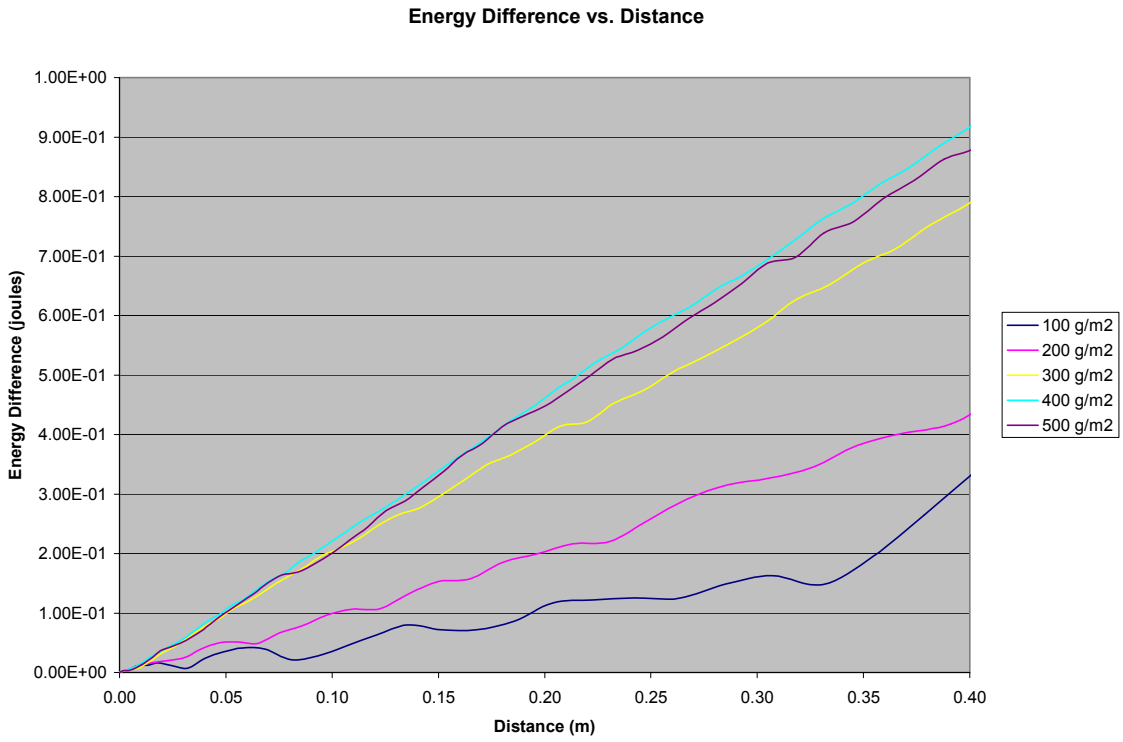

Figure 4.3 – Energy Difference versus Distance for Multiple Basis Weights.

A graph is then produced comparing the energy loss per unit distance (slope on the above graph) versus the basis weight of the sheet sampled. This graph along with a trend line is shown below in Figure 4.4.

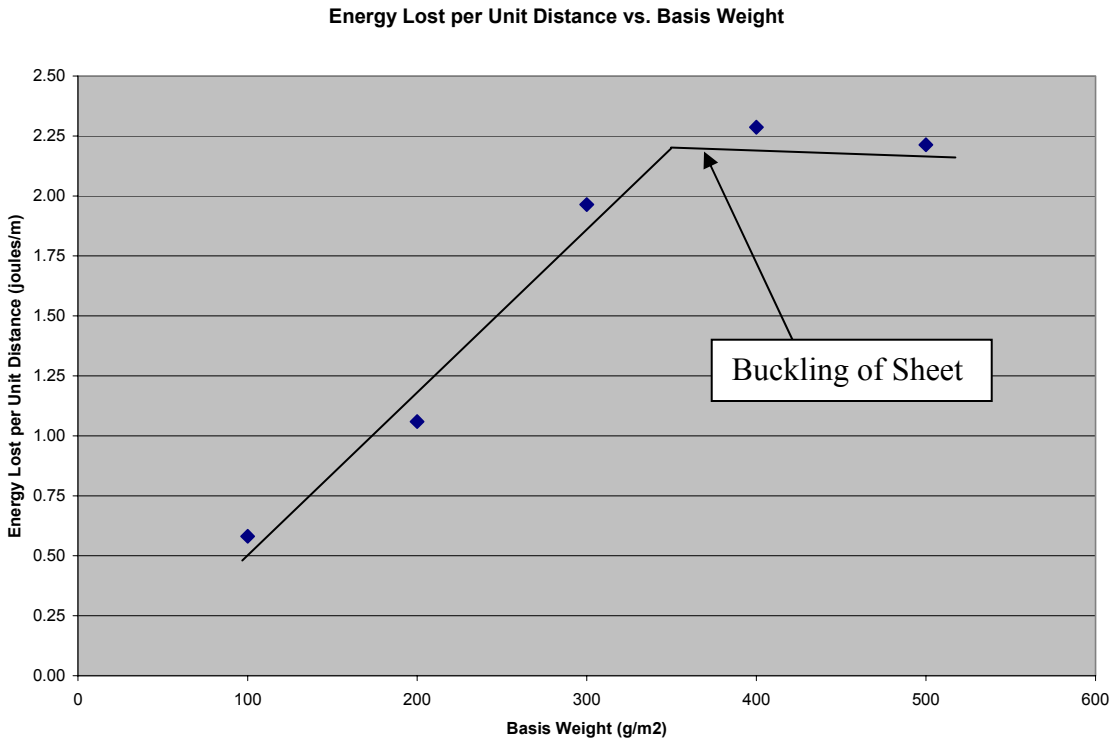

Figure 4.4 – Energy Lost per Unit Distance versus Sample Basis Weight.

The energy lost per unit distance in the above graph represents all of the energy lost by the system, including both the loss due to bending and the loss due to splitting the sheet. As noted earlier, when the system basis weight approaches zero the amount of energy needed to bend the sheet will also approach zero. Therefore, using the equation from the trend line to forecast back to a zero basis weight, the amount of energy that went into splitting (which should remain constant for all basis weights) can be determined. This is solved to be 0.5804 joules/meter. For the fully dried 300 g/m^2 sheet with no additives, the energy lost due to bending is computed as 1.29 joules/meter.

A combination of factors could cause the amount of energy required to bend the test samples to be nonlinear, level off, then decrease at high basis weights. The first action taking place on the samples is the buckling of the compressive side of the bent test sample. This buckling effect can be seen on the test samples themselves. After undergoing the splitting test, small uniform ripples can be seen on the backside of the higher basis weight samples. This buckling occurs in the sheet due to delamination of the fiber layers. Because of the method used to create the sample sheets the material properties of the paper sample are not isotropic. Almost all of the fibers within the sheet run in the MD and CD directions with very few fibers running in the vertical z-direction of the sample. Because of this weakness within the z-direction the possibility for layers delaminating is increased. The exact cause of the layers delaminating is not precisely known because there are multiple methods in which it can occur. The first method is through shear stress created between "layers" of fiber within a sheet. In this case the bottom and top layer would shear off from each other allowing the bottom layer to start buckling. The second method is if the buckling occurs first and creates enough localized z-direction stress at the buckling points to delaminate the sheet. This second method is the more plausible of the two because it results in a more uniform and attached buckled layer with smaller buckles like those seen on some of the test samples.

Different Splitting Masses

The weight chosen for the splitting force was determined by the strength needed to split a fully dried paper sample with no additives. When testing the fully dried sheets

with the bonder additive, the inter-fiber force was too great for the weights to overcome and split the sheet. For these samples, additional weight was used to achieve full splitting.

The equations that were used to manipulate the data from the experiment allow the results from a greater splitting weight to be compared directly to the results of a lower splitting weight. The numerical analysis of the data is done using a simple energy balance of the system. The initial energy of the system is due to the raised weights and is 100% potential energy. Once the split has initiated, the systems energy is a mix of potential energy, from the falling weights position, kinetic energy, from the velocity of the weights, and energy that is lost from the system. This lost energy represents the energy that was used to split the sheet and the frictional loss of energy due to inefficiencies of the system. The equation used to solve for the energy to split the sheet is shown below.

$$\text{Potential Energy}_{\text{initial}} = \text{Potential Energy} + \text{Kinetic Energy} + \text{Frictional Loss} + \text{Splitting Energy}$$

$$m_{total}gh_{Initial} = m_{total}gh_{Instant} + \tfrac{1}{2}\, m_{total}V^2 + Friction + Splitting \qquad \text{eqn. 4.2}$$

Assuming for this model that the amount of energy needed to split the sheet is a combination of the splitting and frictional energy, the initial height of the system is taken as the datum reference point of the system, the mass is two times the individual splitting mass, and the velocity is the average velocity of both of the splitting masses.

"Splitting Energy" is a combination of the splitting and friction energy

$$Splitting\_Energy = Friction + Splitting$$

Total system mass equals two times the individual splitting masses

$$m_{total} = 2m$$

The initial starting position is taken as the y-origin

$$h_{Initial} = 0$$

$$0 = 2mgh_{Ins\tan t} + mV^2 + Splitting\_Energy \qquad \text{eqn. 4.3}$$

The instantaneous height of the sheet is going to be a negative value for all time, therefore the negative value is moved outside of the height value.

$$0 = -2mgh_{Ins\tan t} + mV^2 + Splitting\_Energy \qquad \text{eqn. 4.4}$$

$$2mgh_{Ins\tan t} - mV^2 = Splitting\_Energy \qquad \text{eqn. 4.5}$$

$$m \cdot \left[2gh_{Ins\tan t} - V^2\right] = Splitting\_Energy \qquad \text{eqn. 4.6}$$

The mass acts as a scalar that stays constant. If the weight used for splitting is increased, the amount of splitting energy is scaled inversely by the percent change of the weight to allow it to be compared to the results from other weights. For example, if the weight used for splitting in the above example were twice as large, the measured splitting energy is divided in half to achieve the corrected value.

To test this theory experimentally, different splitting masses are used to split one sample. The splitting mass used in the experiment started at the commonly used mass of

460 grams and incremented in 20 gram divisions up to 560 grams. The splitting material used was a fully dried sample with no additives. Two tests for each weight were averaged to determine the splitting energy. The graph of the total summation of scaled splitting energy values versus the distance split is shown below in Figure 4.6.

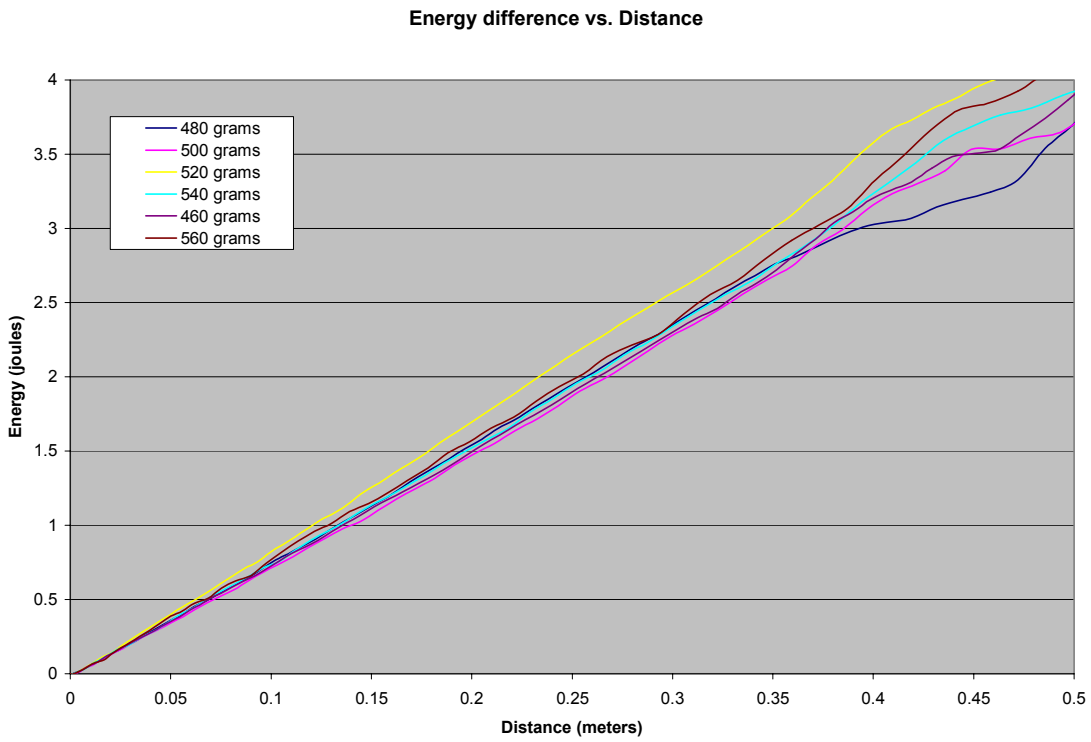

Figure 4.5 – Splitting Energy versus Distance for Different Splitting Weights.

The graph above shows that regardless of the splitting weights all of the results are approximately equal to one another, and more importantly there is no trend that can be developed between the slope and splitting weights. The different splitting velocity created by the splitting masses is shown below in Figure 4.6.

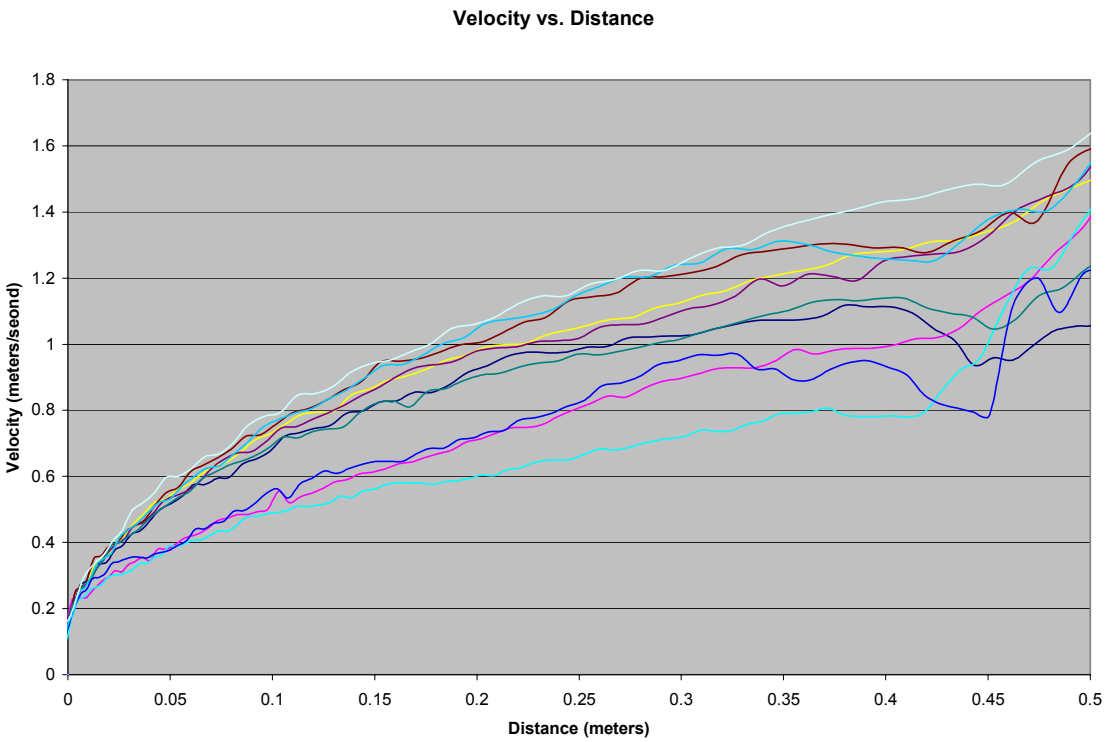

Figure 4.6 – Velocity versus Distance for Different Splitting Weights.

CHAPTER 5 – FINITE ELEMENT MODEL DEVELOPMENT

A mathematical model of the paper splitting system was created in an effort to further understand the results obtained from the experimental data. The model is designed to represent the fiber level properties of a sheet during a split. One of the key aspects of the program is to have the ability to break links between nodes when they reach a maximum given force or displacement threshold.

Finite Element Theory

Paper can be physically broken down into a finite number of fibers held together by multiple interfiber forces. Because of this ability to be broken down, paper lends itself well for being modeled in the finite element method. To accurately model a sheet of paper the number of elements does not need to approach infinity, like it does for an isotropic material. Instead, the number of elements in the model needs to approach the number of bonds present within the sheet.

Multiple assumptions and simplifications were made with regard to the individual elements in the development of the program. To understand where most of these assumptions came from it is helpful to first look at a model of the finite element grid used by the program. This grid is shown below in Figure 5.1.

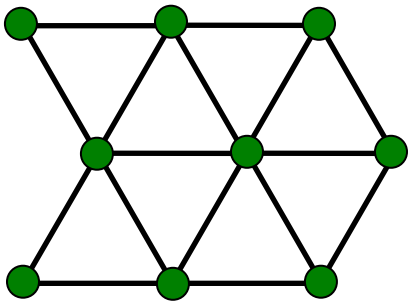

Figure 5.1 – Finite Element Grid.

The finite element grid is made up of multiple nodes (green) and links (black). A node represents some form of interfiber bonding, while a link represents an individual fiber. In saying this, the very generic and misleading assumption that all fibers are the same length and attach to other fibers only at their ends is made.

The mathematical properties used in the finite element model are based on the numerical method known as Newton's iteration. Newton's iteration is simply the first three terms of the Taylor Series. It allows a point in the future to be estimated by using points from the past. The Taylor series of f(x) about the point $x = x_0 + \Delta x$ is shown in equation 5.1 below.

$$f(x_0 + \Delta x) = f(x_0) + f'(x_0)\Delta x + \frac{1}{2} f''(x_0)\Delta x^2 + ... \qquad \text{eqn. 5.1}$$

For every node in the program there are two Taylor Series expansions; one for each the global x and y directions. In these expansions the function shown above in

equation 5.1 is equivalent to either the x or y location of a node and the variable x used in the function is equivalent to time. Rewriting the expansion using the terms used by the program gives the equations shown below in equations 5.2 and 5.3.

$$x(t_n + \Delta t) = x(t_n) + x'(t_n)\Delta t + \frac{1}{2}x''(t_n)\Delta t^2 \qquad \text{eqn. 5.2}$$

$$y(t_n + \Delta t) = y(t_n) + y'(t_n)\Delta t + \frac{1}{2}y''(t_n)\Delta t^2 \qquad \text{eqn. 5.3}$$

Truncating the terms to the third order makes the assumption that the acceleration term (x" or y") is constant over the time step.

To solve the equations shown in equations 5.2 – 5.3, the position, velocity, acceleration, and mass of the node must be solved for. The easiest of these to compute is the nodal mass. The nodal mass is calculated as the sheet basis weight divided by the area surrounding one node, the area being found by multiplying the x-nodal spacing by the y-nodal spacing.

The remaining terms are all determined through force calculations on the nodes. Six other nodes surround each node unless it is along an edge of the array. The distance, velocity, and link properties between the node in question and a surrounding node are used to determine the force that is acting between the nodes. This force along with the force from the other five nodes is split into their corresponding x and y components and is summed for the node. Using Newton's second law of motion, the x and y force and the nodal mass are used to determine the nodal acceleration. This nodal acceleration is then

used with a second order Taylor series expansion to determine the corresponding nodal velocity. This velocity along with the acceleration and past nodal position is then used in the equations shown above in equations 5.2 and 5.3 to determine the new nodal position. Due to the small size of the time steps and magnitude of forces involved, the process for determining the nodal locations has to be repeated a great number of times to achieve even nominal nodal displacements

Finite Element Program Development

The first step in program development is the setting up of an array of nodes that will be used in the finite element model. In a first run the default number of nodes per row was set at four. This allowed the split to occur between the center two nodes and some interaction to take place on either side of the break. The number of rows in the array is a variable supplied by the user. Each node is assigned a single number starting from 1 in the top left corner and progressing to the right and down. At the same time node numbering is occurring, two matrices size n x 1 (with "n" being the total number of nodes) are constructed with the x and y coordinates of each node. The system origin is set at the top left node.

The program then assigns nodal relationships relative to one another. This is done as a four row column vector in which the column number represents the node being assigned. The first row is the number of the node that is above, second is the number of the node that is to the right and so on in a clockwise direction. If a node is not connected

to another node on a particular face, which would occur on an edge node or a node with a broken link, then the number zero is put in place of a node number.

After all of the nodes and their relationships have been created the array is plotted in black and the dynamics section of the program starts. The dynamics section has two loops, one nested inside the other, with the outer loop cycling through every node and the inner loop cycling through the relationships between the node that is being looked at and all of its neighboring nodes. A distance and angle between nodes is calculated and the resulting x and y forces for a particular node is determined. This force along with a nodal mass is used to calculate the current acceleration, displacement, and velocity of the node. After this process finishes for each node the time is stepped forward and the process is begun again. Once a predetermined ending time is reached the loops are exited and the final array configuration is drawn in red (all intermediate nodal locations are drawn as blue dots at every time step), as seen in Figures 5.2 – 5.13.

The dynamics of the system are defined by the nodal mass and the model used for the links. In the first model, the links between nodes were comprised solely of springs with one spring constant. This was done because the results from this model are more intuitive and it was a check to see if the program was running correctly thus allowing troubleshooting at an early development stage. The first displacement used was a step input where the top two corner nodes were shifted to a new position at time equal to zero and held there for all time. Since the dynamics of the system rely only on the

displacement between nodes without any damping effects, the system never relaxed and just vibrated for all time. See Figure 5.2 below:

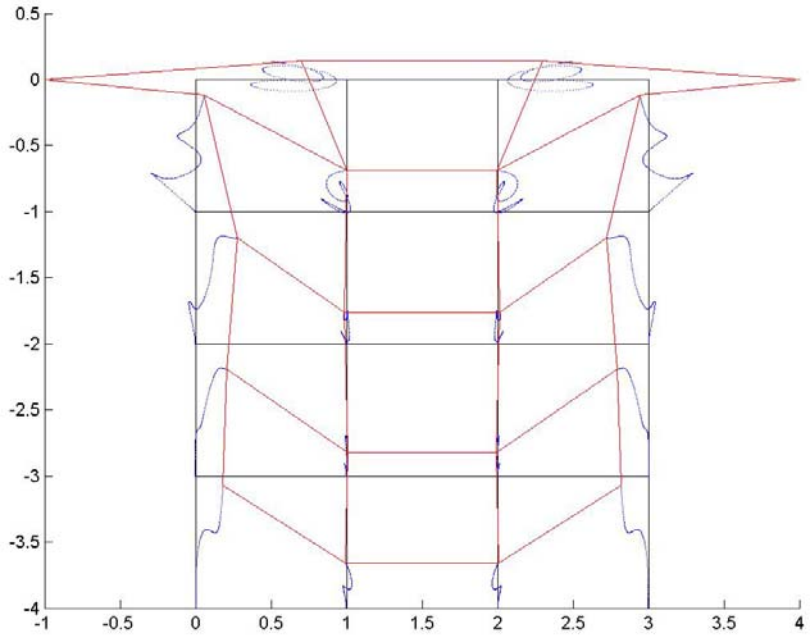

Figure 5.2 – Plot of Nodal Displacements for System with Springs and no Damping.

The next step was to add a dashpot in series with the spring. In viscoelastic models this is generally known as a Maxwell fluid. By adding this dashpot the system could be damped to allow for better system relaxation. This relaxation can be seen in the Figure 5.3 below which shows the same system as Figure 5.2 but with damping.

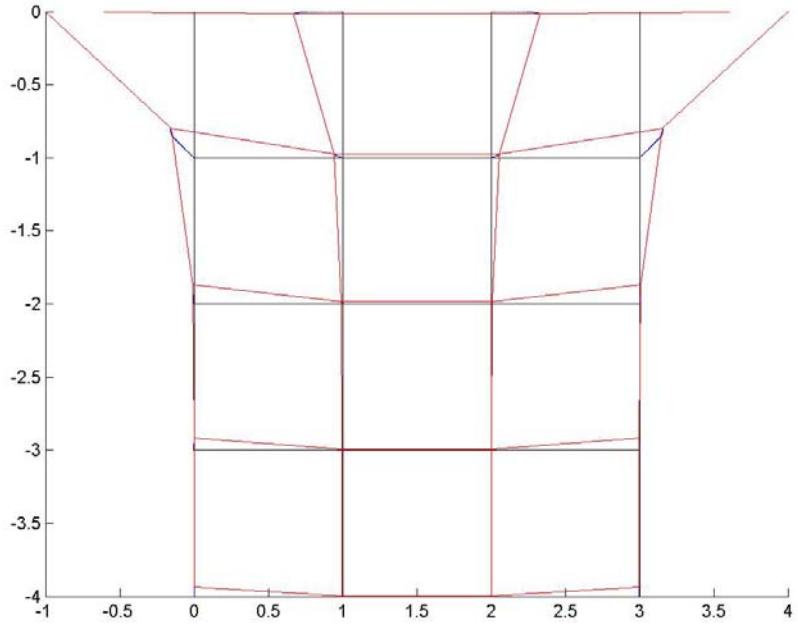

Figure 5.3 - Plot of Nodal Displacements for System with Springs and Damping.

The next progression of the system was to add the ability for nodes to break apart when the sheet is overstretched or over forced. Without this ability the program would just be a viscoelastic sheet that could be stretched and deformed but would never split. This capability was easily added to the program through a check of the inter-nodal force and distance values and setting the relative node value to a zero if the values are above a particular user defined threshold value. When the program was run again an issue arose when the nodes were allowed to split. In the model the two corner nodes that were given the initial displacement were separating from the array because their strain was immediately greater than the displacement threshold. To overcome this dilemma the top two nodes on each side were pulled together maintaining their spacing. In retrospect this is a better way to model the split because in the experiment a sheet is not being pulled by

the corners but by the whole end (while maintaining spacing). In addition, instead of the initial crude step displacement, the top nodes are driven at a constant speed and are later modified to be pulled with a constant force. This technique works well in the model, however to achieve a full split, the split propagation speed, the damping constant, and spring constant have to be fine tuned to allow the greatest strain to occur in the exact center of the piece. If it occurs anywhere else the top nodes that are being driven will separate from the body. Shown in Figure 5.4 below is a 20 node model of the sheet with spring-dashpot type links being pulled apart at a constant velocity.

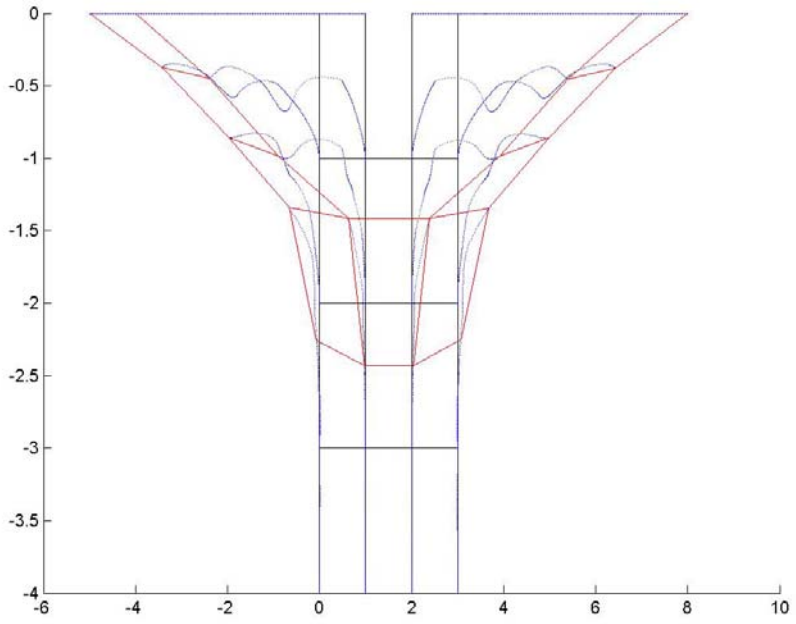

Figure 5.4 - Plot of Nodal Displacements for System with Springs, Damping and Fracture.

The next step in the program development is to allow a user to define the number of nodes in the width of the model. Having additional nodes in the width more accurately describe the action of the sheets that are currently being split because it allows more inter-node interactions away from the fracture. This includes stress distribution and sheet bending. Shown below in Figure 5.5 is the same sample pulled apart in Figure 5.4 with twice the width, or eight nodes across.

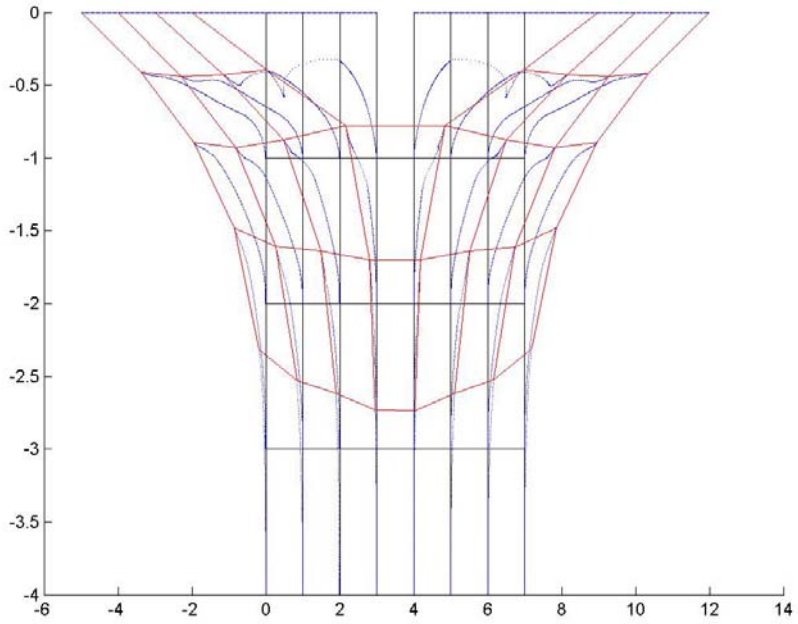

Figure 5.5 – Plot of Nodal Displacements for System with Springs, Damping and Fracture with Variable Width Number of Nodes.

The links of these early models were comprised of a spring in series with a dashpot. While this model represents a viscoelastic material, a three-parameter solid may better describe what is taking place when the paper is fracturing. In a sheet of paper

undergoing fracture there are two main modes of failure, breakage of a well bonded fiber-fiber link and fiber pullout. The three-parameter solid tries to take both of these properties into account. The bonds in this model are represented by springs, and the fiber entanglement properties are represented by a viscous dampener in series with a spring. Both of these are placed in parallel so they can work independently of one another. A sample link using the three parameter solid is shown below (Figure 5.6a) in contrast to the previous Maxwell fluid – Kelvin solid model (Figure 5.6b).

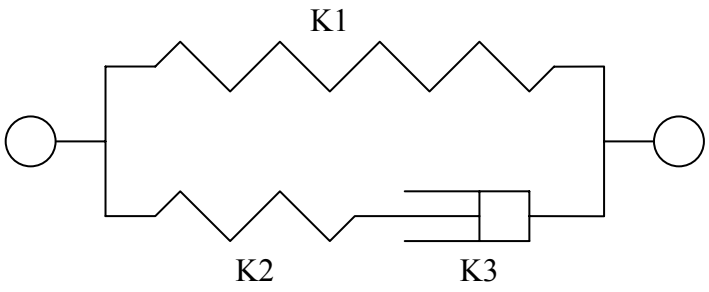

Figure 5.6a – Three-parameter Solid Model.

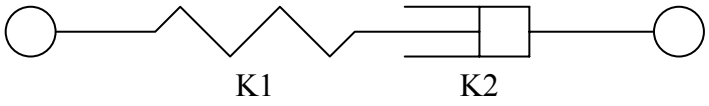

Figure 5.6b – Maxwell Fluid Model.

The governing differential equation for the three-parameter model is shown below:

$$K2 \cdot \sigma + K3 \cdot \frac{d\sigma}{dt} = K1 \cdot K2 \cdot \varepsilon + (K1 + K2) \cdot K3 \cdot \frac{d\varepsilon}{dt} \qquad \text{eqn. 5.4}$$

In the program time is stepped through and the equation above is transformed into the one shown below:

$$K2 \cdot \sigma_n + K3 \cdot \left[\frac{\sigma_n - \sigma_{n-1}}{\Delta t} \right] = K1 \cdot K2 \cdot \varepsilon_n + (K1 + K2) \cdot K3 \cdot \left[\frac{\varepsilon_n - \varepsilon_{n-1}}{\Delta t} \right] \qquad \text{eqn. 5.5}$$

Solving for the stress in terms of the strain:

$$\sigma_n = \frac{K1 \cdot K2 \cdot \varepsilon_n + (K1 + K2) \cdot K3 \cdot \left[\frac{\varepsilon_n - \varepsilon_{n-1}}{\Delta t} \right] + \frac{K3}{\Delta t} \cdot \sigma_{n-1}}{K2 + \frac{K3}{\Delta t}} \qquad \text{eqn. 5.6}$$

When this equation is graphed with estimated constants it starts to take on the form of the viscoelastic stress-strain graphs seen in the testing of the paper samples. This graph is shown below in Figure 5.7.

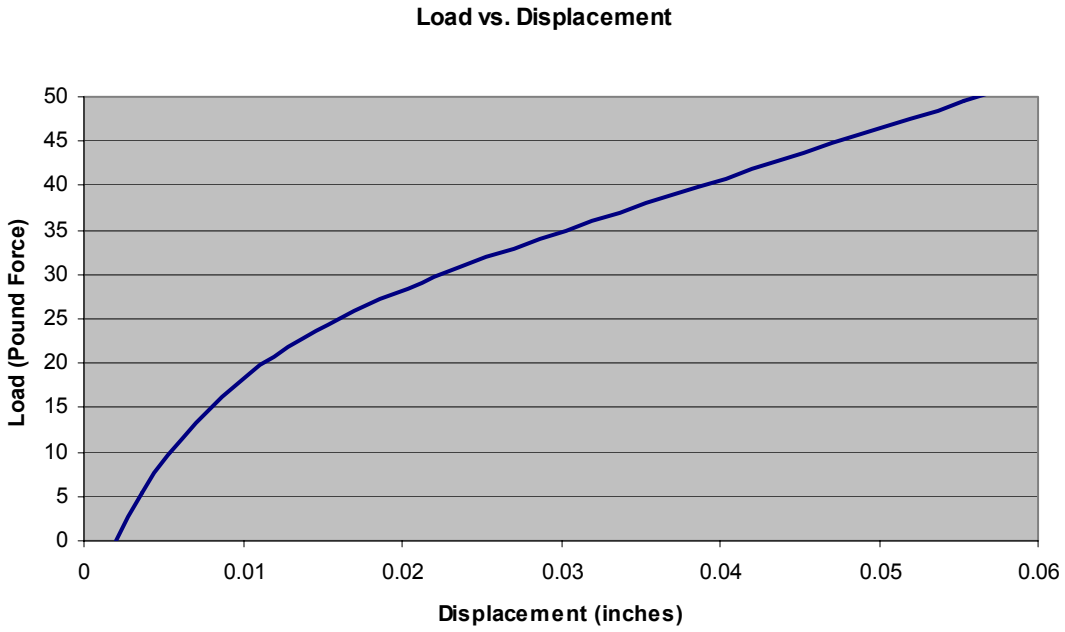

Figure 5.7 – Stress Strain Graph Produced from the Three-Parameter Solid Governing Differential Equation.

Initially it was thought that a single link following the three-parameter solid equation and representing both the fiber bond and fiber entanglement would be ideal. However, when both were joined it was impossible to decouple the system to see the effect of having a greater percentage of one bonding type versus the other. To fully decouple the system some links were defined as fiber entanglement and some as fiber bonds instead of being combined. By modeling the two separately it adds randomness to the program that would be similar to that seen in an actual sheet. A random number generator was used to create a variable number between 0 and 1 for every link to achieve this uncertainty. This number was then used in a comparative statement that determines whether or not the link will be modeled as a bond or a fiber entanglement. Once this is

determined the equation is run to calculate the force exerted on the nodes by the link. An issue created by this is that with such limited numbers of nodes, assigning each node a value for all time the system is not averaged out and can stray from its course. An example of this non-averaging effect can be seen in the lack of symmetry within Figure 5.8 below:

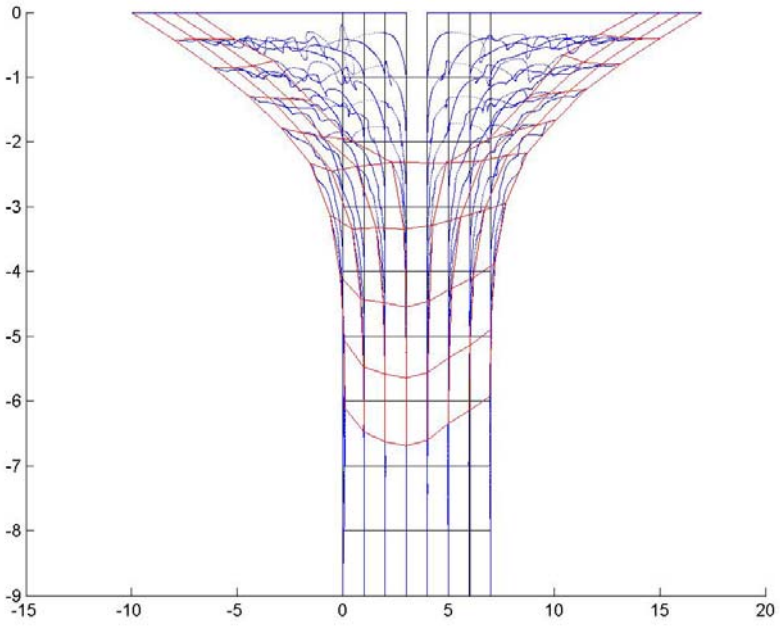

Figure 5.8 – Splitting Result with Half Bonds Half Fiber Entanglement.

The tests were run again with the node types changing every time step so that on average a node would act as bond half the time and as a fiber entanglement point half the time (assuming that the if/then statements are set to a 50% duty cycle). The results of doing this are shown below in Figure 5.91 and it can be seen that the system has averaged out.

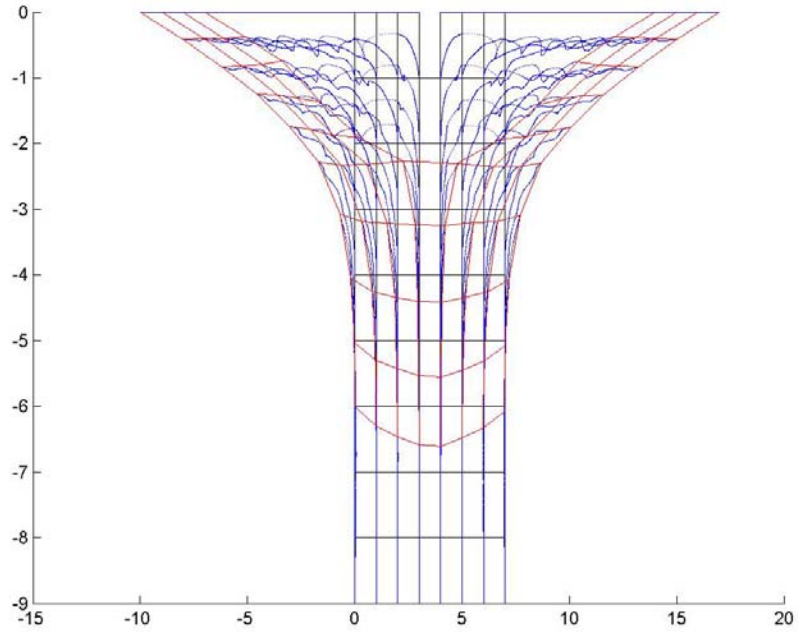

Figure 5.9 – Splitting Result with Random Bonding Type set Every Time Step.

Up until this point in the programming all of the nodal analysis was done using a uniform square nodal array. This worked well but did not truly model the sheet in our application. This model was neglecting any shear stress within the sheet during fracture. In theory behaving more as a liquid being split apart then a solid.

To correct for this, the nodal spacing was changed into a triangular spacing and the relative node matrix was expanded to include all six of the boundary nodes instead of the previous four. The nodal spacing that was created is shown below in Figure 5.10 for an eight by eight matrix:

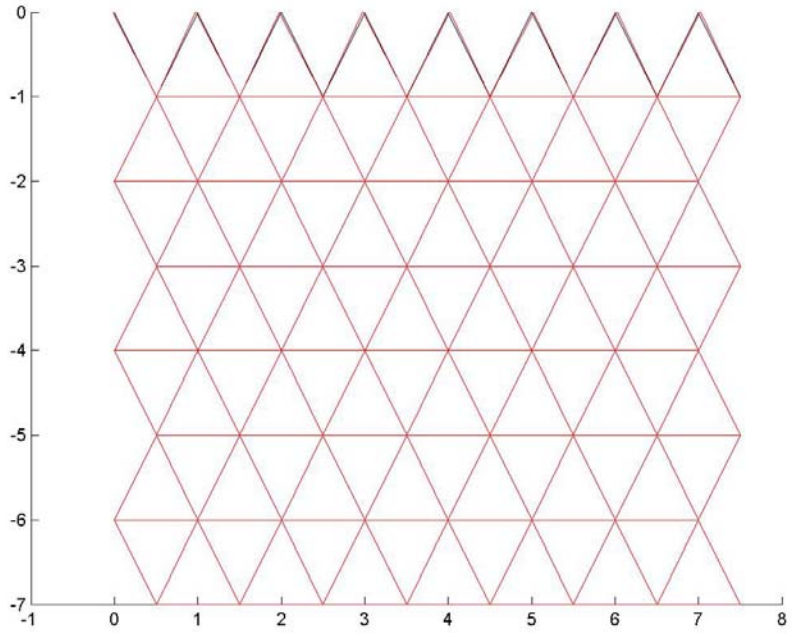

Figure 5.10 – Eight by Eight Nodal Spacing for Triangular Nodes.

Due to the fact that there is no symmetrical way to split the matrix in two like there was with the square nodal spacing the fracture tends to veer as the split propagates. This veering is similar to that seen during the actual sheet splitting experiment. In addition to changing from square to triangular nodes the nodal spacing in the x-direction was disassociated with the nodal spacing in the y-direction allowing for a greater linear density of nodes in the sheet z-direction that in the in-plane direction. By increasing the ratio of the y-distance to the x-distance in the model the previous problem with veering was decreased. The triangular nodal spacing as well as a ratio of y-distance to x-distance of 5 is shown below in Figure 5.11.

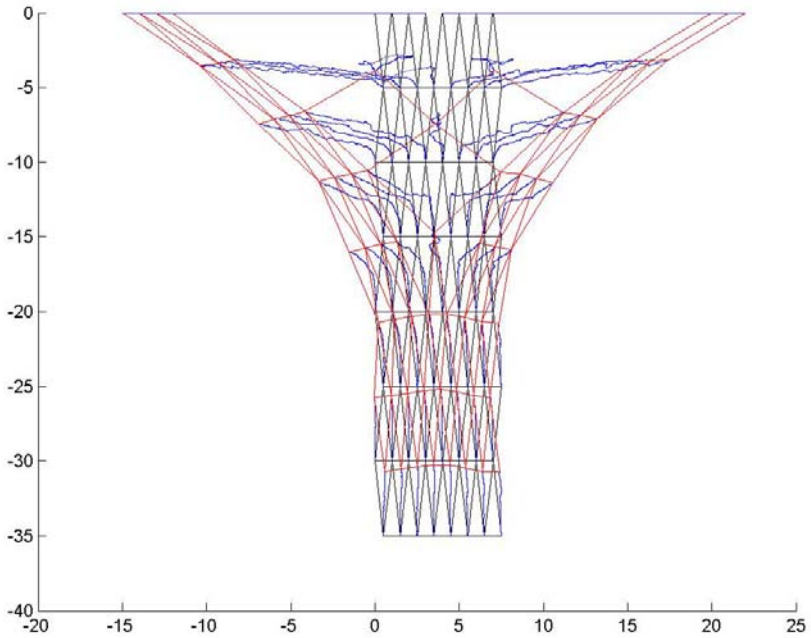

Figure 5.11 - Eight by Eight Nodal Spacing with 5:1 Nodal Spacing.

At this stage in the development process the program is completed however almost all of the variables associated with the program are randomly chosen. Most of the variables such as unit mass, nodal spacing, and number of nodes are determined through the geometry of the system whereas some others such as the spring, damper, and time constants need to be determined experimentally.

CHAPTER 6 – RESULTS

Paper Splitting Results

The splitting velocities in the experiment varied from approximately 1 meter per second for sheets low in moisture content to 2.6 meters per second for sheets high in moisture content. The velocity never reached equilibrium during testing because more than enough weight was used to overcome the cohesion forces of the paper. To achieve a constant splitting velocity the ability to make real-time adjustments to the splitting force would be required because the amount of internal sheet strength is not constant enough.

For every sample that is split the voltage values recorded through the data acquisition program are converted into RPM, linear velocity, distance, and kinetic energy values. A graph of the difference between the potential energy (determined by the splitting masses and the split distance) and the kinetic energy versus distance was created. A sample of this graph showing both of the moisture extremes and all three additives is shown below in Figure 6.1. All of the graphs that were created are located in Appendix A.

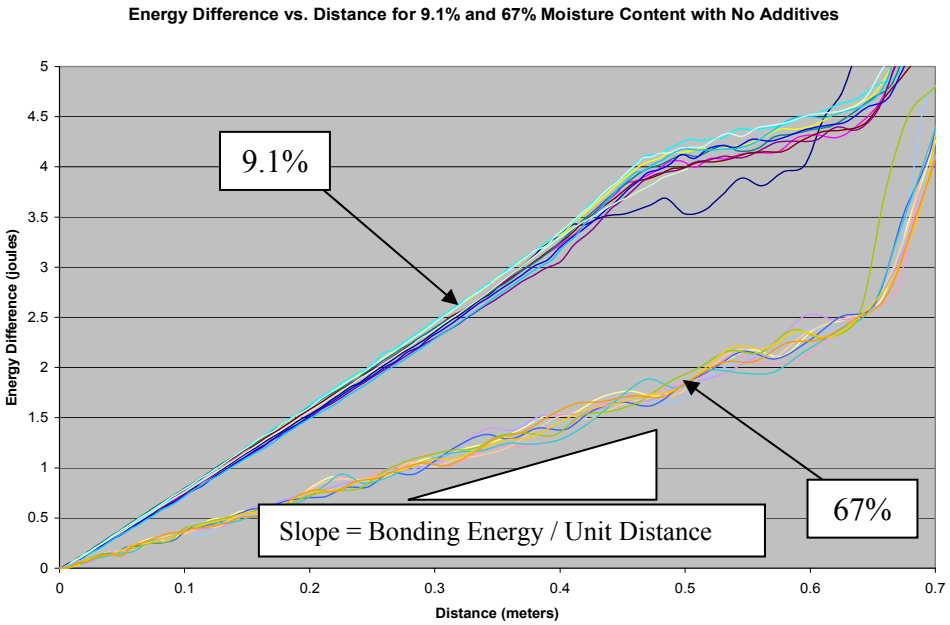

Figure 6.1a – Splitting Energy versus Distance for 9.1% and 67% Moisture Content with No Additives.

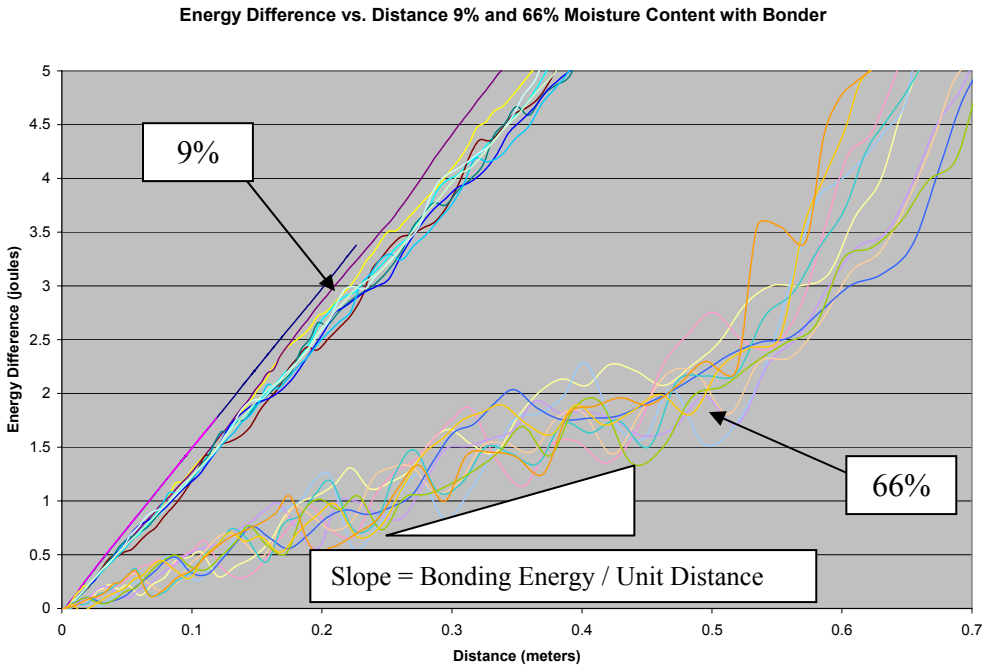

Figure 6.1b – Splitting Energy versus Distance for 9% and 66% Moisture Content with Bonder.

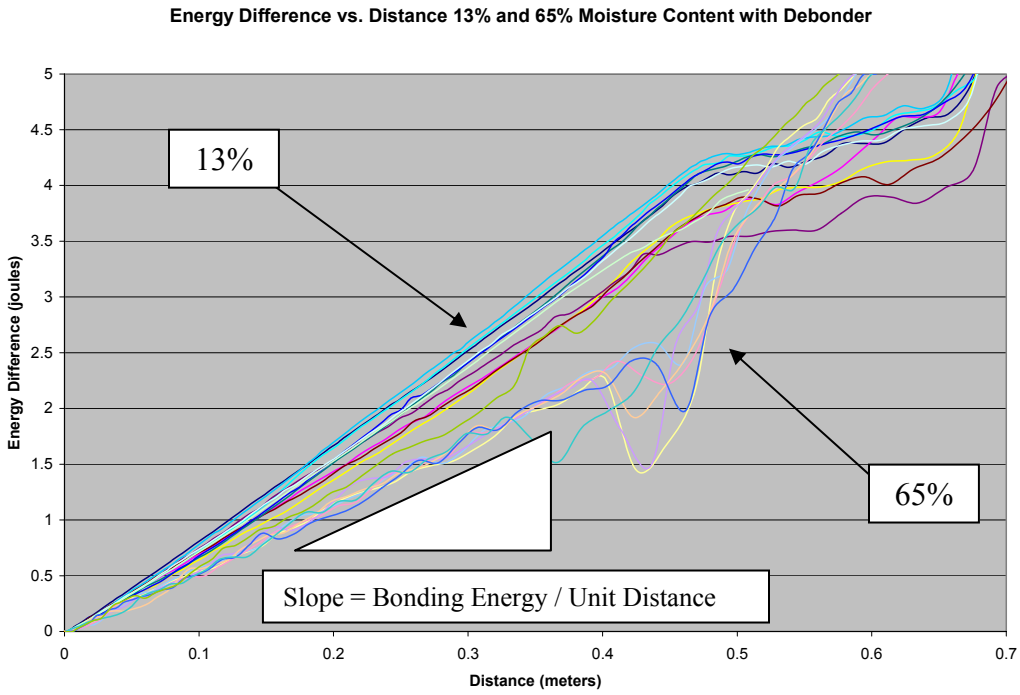

Figure 6.1c – Splitting Energy versus Distance for 9.1% Moisture Content with Debonder.

The linear dependency of the graphs can easily be seen and a slope for all of the samples was recorded for the first 0.4 meters using an average of all of the fully split tests. This slope represents the amount of energy needed per unit length of splitting, keeping in mind that this value is also for a sheet width of 2 inches. All of these slopes were then graphed together as a function of sheet moisture content taking into account the sheet width. This graph showing the work of cohesion is shown below in Figure 6.2.

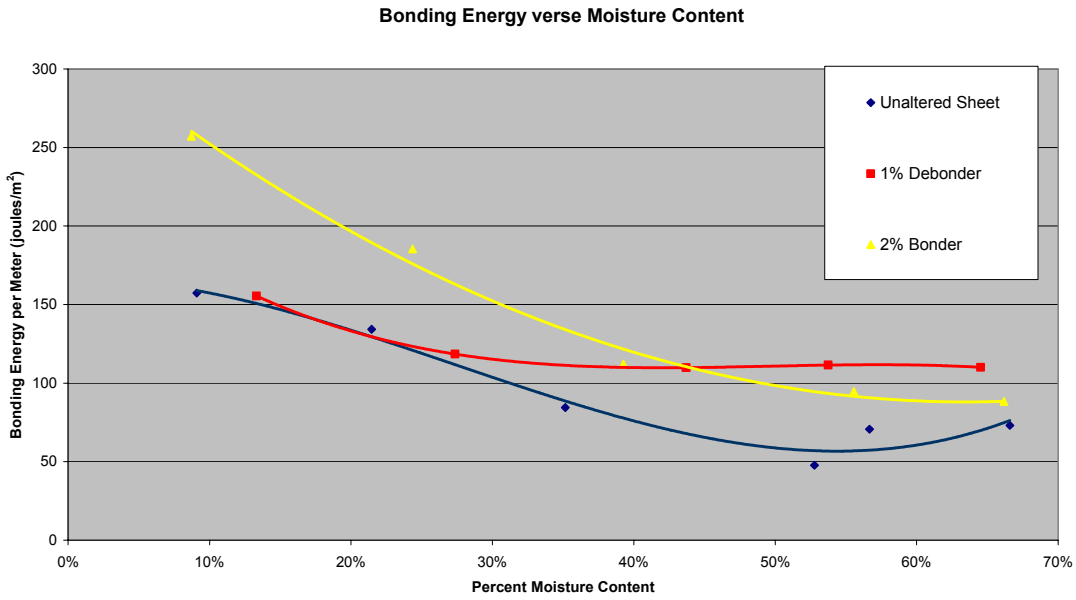

Figure 6.2 – Bonding Energy per Meter versus Sheet Moisture Content.

The values for the work of cohesion shown in the graph above are important in determining when a sheet is going to fail in the z-direction. Picking and peeling of fibers from the sheet during pressing and drying is a direct result of this failure of the sheet. To fail in the z-direction the work of adhesion to a surface must surpass the work of cohesion within the sheet.

To understand what is occurring during picking and peeling the work of cohesion values are compared with the work of adhesion values obtained experimentally by Ahrens et al (1). For a dried sample the work of cohesion is many times greater than the work of adhesion needed to remove a similar sheet from a surface. However, as the moisture content in the sample is increased the work of cohesion decreases very rapidly and the work of adhesion is slightly increased. In a very wet sheet (70% moisture

content) the work of cohesion value is only three times greater than the work of adhesion. Because the values calculated for the work of cohesion never become less then the work of adhesion the cause of peeling and picking of fibers from the surface has to be a localized phenomenon. This is most likely due to the fact that the work of cohesion and adhesion are both average values taken over a large area. While pressing and drying a wet sheet there is a good chance that the work of adhesion is greater than the work of cohesion at some location on the sheet allowing the fibers to be pulled from the surface.

The work of separation for all of the results is then used in Osterberg's equation 2.9 to determine the amount of straining occurring in all of the sheets. To perform this calculation the tension in the web must be found. The velocity measurements of the sheets are differentiated to determine the acceleration of the sheets as they are being pulled apart. This acceleration along with the splitting mass gives the tension force that is being applied to pull the sheet apart. A sample of the graph of tensile force versus time is shown below in Figure 6.3.

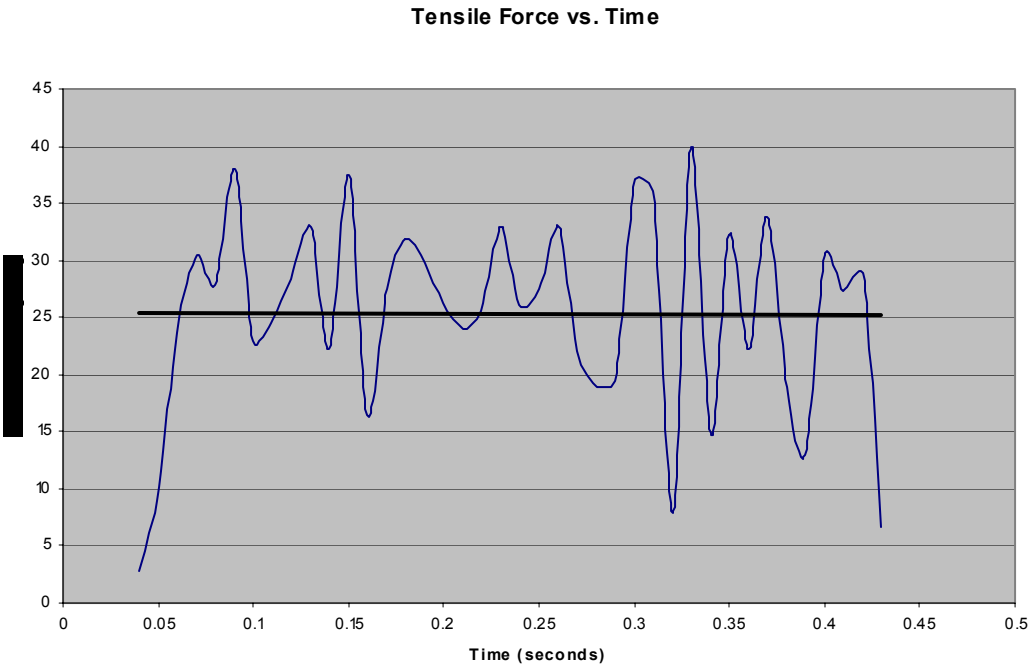

Figure 6.3 – Tensile Force per Unit Width versus Time.

Two things to be noted for the graph above, the first is that in determining the strain the data for approximately the first 0.07 seconds was discarded due to the fact that at this point in the experiment the sample is not being split and any energy going into the experiment is going solely into sheet strain and other terms that we are not as interested in. The second thing to note about the graph in Figure 6.3 is that the tension is not very uniform and jumps around a lot. This fluctuation in the tension is due to the surging in the velocity that occurs during the sheet splitting.

For every data point the tension and velocity are used to compute the strain. Osterberg's equation for work of separation is used to do this. This equation along with the equation used to solve for strain are shown below in equations 5.1 and 5.2.

$$W_s = (T - mV^2) - T\varepsilon \qquad \text{eqn. 5.1}$$

$$\varepsilon = \frac{W_s + mV^2 - T}{T} \qquad \text{eqn. 5.2}$$

The strains are graphed against the split distance for all of the samples. A sample of the resulting graphs is shown below in Figure 6.4 and all of the strain graphs are shown in Appendix B.

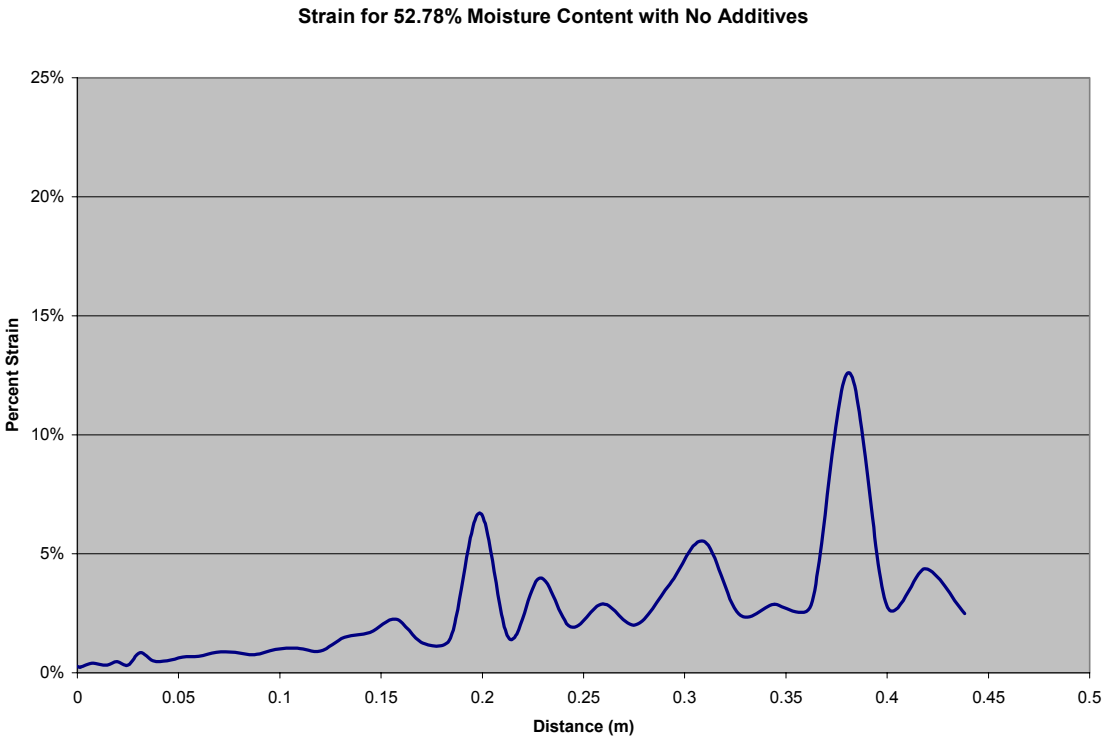

Figure 6.4 – Strain versus Distance graph for 52.78% Moisture Content.

At first glance the data recorded and obtained from Osterberg's equation seems quite feasible. However, when all of the results for varying moisture content sheets are looked at simultaneously, the trend seems to be backwards from what was predicted with the lower moisture content sheets experiencing greater strain than those with higher

moisture content. This trend can be seen if all of the strain versus distance graphs are laid on top of one another, shown in Figure 6.5 for the no additive case.

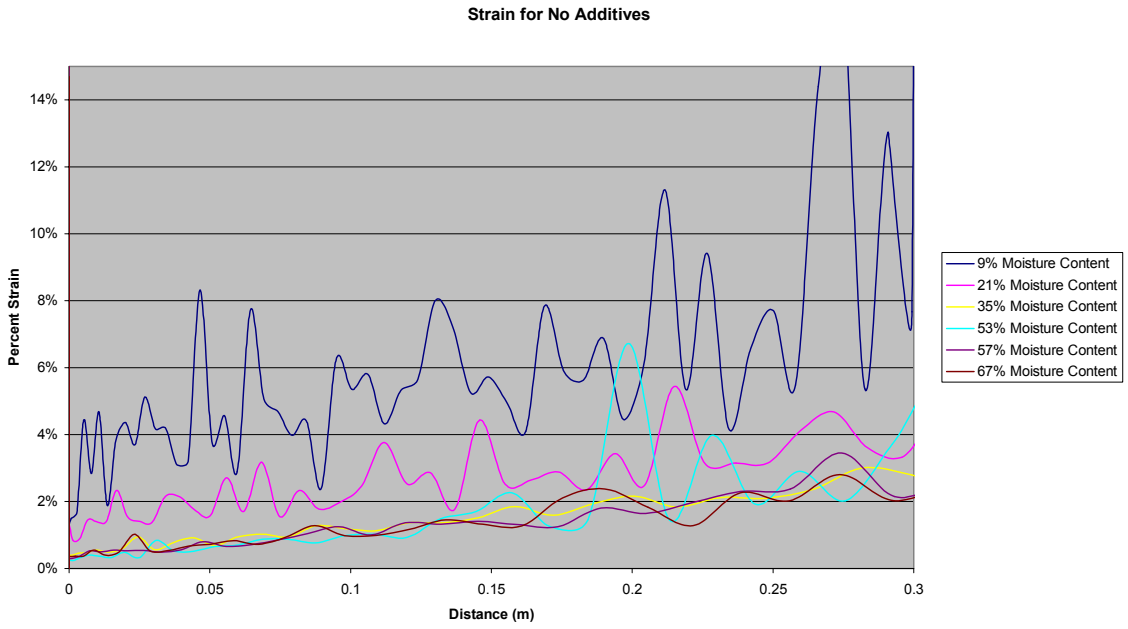

Figure 6.5 – Percent Strain versus Distance for No Additives.

It is thought that the computed strains of the higher moisture content sheets are fairly close to the actual values. However, as the sheets begin to dry out some other factor not included in the work of separation is affecting the computed strain results. This additional factor is thought to be the energy that is used in bending the sheets. The form of Osterberg's equation that was used to determine the strain of the sheet does not take into account the bending. However, the work of separation value that was determined experimentally and plugged into the equation does have the bending stress included. Although it was not done, these percent strain results could be used to estimate a value for the amount of energy that went into the bending of the sheets.

In addition to measuring the velocity of splitting, the calipers of all the split ends were recorded. This information reveals an interesting look at how cracks propagate through the sheet during splitting. Graphs showing the cross section thickness for each sample were created. An example of these graphs is shown below in Figure 6.6, all of the other graphs created from this data are contained in Appendix C.

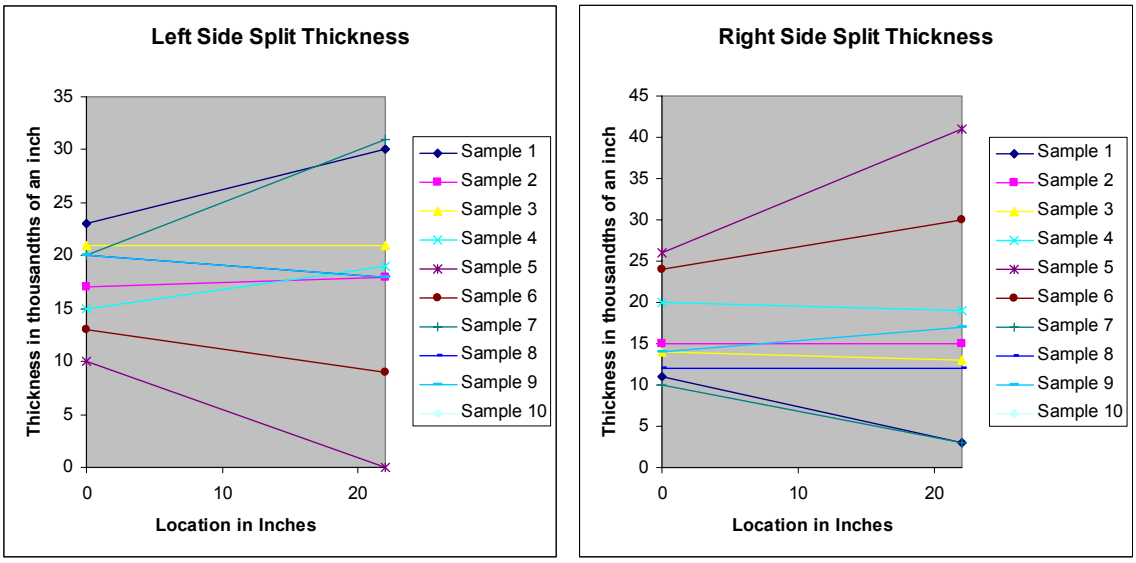

Figure 6.6 – Thickness of Sheet Versus Split Location for 53% Moisture Content Sheet with No Additives.

Using the graphs shown above and in Appendix C an average thickness was calculated for all four split locations (Top Right, Top Left, Bottom Right, Bottom Left). Using these average thicknesses along with the actual results allowed for an average stray term to be calculated. This average stray term is an absolute value number that reflects on the ability of the sheet to split down its center. For example, a stray term of zero would mean that the sheet stayed completely centered during the split whereas a stray term of

five would mean that on average the sheet would stray either positive or negative five-thousandths of an inch while being split. Because all of the tests were conducted with the forming screen side of the sheet oriented in the same direction the affect on the direction of stray was investigated but the results did not suggest the sheet orientation affected the stray direction. The calculated stray terms are then graphed against the moisture contents of the sheets to produce Figure 6.7.

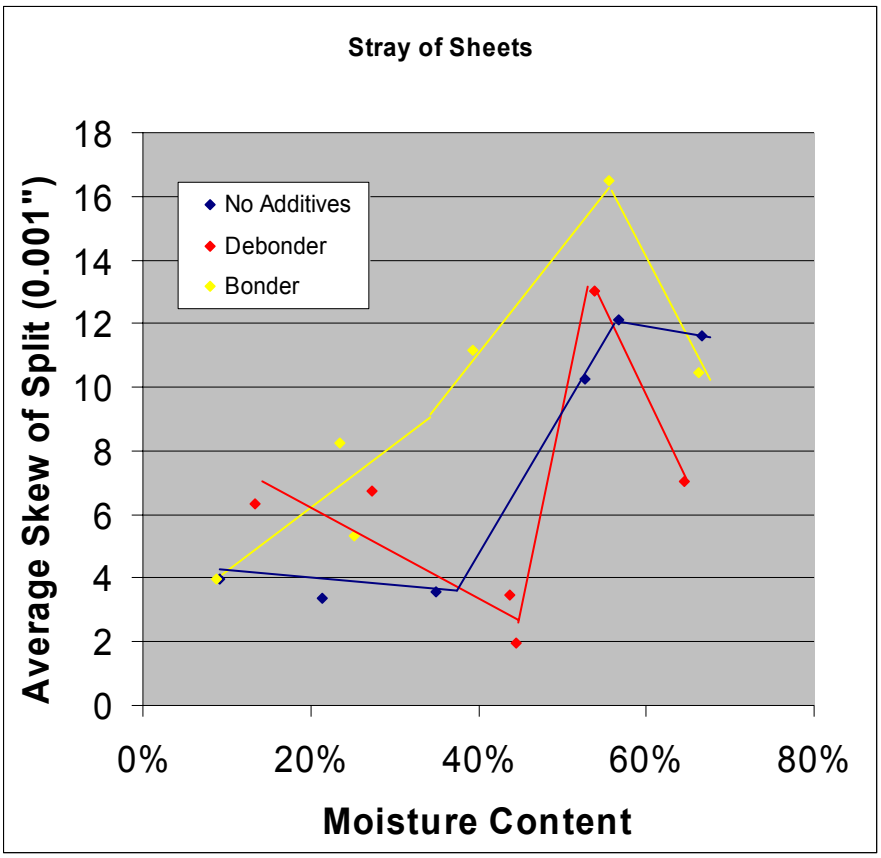

Figure 6.7 – Average Skew of Split versus the Moisture Content. (trend lines are freehanded and represent the general tendency of the graph)

This graph shows a couple of interesting features that need to be further explained. The first feature is the overall general shape of the three curves. As the

moisture content of the sheet decreases the amount of skew within the split also decreases regardless of the sheet additive. In all three cases at approximately 50% moisture content the skew of the split sheet begins to decrease rapidly. Interestingly enough, this is also the same location on the moisture content scale where bonding begins to increase rapidly. Thus it is fair to say that with an increase in bonding the amount of skew in a split will decrease. However, the results also suggest that the addition of the bonding agent increases the amount of skew within the sheet.

It is thought that the results in the graph above are created through the interaction of the papers internal geometries with the bonding present within the sheet. Inside the paper sheet are many fibers crossing over one another that mainly exist in the MD-CD plane, see Figure 6.8.

Figure 6.8 – Magnified Paper Corner. (2)

Because most of the fibers are in the MD-CD plane, most of the fibers they are touching are also in that plane. It is for this simple reason that as the amount of bonding

within a sheet is increased the strength of each parallel MD-CD plane is also increased. Because of this increase in the planer strength it is much more difficult for a split to propagate in the z-direction. This difficulty of propagating in the z-direction directly minimizes the amount of stray within the split.

To account for the increased stray with the bonder additive the bonder also needs to be looked at close up. The bonder under a microscope looks like very small fibers. These small fibers are dispersed everywhere within the sheet including between the MD-CD layers created during shear formation. These small fibers increase the number of bonds connecting the parallel MD-CD layers which in turn allows the load created by a split to transfer from one MD-CD layer to another much easier. This ease of the split to travel from one MD-CD plane to the next results in a greater stray within the sheet.

At about 60% moisture content the effect of the bonding begins to dominate the graph in Figure 6.7. This is approximately the point where the surface tension has reached a maximum and air filled voids appear within the sheet. It can be seen in the Figure 6.2 that this point occurs a little earlier when the surface tension is decreased in the debonder case and a little later when the fines in the bonder case are able to allow the sheet to reach a maximum surface tension at a drier state.

An interesting phenomenon that is also seen in Figure 6.9 is the definite decrease of the amount of skew in sheets where no bonding has started to occur. This is mainly due to the planer MD-CD fiber orientation that was created during sheet formation.

Tensile Test Results

A section from each sheet was reserved for tensile tests. Six different moisture contents were tested for each of the three sheet additives. At each moisture content four tensile tests were conducted, two wet and two dry, giving a total of 24 tensile tests for each sheet additive. Three values are obtained directly from the tensile tests, the maximum tensile load, percent strain at maximum load and the modulus of elasticity of the stress strain curves. The maximum tensile load (per unit width) versus moisture content for all three of the additives is shown below in Figure 6.9.

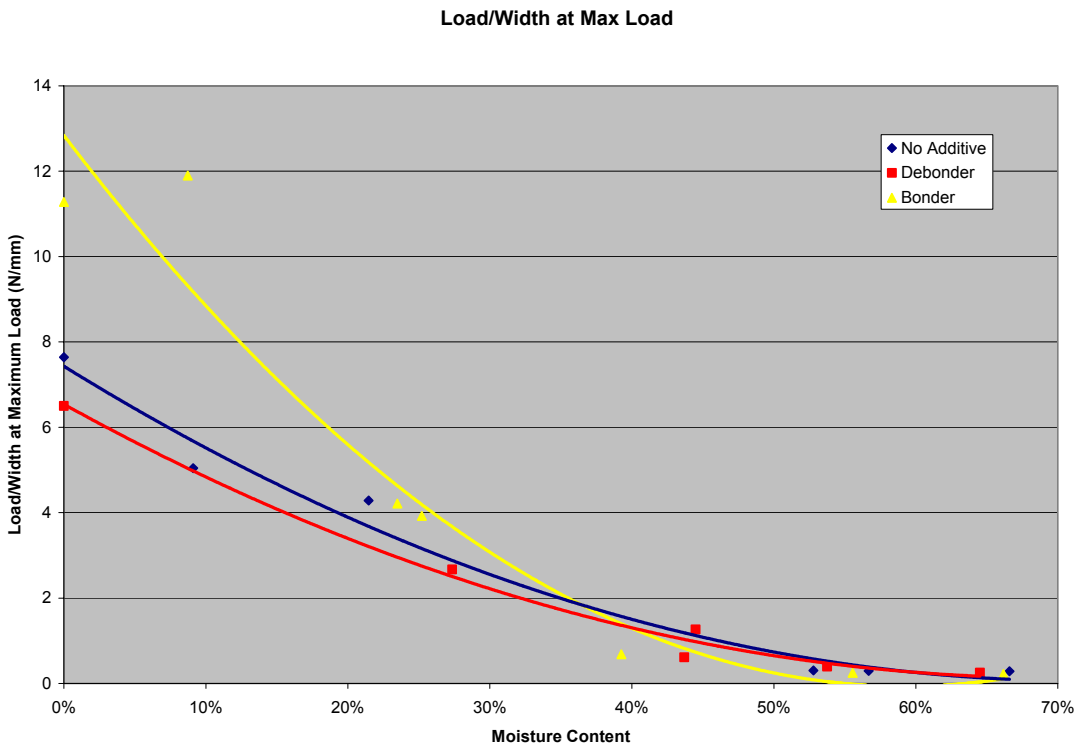

Figure 6.9 - Maximum Load per Unit Width versus Moisture Content for Tensile Samples.

This graph supports the results seen in Figure 6.2 that show that the bonder actually decreases the overall strength of the sheet at high moisture contents. The addition of the bonder adds strength to the sheet only when the moisture content is low enough for bonding to start to occur within the sheet.

The graph of the percent strain versus moisture content for all of the sample additives is shown below in Figure 6.10.

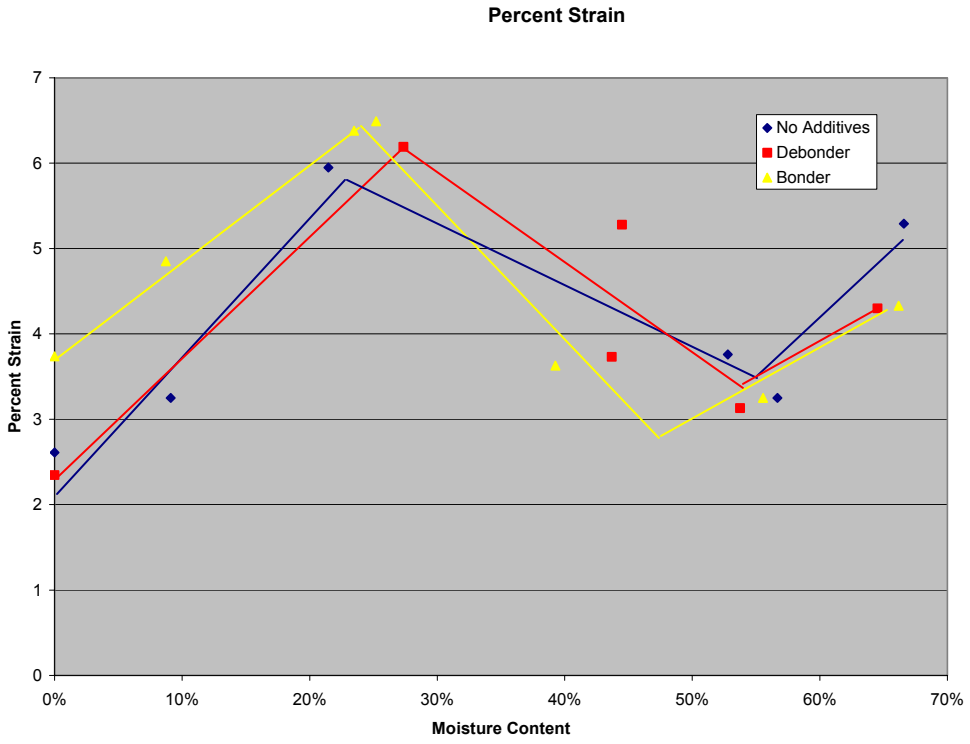

Figure 6.10 – Percent Strain Versus Moisture Content. (trend lines are freehanded and represent the general tendency of the graph)

The percent strains of the samples seem to behave inversely to the skew of the samples. The theory describing the straining of the fibers is shown below in Figure 6.11 and 6.12. The first figure shows a sample of fibers within the sheet at varying moisture contents. The second figure shows a theoretical division of the total stiffness into that from bonding and that from surface tension. At 100% to 80% moisture content no fibers have started to bond and the amount of fiber entanglement is low because of the large quantity of free inter fiber water within sheet. As the moisture content decreases to the 70% to 60% range the inter fiber free water has been eliminated and the fiber entanglement is near its greatest value because of the increased surface tension. Fiber bonding then begins to take place randomly within the sheet as the moisture content goes from 60% to 30%. The air intrusion into the sheet rapidly decreases the amount of surface tension present in the sheet. As the moisture content approaches the 30% to 0% value bonding increases in the sheet and reaches a point where the randomly distributed bonds account for all of the stiffness of the sample. At this point within the sheet

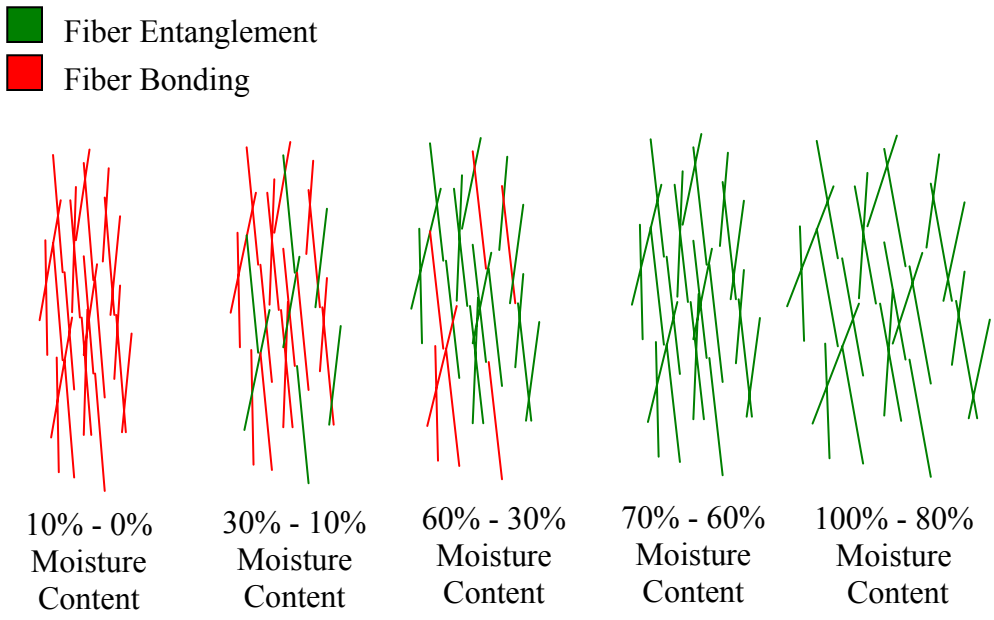

Figure 6.11 – Theory of Straining as a Function of Moisture Content.

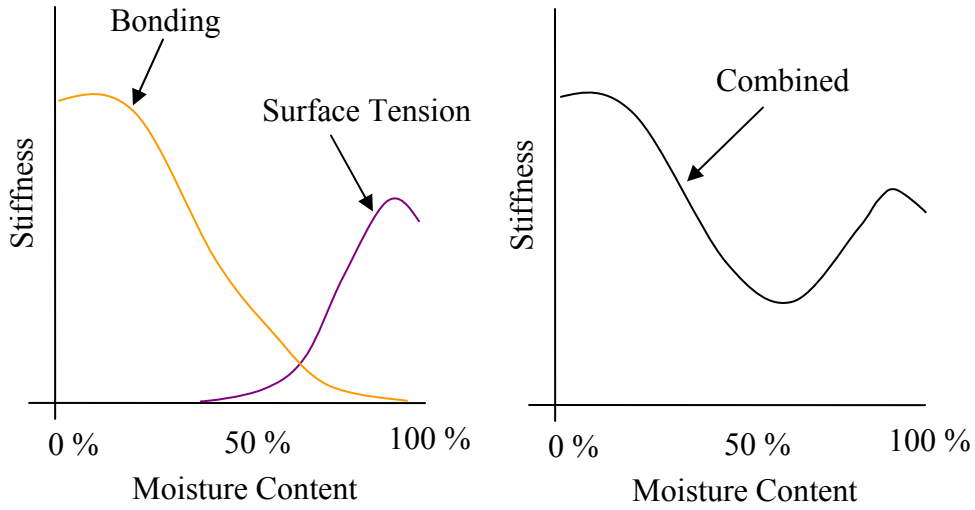

Figure 6.12 - Theory of Straining as a Function of Moisture Content.

As can be seen in Figure 6.12 the stiffness of the sheet, which is inversely related to the strain of the sheet, is a combination of the bonding related stiffness and the surface tension related stiffness.

The graph of the modulus of elasticity versus moisture content for all sample additives is shown below in Figure 6.13.

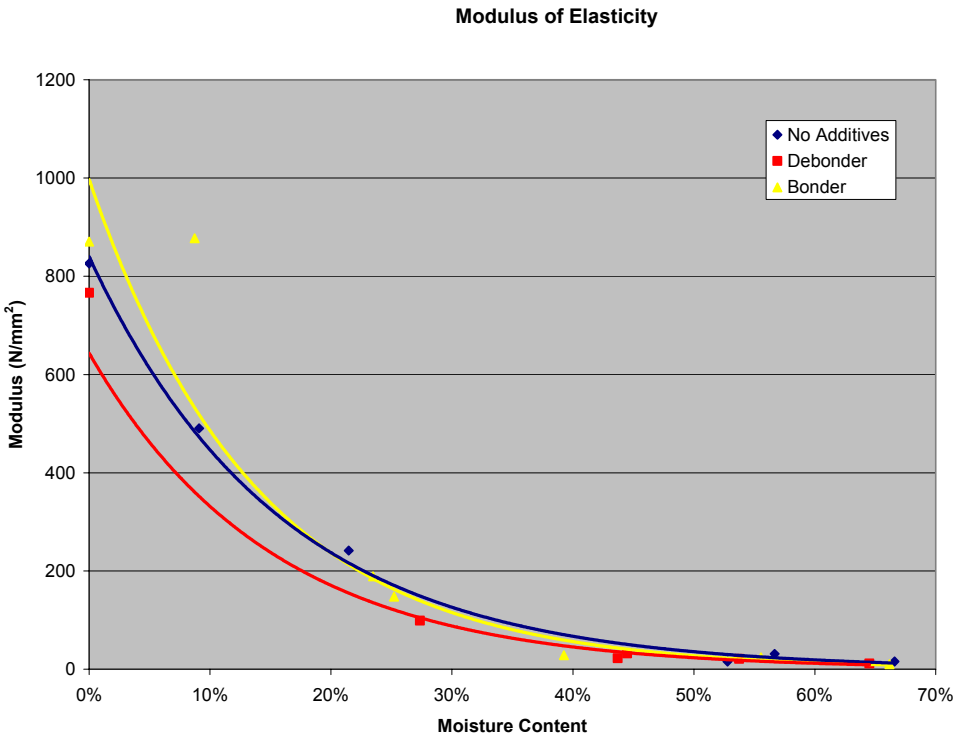

Figure 6.13 – Modulus of Elasticity Versus Moisture Content.

The results from this graph are as predicted and were used in the development of the finite element program to determine the stiffness values of the three-parameter solid.

In addition to the results shown in the figures above graphs of average load versus displacements were developed for all of the test samples. A sample of an average load versus displacement graph for 30% moisture content is shown below in Figure 6.14. All of the other average load versus displacement graphs are shown in Appendix D.

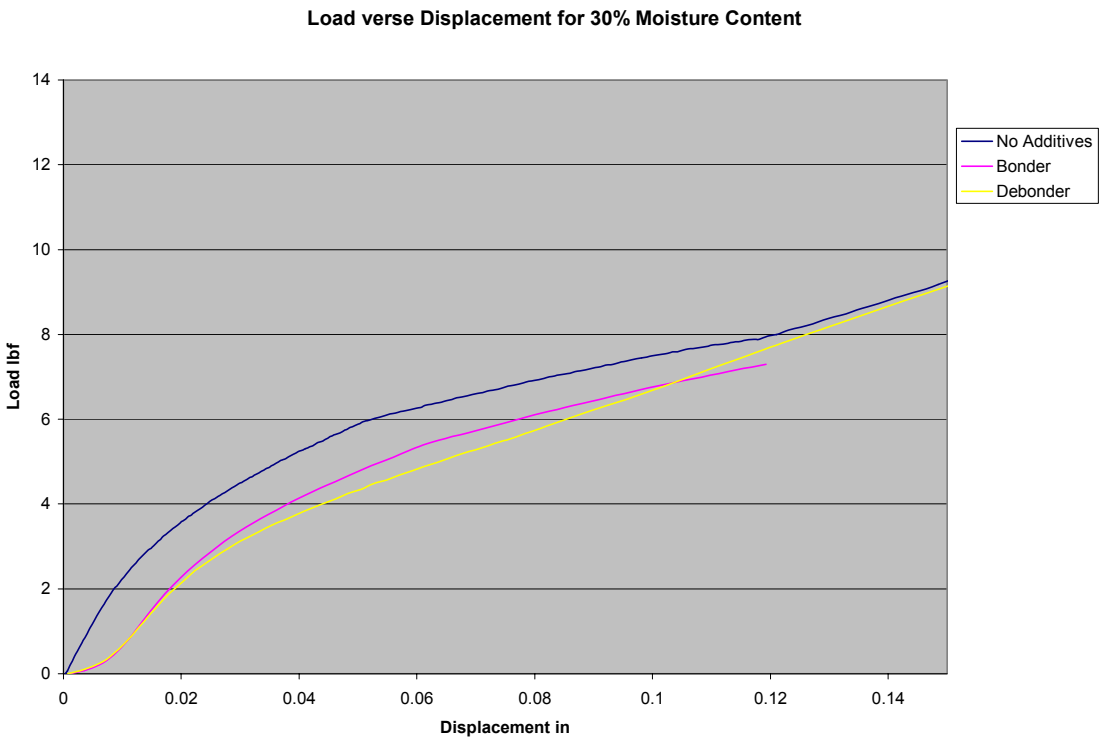

Figure 6.14 – Load Versus Displacement Graph for 30% Moisture Content.

Z-Direction Test Results

Z-direction tests are conducted using a completely dried sheet that has been dried on a steam drum dryer. At each moisture level two z-direction tests are conducted, giving a total of 24 z-direction tests for each sheet additive. The results from this test can be loosely correlated to the data obtained in the paper splitting experiment. Two sections from each sample are tested and the results for all of the samples are shown below in Figure 6.15.

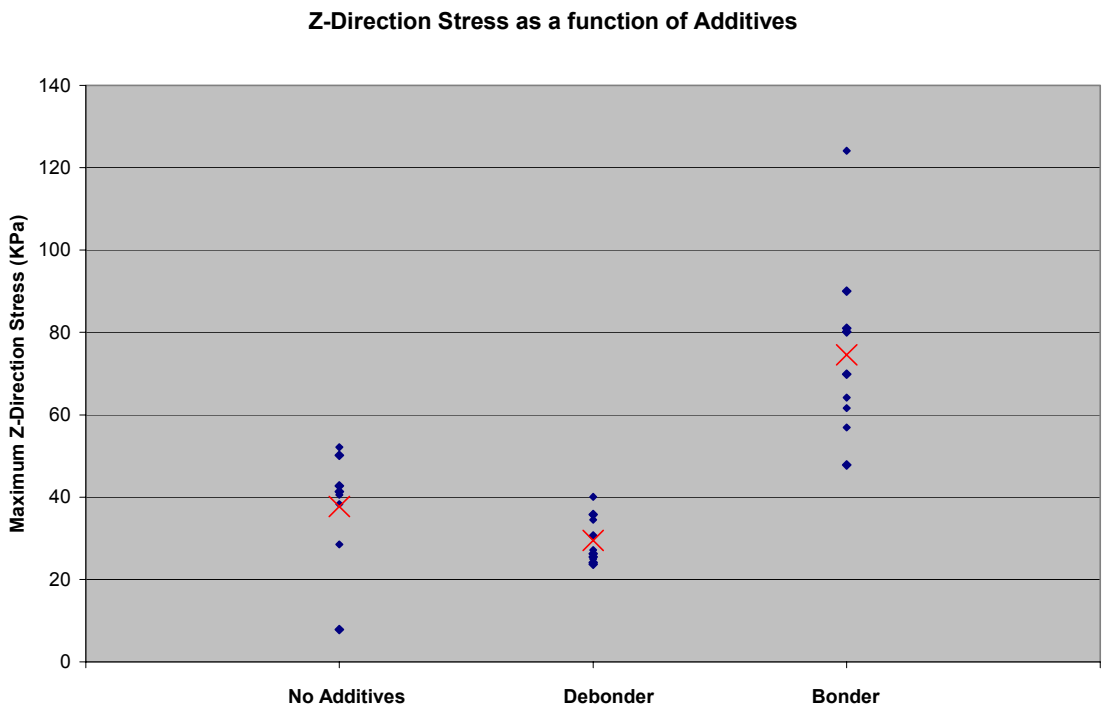

Figure 6.15 – Z-Direction Stress as a Function of Sheet Additives.

Not a tremendous amount can be determined from the graph other than the fact that the bonder increased the strength of the samples more than the debonder decreased the strength. This supports the experimental results of the splitting apparatus shown in Figure 6.2 that showed little change of the energy required to split per meter with the addition of debonder as compared to the addition of bonder.

Finite Element Results

The first test that was run using the paper splitting program was to model the tensile tester and determine the appropriate spring and damper constants that would be needed to simulate the paper sample. To model the tensile tester all of the top nodes in

the matrix were driven upwards at the constant rate used by the tensile tester (1 in/min) and all of the bottom nodes were held stationary. An average of the vertical loads across the top of the sample was taken and was graphed against their displacement. This graph was then overlaid on top of the experimentally determined load versus displacement graph produced from the actual tensile test. The values of the springs and dampers were then changed and the program was run again. After multiple iterations the following spring and damping constants were determined for the three-parameter solid.

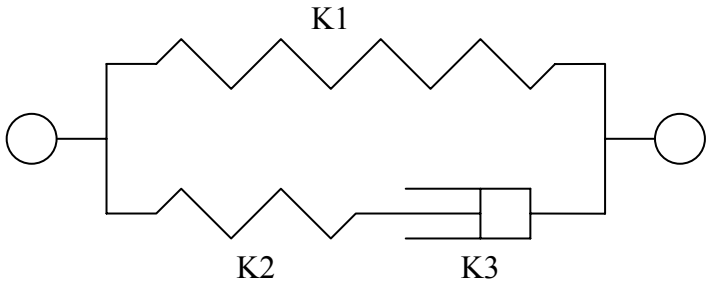

K1 = 25000 N/m Spring Constant

K2 = 400000 N/m Damping Spring Constant

K3 = 210000 N/m/s Damping Constant

Figure 6.16 – Computed Spring Constants for Three-Parameter Solid.

The graph of load versus displacement for both the experimental and theoretical sheets using the determined spring constants are shown below in Figure 6.17.

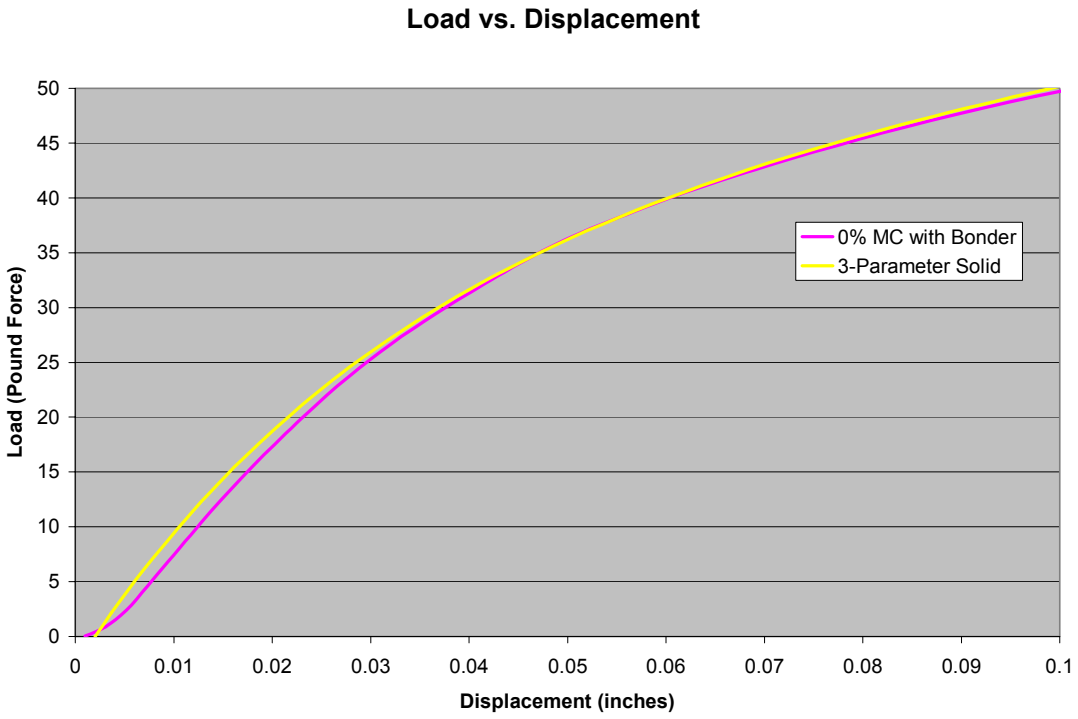

Figure 6.17 – Load versus Displacement for Experimental and Theoretical Data.

Unfortunately when these spring constants were used in the program running in the splitting mode the results were highly unstable. This was due to a combination of the fact that Newton's iteration method was used and the high stiffness of the paper. To increase the stability of the system and results the time step had to be optimized. The optimized time step was very small and allowed the program to run but could not complete (or even begin) a split in the paper. To correct this problem a more accurate system for solving differential equations needs to be used instead of Newton's iteration method. Future programs also need to be better optimized to handle more calculations using matrices to reduce the required number of computations.

CHAPTER 7 - CONCLUSION

The internal strength of a sheet of paper is known to be a combination of three different properties: the amount of interfiber bonding, the amount of surface tension as a result of fiber entanglement, and the individual fiber strength. In a wet sheet overall bonding is reduced and fiber strength is not necessarily the controlling factor. Because of this knowledge, three experiments isolating the bonding mechanism and measuring the bonding energy of a sheet were conducted using a paper splitting apparatus. The first experiment was performed using control sheets that were manufactured with no additives and the second and third were performed using sheets that had either a bonding or debonding agent added during sheet formation. All three of these experiments were conducted at the full range of moisture contents that would be seen during paper manufacturing.

The results from these tests show that the effect of bonding on the internal strength in the sheet begins to dominate at 50% moisture content. As anticipated this increase in internal strength is much greater in the bonder case than either the no additive or the debonder case. In the case of the debonder additive the sheet strength at moisture contents above 40% is counter intuitively greater than both the bonder and no additives. Perhaps the most interesting of the results obtained was the amount of stray in the sheet splits and the percent strain of the wet tensile tests. The results from the stray in the splits test show that the addition of the bonder additive greatly increases the amount of stray in a sheet split. The results also show that the greatest stray in the splits regardless of the

additive occurs around 55% moisture content. The percent strain results of the wet tensile tests are inversely related to the stray in the splits with the least amount of strain occurring at 55% moisture content. Also of interest is the fact that the percent strain of all of the samples is greatest at the 25% moisture content level.

All of these results can be directly related to the paper production process. The percent strain results indicate that the greatest straining of the sheet does not occur early in production during periods of high moisture content but rather later when a large majority of the bonding in the sheet has already occurred. The stay of splits along with the overall sheet strength can be directly related to the picking and peeling of fibers during pressing and drying. Any picking or peeling that begins on a press or drying roll has a greater possibility to be larger if a bonder additive is added to the sheet during formation. This potential increase in size is due to the higher amount of stray that occurs in sheets with the bonder additive.

The internal strength mechanisms present within a sheet of paper were investigated throughout a high range of moisture contents. Traditional tests such as tensile and z-direction strength were conducted on the samples. In addition to the traditional tests, results were also obtained using a paper splitting apparatus designed and constructed specifically for measuring internal sheet bonding. The paper splitting apparatus that was designed and constructed for this thesis can measure the internal bond strength of a sheet with a high degree of repeatability and has helped develop a better

understanding of the cohesive and tensile properties of wet paper and how these properties change throughout the paper making process.

CHAPTER 8 – RECOMMENDATIONS FOR FUTURE WORK

The results obtained using the paper splitting apparatus seem to be accurate and repeatable, but there are some downfalls to testing using the splitting apparatus. One disadvantage of the system the maximum length that can be tested is two feet. This length is limited due to the spacing of the rotation sensors and the veering within the sample sheet. In an effort to maintain a centered split, which would be critical for any long length splitting machine, a sheet could be produced with multiple thin monofilament strands in the MD direction and centered in the thickness. This type of sheet would be very difficult to produce on a Formatte machine but could be made on a small Fourdrinier type machine. A Fourdrinier machine with a split head-box to allow for the monofilament spool and tension regulator is shown below in Figure 8.1.

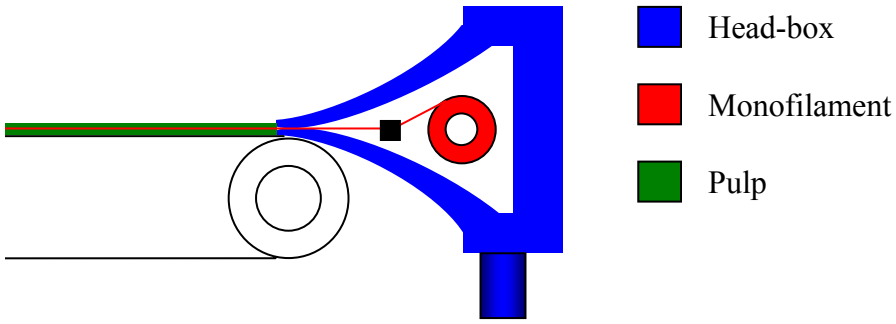

Figure 8.1 - A Fourdrinier Machine with a Split Head-box.

The main advantage of a sheet fabricated with monofilaments is that the split location in the z-direction can be controlled to allow for longer splits to take place. A

device that could be constructed using drums to split the sheet would allow samples to be split over a longer length. Such a device would allow an almost unlimited length of sample to be split leading to more accurate results due to averaging.

With the addition of a microprocessor the amount of energy needed to split the sample could be calculated real time or averaged for a particular sample. A diagram for such a device is shown below in Figure 8.2.

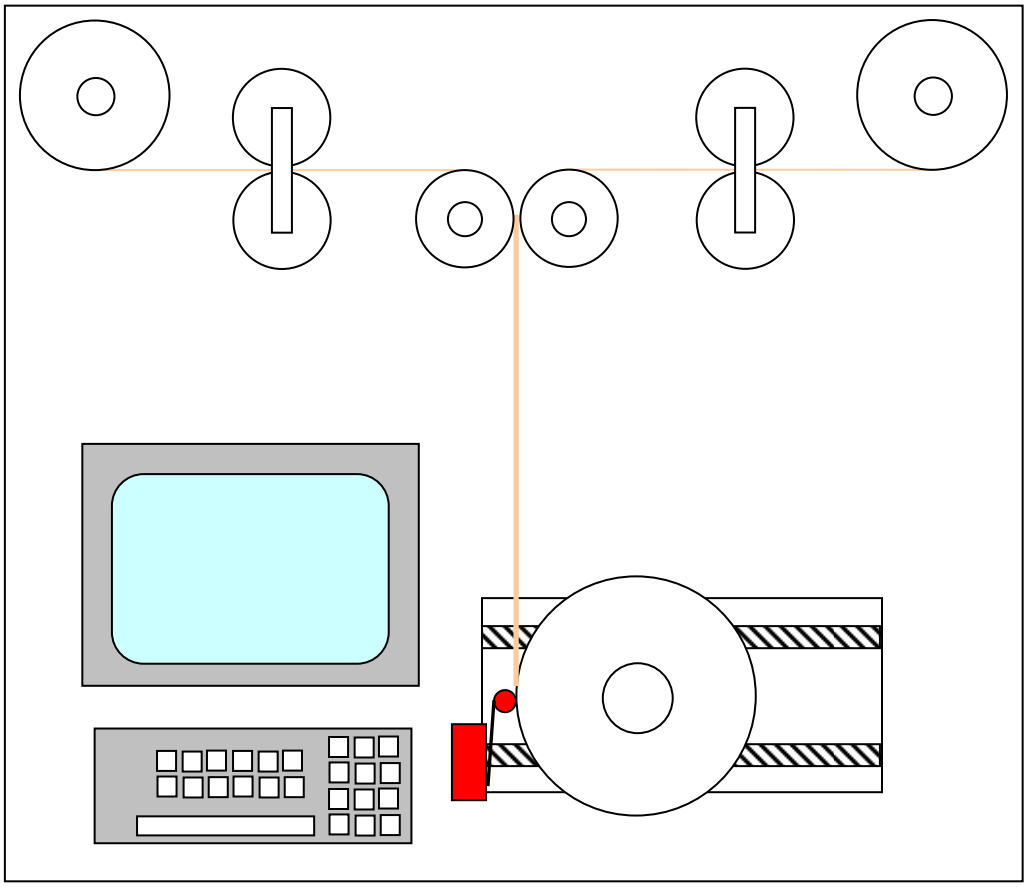

Figure 8.2 - New Design for Paper Splitting Apparatus.

In this apparatus the paper would be loaded on the roll located at the bottom of the figure. This roll has the ability to translate in the x-direction to allow a given peel angle to be maintained throughout the test. The two rolls located in the center of the device would be used to define the peel radius of the sheet. These rolls could be interchanged with others of a different diameter. Located on both sides of the radius of peel rolls would be the driving rolls. The driving rolls would be directly attached to stepper motors and would have the ability to monitor both torque and rotation rate. This arrangement along with the microprocessor would allow the sheet to be split at a constant torque, velocity or any other programmed velocity and torque scheme. Finally, the split sheet would be taken up on two rolls on either side of the apparatus. All of the rolls on the device would be driven at a velocity that would be a function of the measured rotation rate of the driving rolls. This would be done in an attempt to limit the amount of energy going into the inertial properties of the system.

APPENDIX A: PAPER SPLITTING RESULTS

Paper Splitting Results without Additives

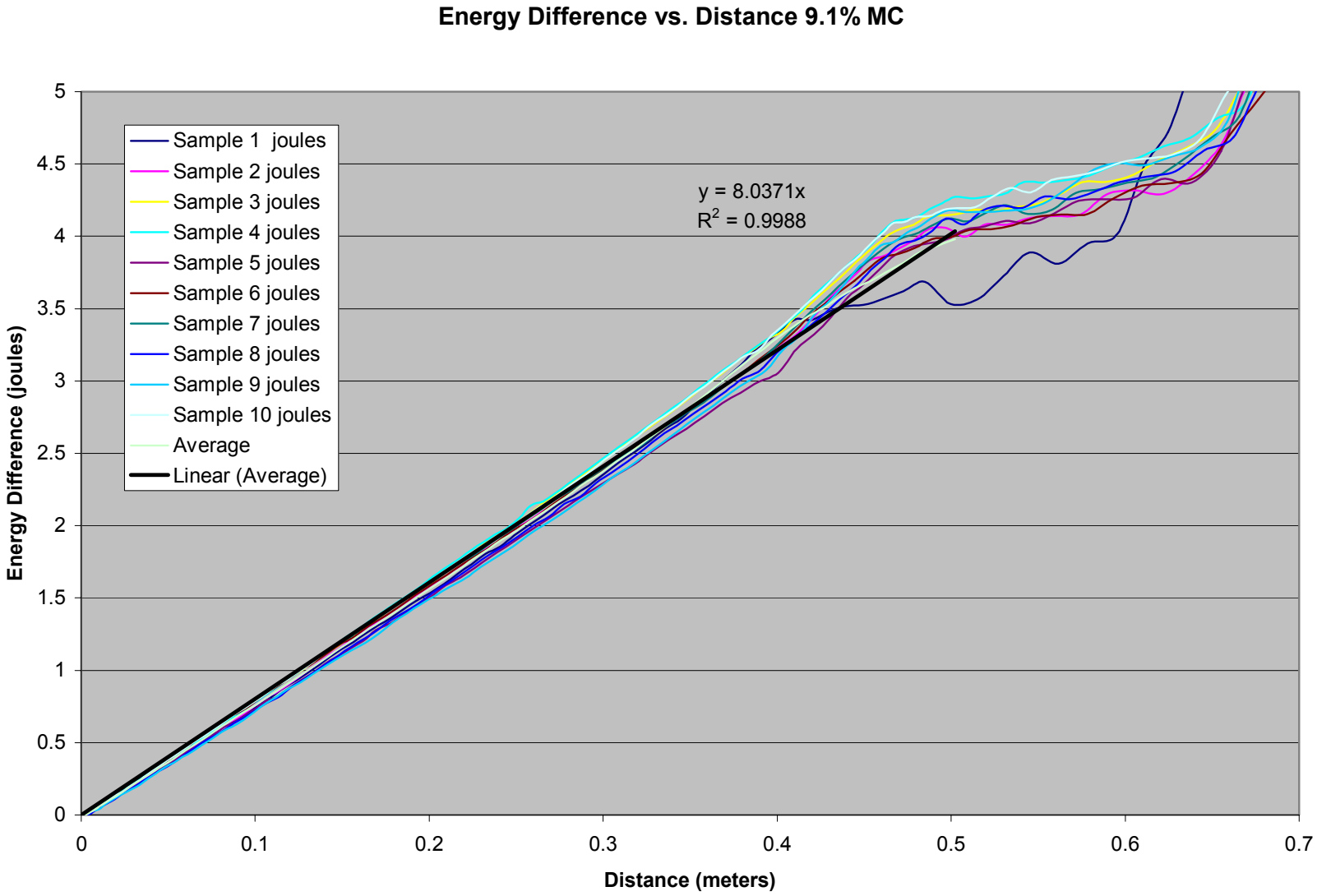
Energy Difference vs. Distance 9.1% MC
Energy Difference (joules)
Distance (meters)
y = 8.0371x
R2 = 0.9988
Sample 1 joules
Sample 2 joules
Sample 3 joules
Sample 4 joules
Sample 5 joules
Sample 6 joules
Sample 7 joules
Sample 8 joules
Sample 9 joules
Sample 10 joules
Average
Linear (Average)
0
0.5
1
1.5
2
2.5
3
3.5
4
4.5
5
0
0.1
0.2
0.3
0.4
0.5
0.6
0.7

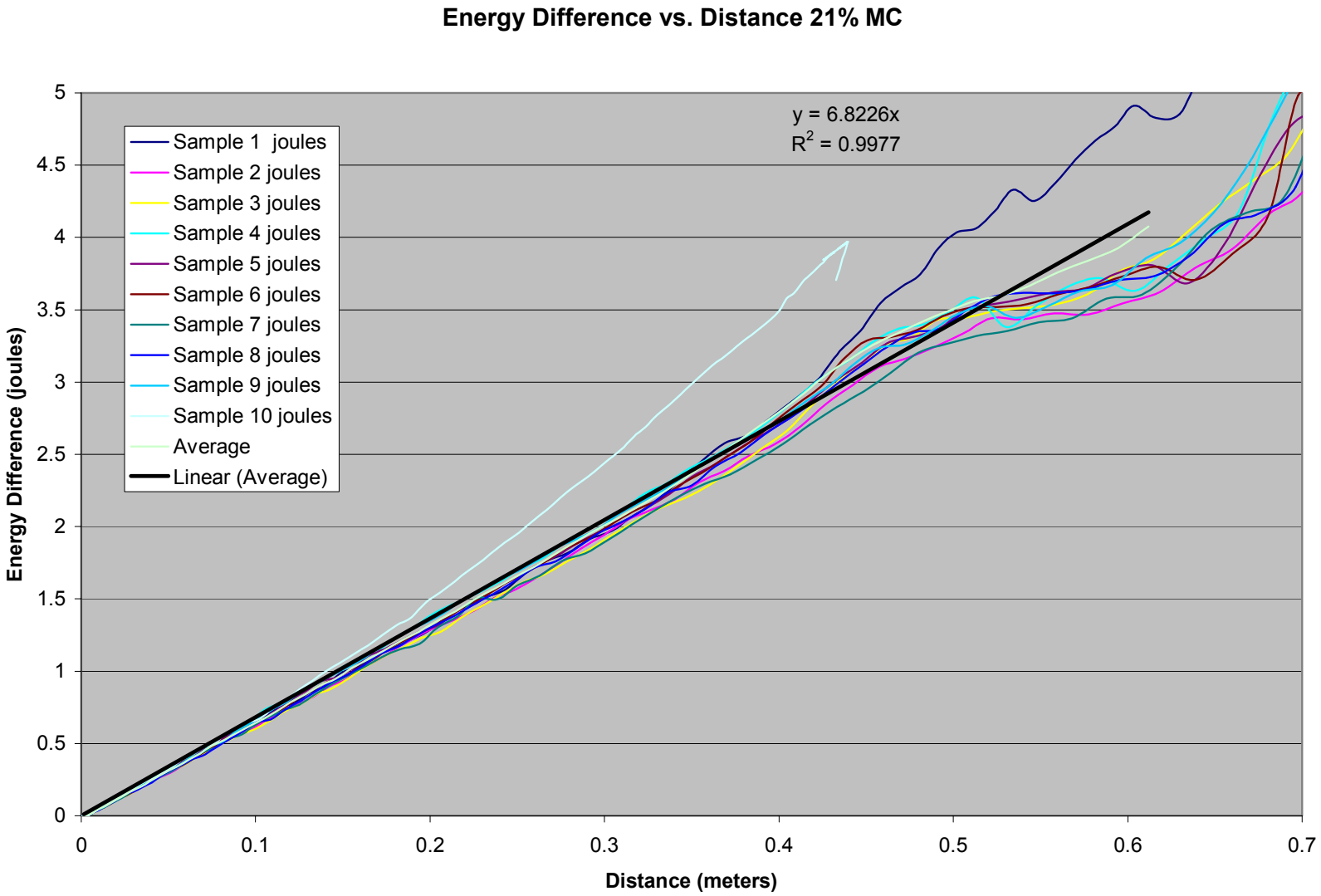
Energy Difference vs. Distance 21% MC
y = 6.8226x
R2 = 0.9977
Sample 1 joules
Sample 2 joules
Sample 3 joules
Sample 4 joules
Sample 5 joules
Sample 6 joules
Sample 7 joules
Sample 8 joules
Sample 9 joules
Sample 10 joules
Average
Linear (Average)
Energy Difference (joules)
Distance (meters)
0
0.5
1
1.5
2
2.5
3
3.5
4
4.5
5
0
0.1
0.2
0.3
0.4
0.5
0.6
0.7

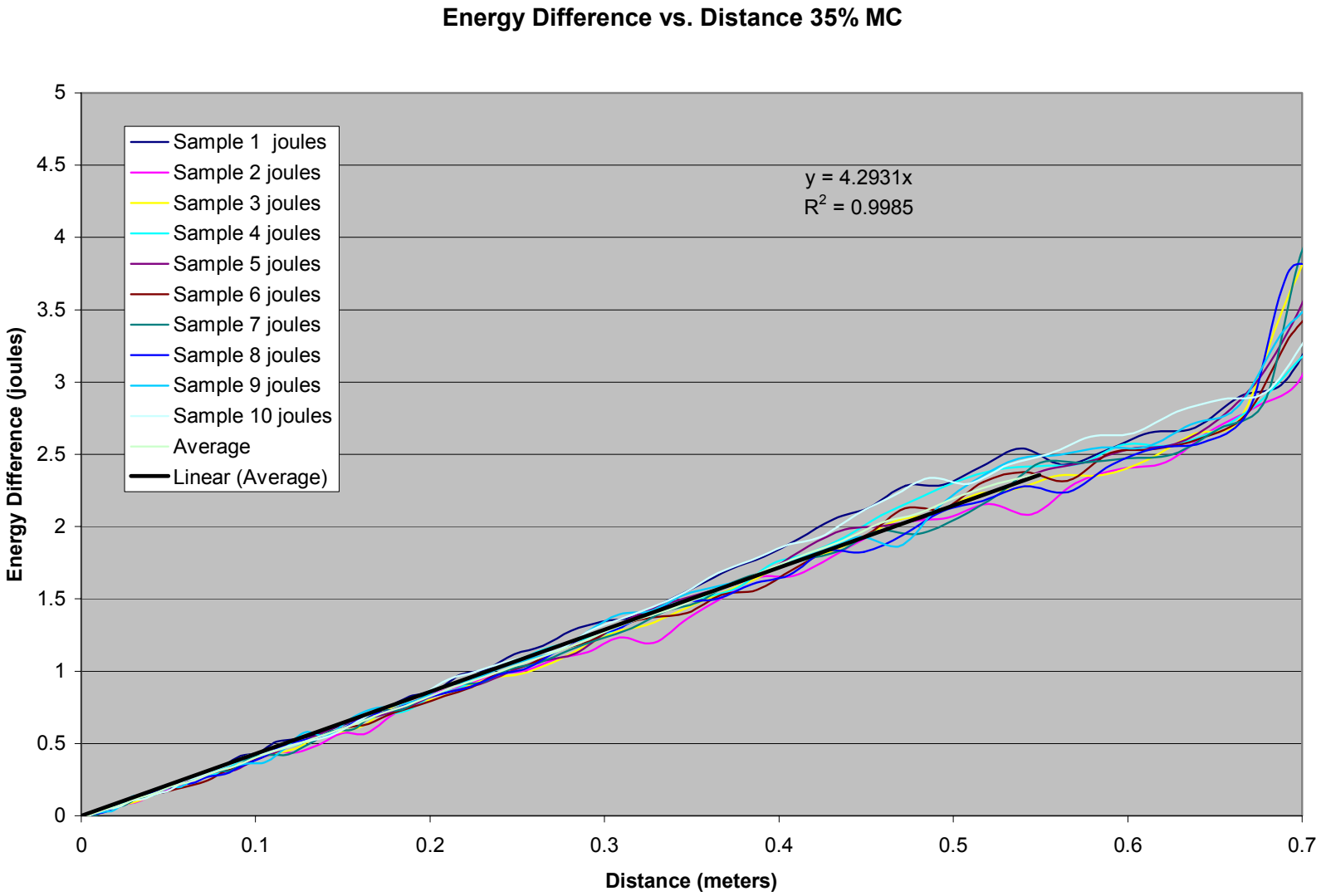
Energy Difference vs. Distance 35% MC
Energy Difference (joules)
Distance (meters)
y = 4.2931x
R2 = 0.9985
Sample 1 joules
Sample 2 joules
Sample 3 joules
Sample 4 joules
Sample 5 joules
Sample 6 joules
Sample 7 joules
Sample 8 joules
Sample 9 joules
Sample 10 joules
Average
Linear (Average)
0
0.5
1
1.5
2
2.5
3
3.5
4
4.5
5
0
0.1
0.2
0.3
0.4
0.5
0.6
0.7

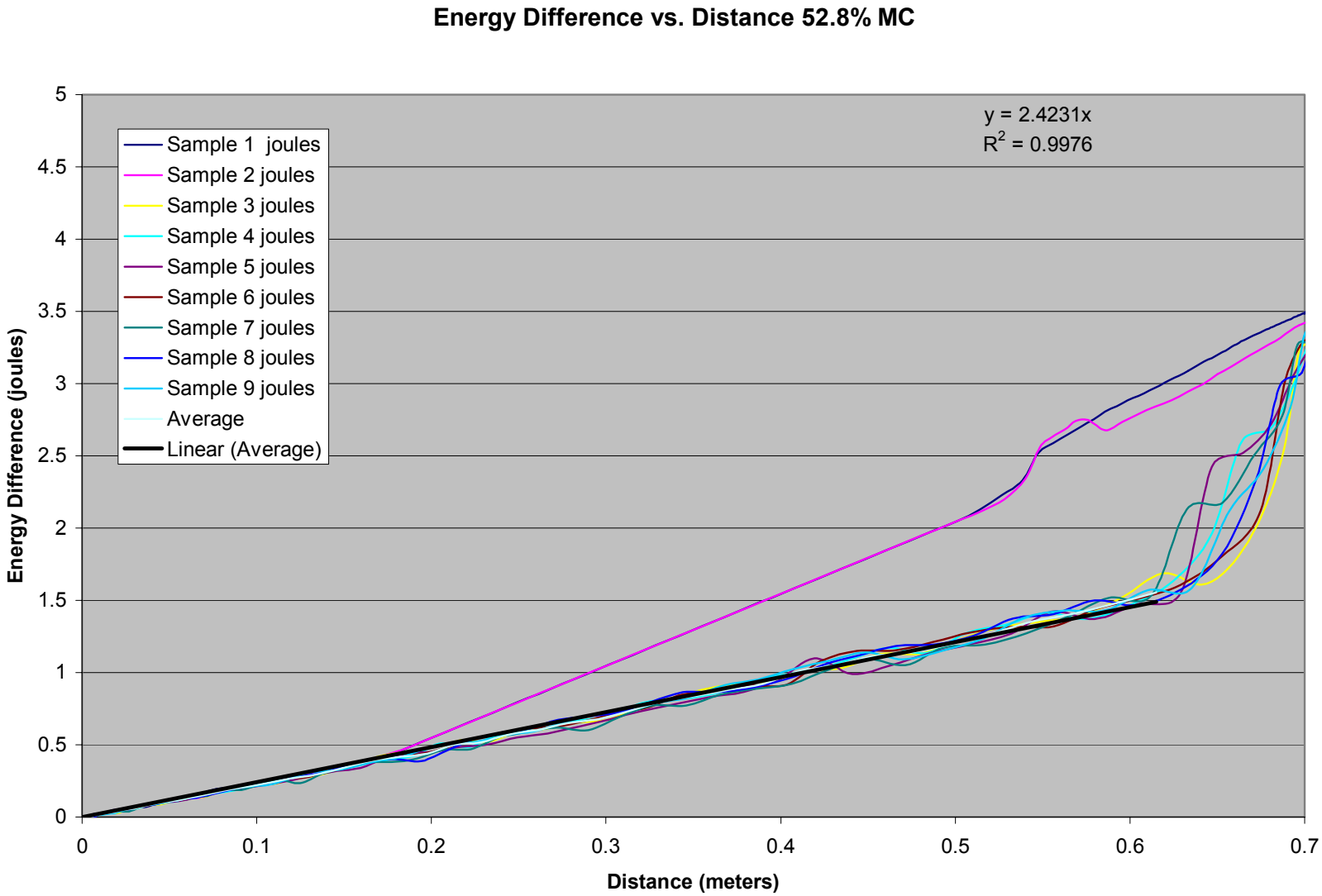
Energy Difference vs. Distance 52.8% MC
y = 2.4231x
R2 = 0.9976
Sample 1 joules
Sample 2 joules
Sample 3 joules
Sample 4 joules
Sample 5 joules
Sample 6 joules
Sample 7 joules
Sample 8 joules
Sample 9 joules
Average
Linear (Average)
Energy Difference (joules)
Distance (meters)
0
0.5
1
1.5
2
2.5
3
3.5
4
4.5
5
0
0.1
0.2
0.3
0.4
0.5
0.6
0.7

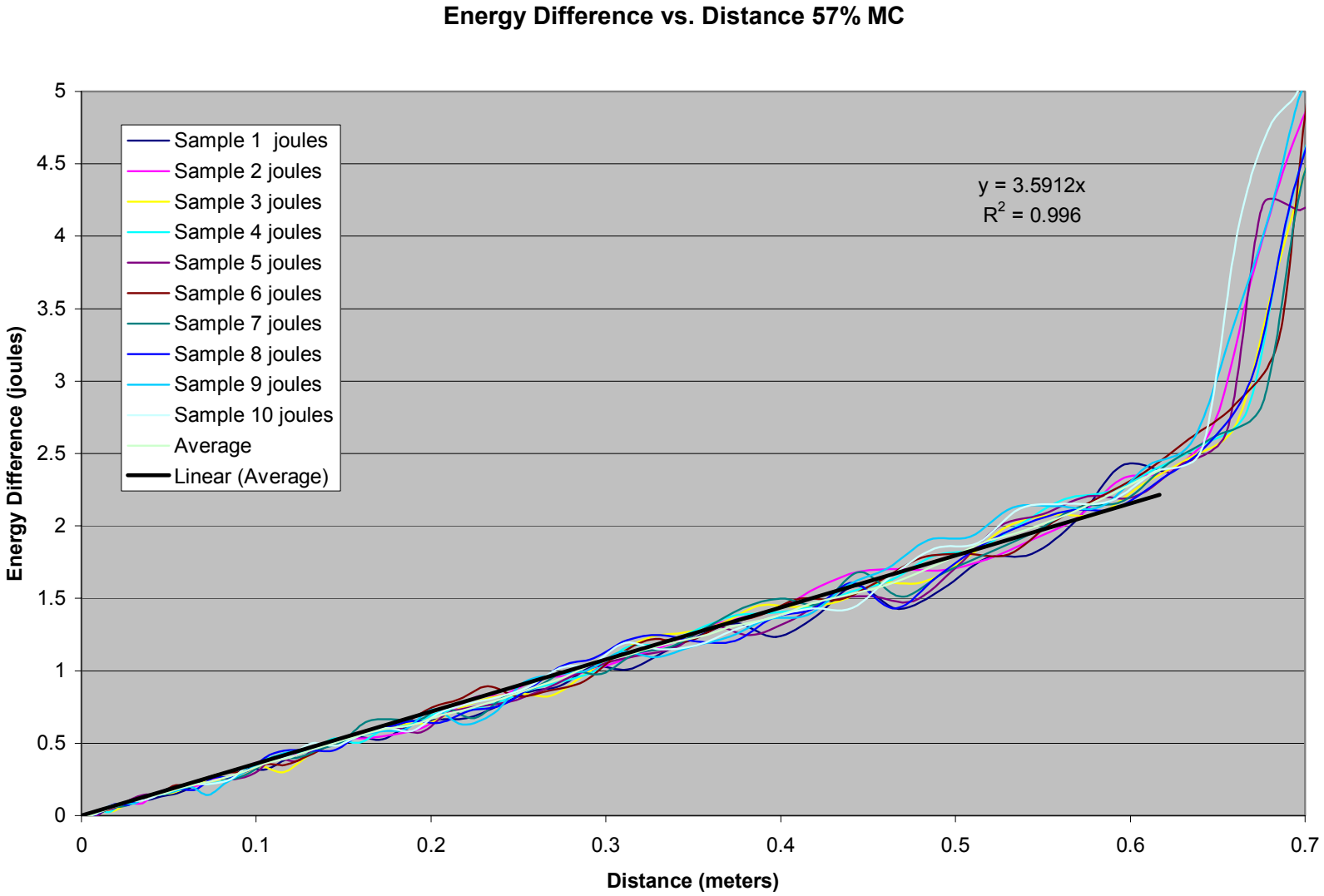
Energy Difference vs. Distance 57% MC
Energy Difference (joules)
Distance (meters)
Sample 1 joules
Sample 2 joules
Sample 3 joules
Sample 4 joules
Sample 5 joules
Sample 6 joules
Sample 7 joules
Sample 8 joules
Sample 9 joules
Sample 10 joules
Average
Linear (Average)
y = 3.5912x
R2 = 0.996
0
0.5
1
1.5
2
2.5
3
3.5
4
4.5
5
0
0.1
0.2
0.3
0.4
0.5
0.6
0.7

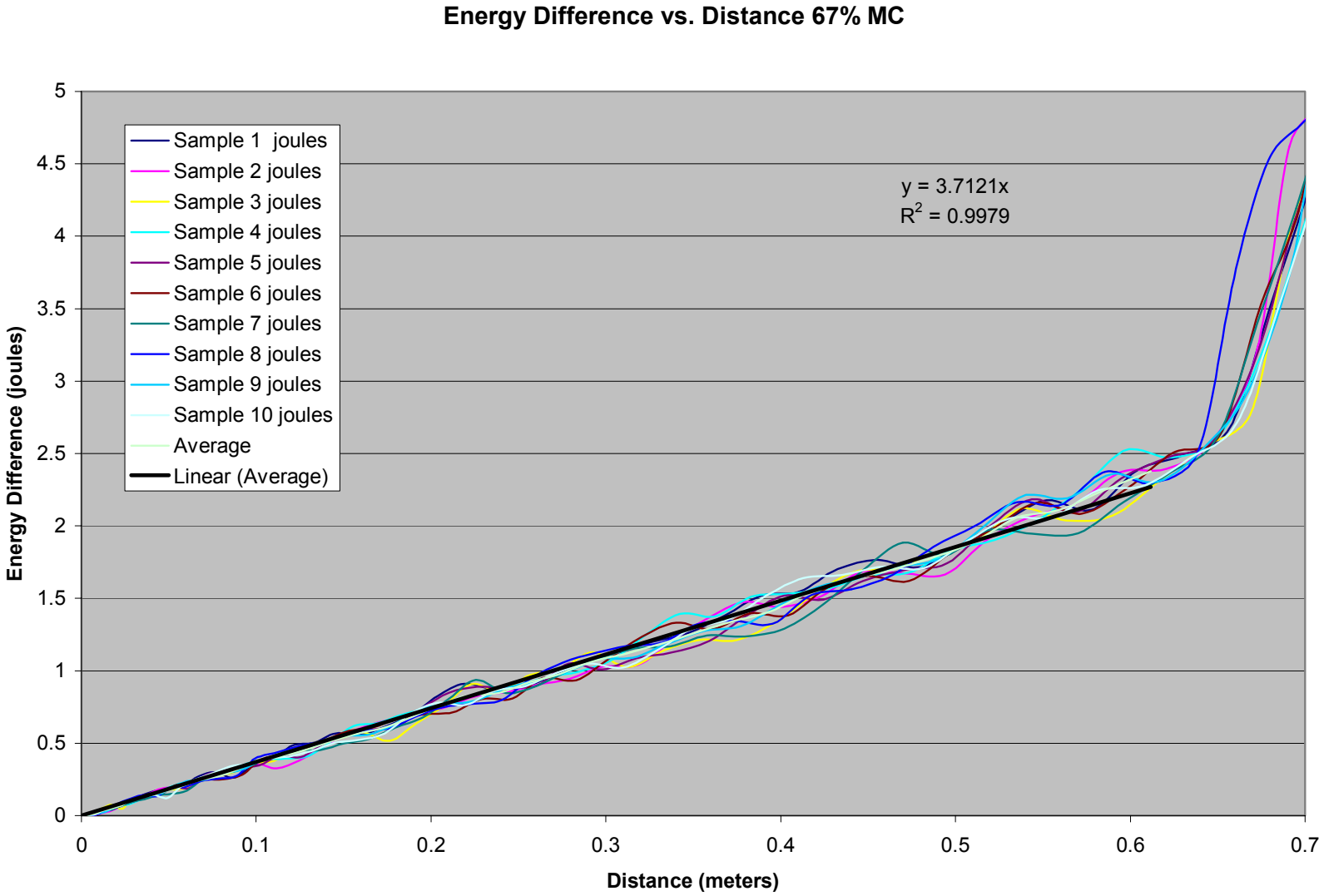
Energy Difference vs. Distance 67% MC
Energy Difference (joules)
Distance (meters)
Sample 1 joules
Sample 2 joules
Sample 3 joules
Sample 4 joules
Sample 5 joules
Sample 6 joules
Sample 7 joules
Sample 8 joules
Sample 9 joules
Sample 10 joules
Average
Linear (Average)
y = 3.7121x
R2 = 0.9979
0
0.5
1
1.5
2
2.5
3
3.5
4
4.5
5
0
0.1
0.2
0.3
0.4
0.5
0.6
0.7

Paper Splitting Results with Debonder

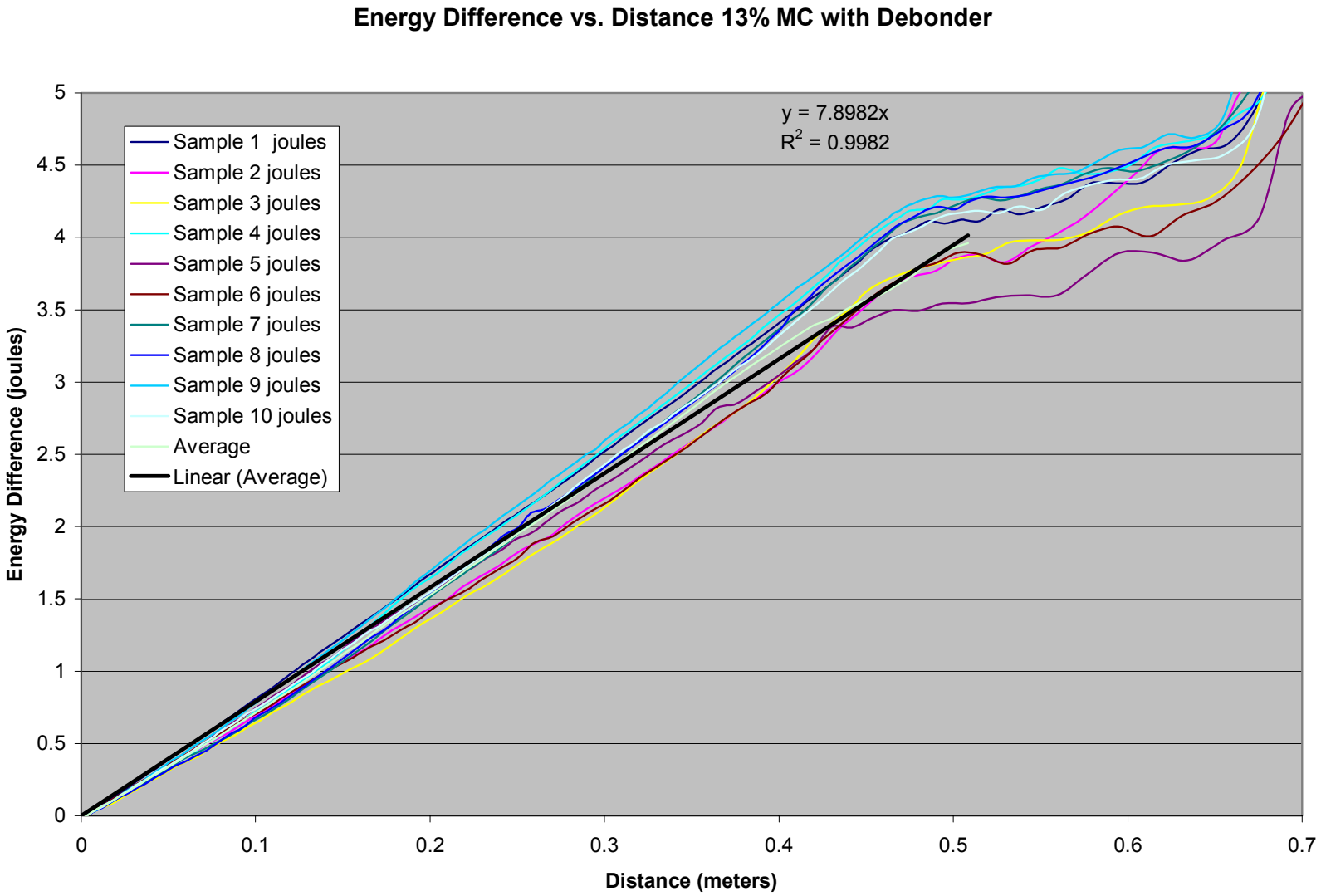
Energy Difference vs. Distance 13% MC with Debonder
y = 7.8982x
R2 = 0.9982
Sample 1 joules
Sample 2 joules
Sample 3 joules
Sample 4 joules
Sample 5 joules
Sample 6 joules
Sample 7 joules
Sample 8 joules
Sample 9 joules
Sample 10 joules
Average
Linear (Average)
Energy Difference (joules)
Distance (meters)
0
0.5
1
1.5
2
2.5
3
3.5
4
4.5
5
0
0.1
0.2
0.3
0.4
0.5
0.6
0.7

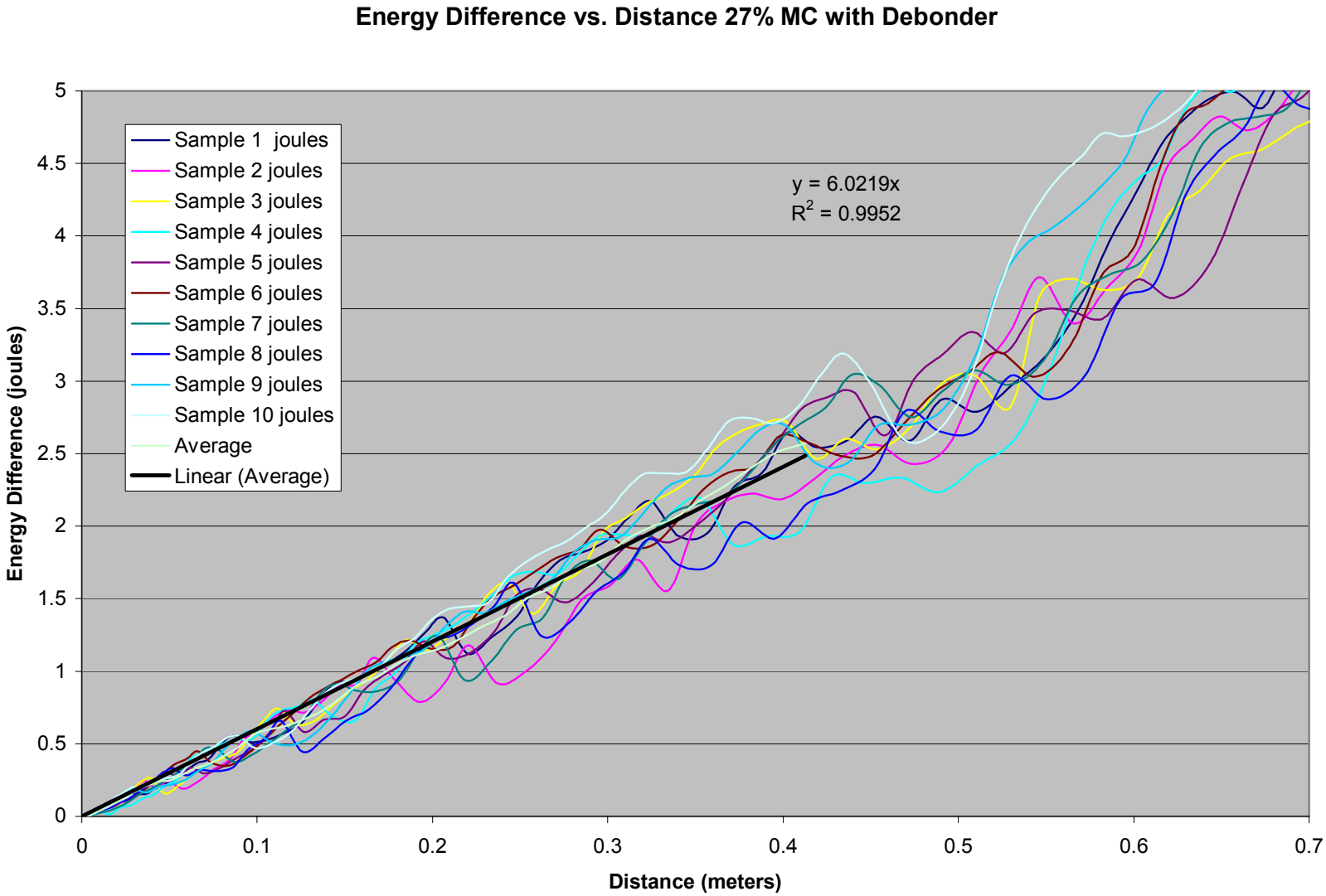
Energy Difference vs. Distance 27% MC with Debonder
Energy Difference (joules)
Distance (meters)
Sample 1 joules
Sample 2 joules
Sample 3 joules
Sample 4 joules
Sample 5 joules
Sample 6 joules
Sample 7 joules
Sample 8 joules
Sample 9 joules
Sample 10 joules
Average
Linear (Average)
y = 6.0219x
R2 = 0.9952
0
0.5
1
1.5
2
2.5
3
3.5
4
4.5
5
0
0.1
0.2
0.3
0.4
0.5
0.6
0.7

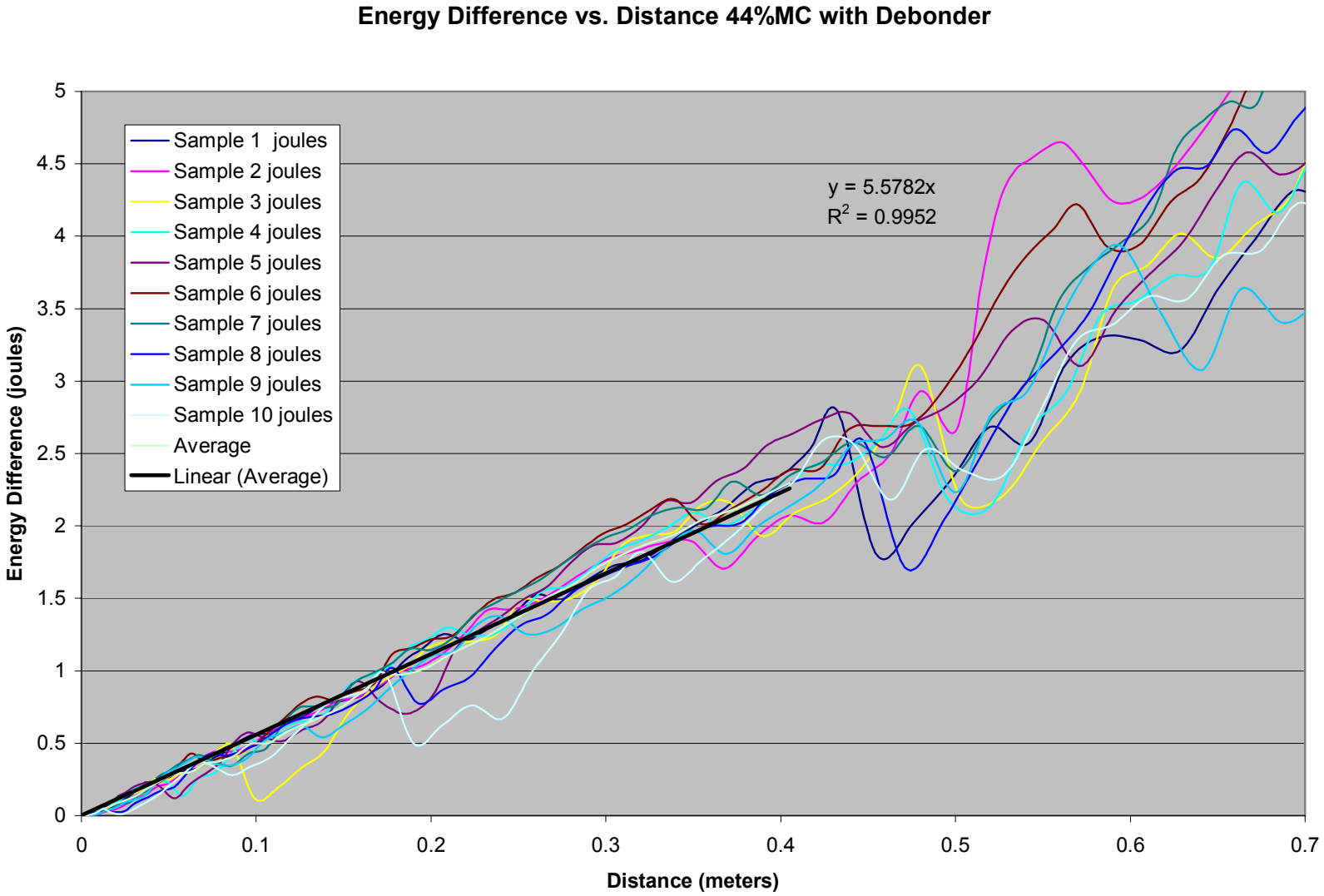
Energy Difference vs. Distance 44%MC with Debonder
Energy Difference (joules)
Distance (meters)
Sample 1 joules
Sample 2 joules
Sample 3 joules
Sample 4 joules
Sample 5 joules
Sample 6 joules
Sample 7 joules
Sample 8 joules
Sample 9 joules
Sample 10 joules
Average
Linear (Average)
y = 5.5782x
R2 = 0.9952
0
0.5
1
1.5
2
2.5
3
3.5
4
4.5
5
0
0.1
0.2
0.3
0.4
0.5
0.6
0.7

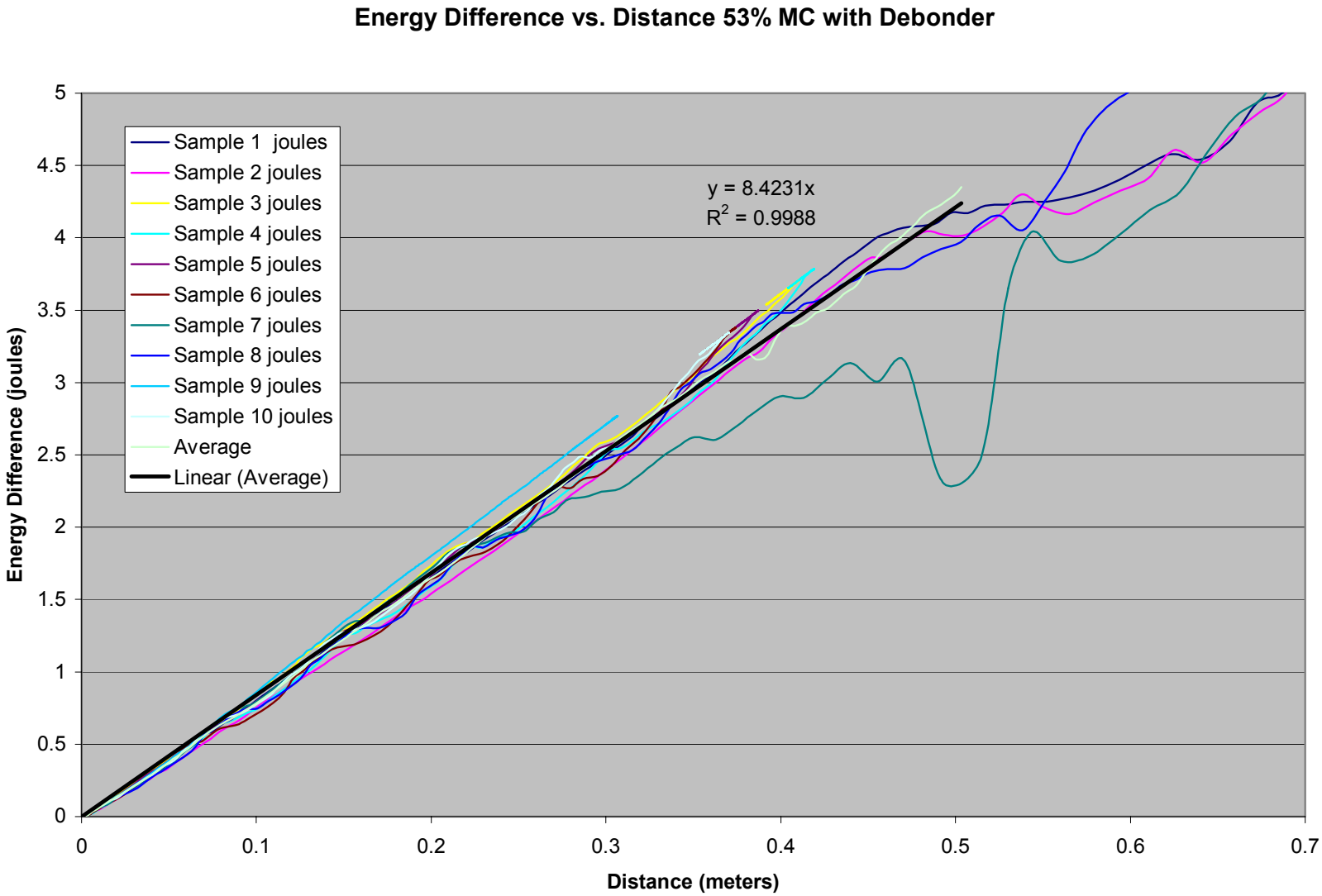
Energy Difference vs. Distance 53% MC with Debonder
Energy Difference (joules)
Distance (meters)
y = 8.4231x
R2 = 0.9988
Sample 1 joules
Sample 2 joules
Sample 3 joules
Sample 4 joules
Sample 5 joules
Sample 6 joules
Sample 7 joules
Sample 8 joules
Sample 9 joules
Sample 10 joules
Average
Linear (Average)
0
0.5
1
1.5
2
2.5
3
3.5
4
4.5
5
0
0.1
0.2
0.3
0.4
0.5
0.6
0.7

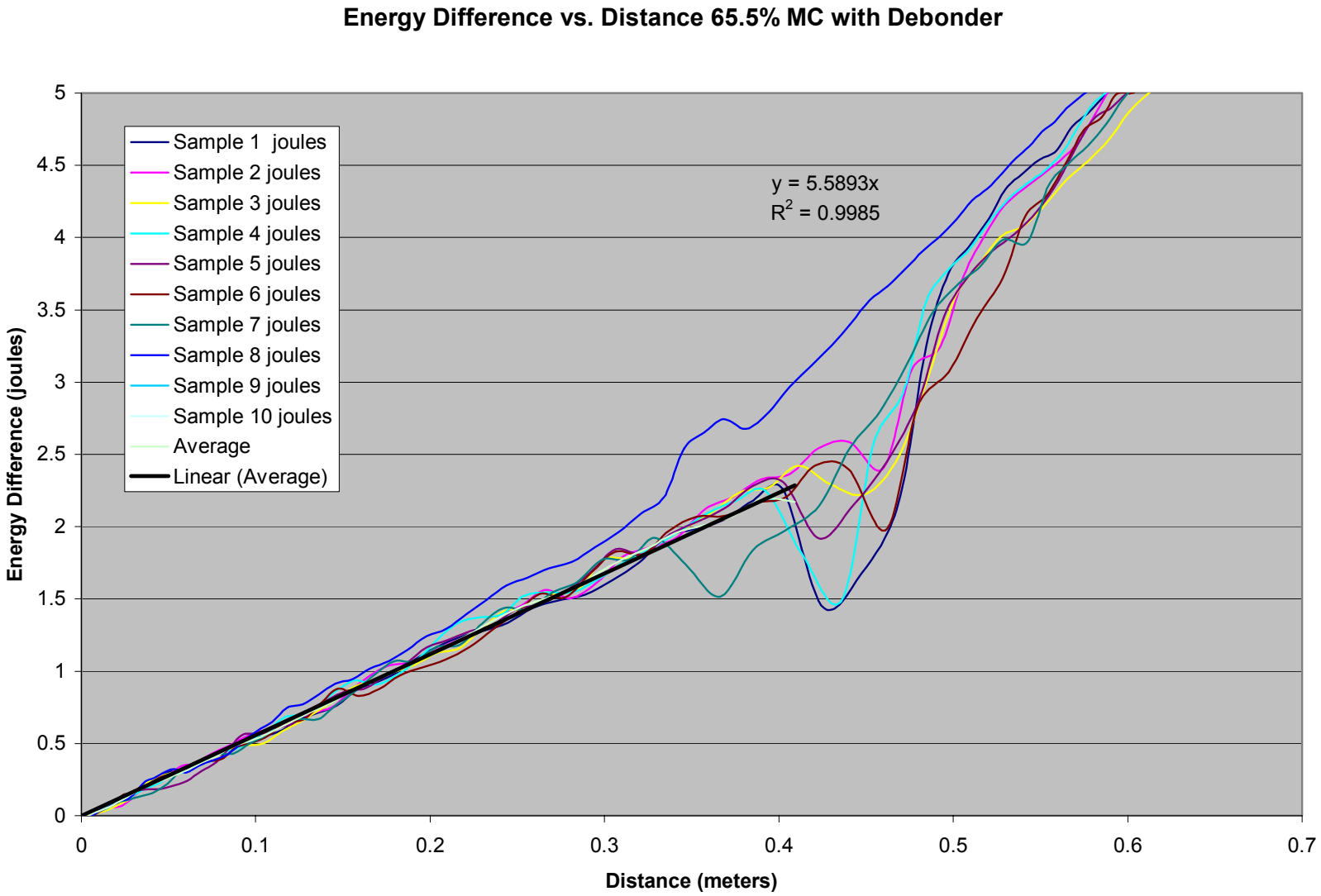
Energy Difference vs. Distance 65.5% MC with Debonder
Energy Difference (joules)
Distance (meters)
y = 5.5893x
R2 = 0.9985
Sample 1 joules
Sample 2 joules
Sample 3 joules
Sample 4 joules
Sample 5 joules
Sample 6 joules
Sample 7 joules
Sample 8 joules
Sample 9 joules
Sample 10 joules
Average
Linear (Average)
0
0.5
1
1.5
2
2.5
3
3.5
4
4.5
5
0
0.1
0.2
0.3
0.4
0.5
0.6
0.7

Paper Splitting Results with Bonder

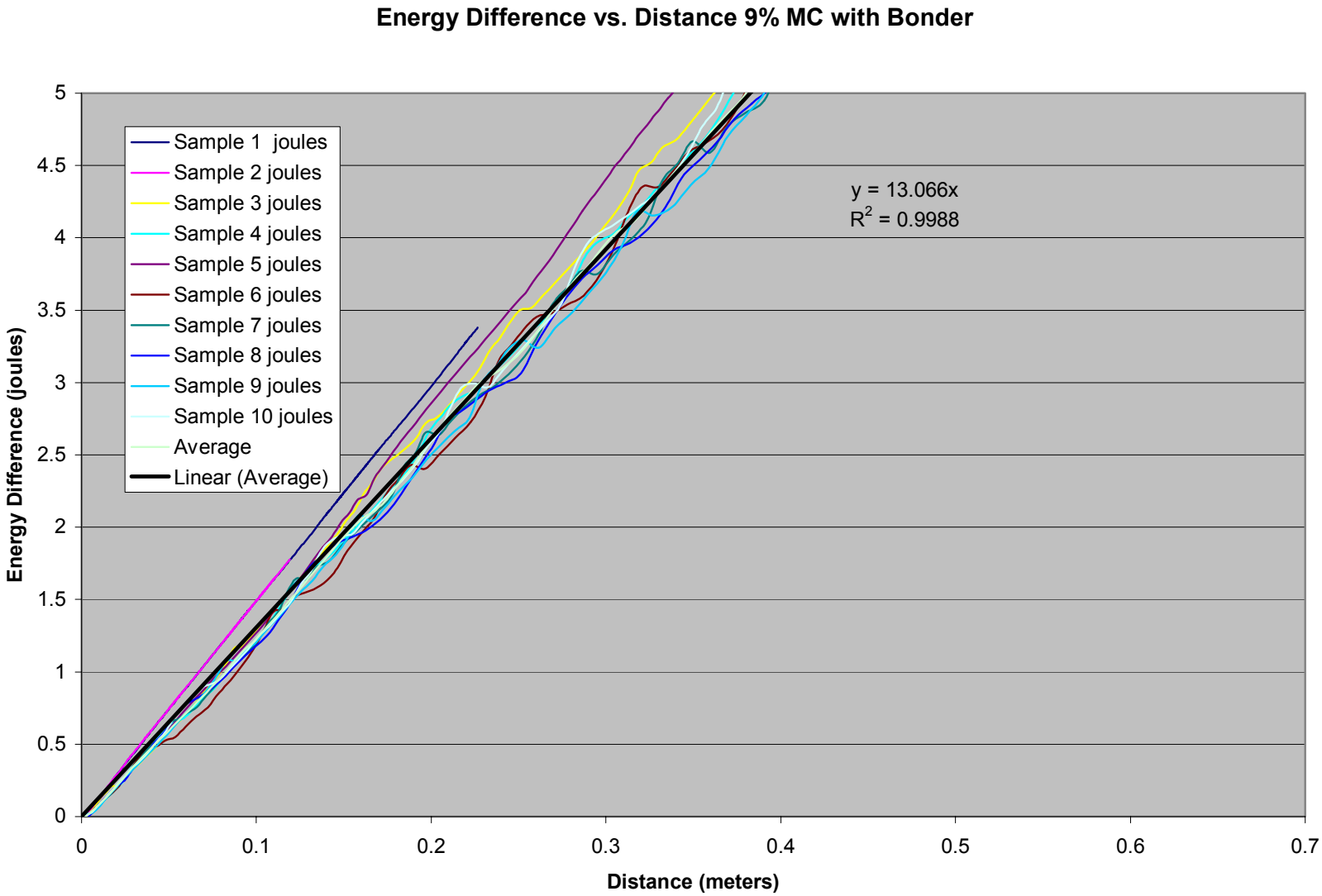
Energy Difference vs. Distance 9% MC with Bonder
Energy Difference (joules)
Distance (meters)
Sample 1 joules
Sample 2 joules
Sample 3 joules
Sample 4 joules
Sample 5 joules
Sample 6 joules
Sample 7 joules
Sample 8 joules
Sample 9 joules
Sample 10 joules
Average
Linear (Average)
y = 13.066x
R2 = 0.9988
0
0.5
1
1.5
2
2.5
3
3.5
4
4.5
5
0
0.1
0.2
0.3
0.4
0.5
0.6
0.7

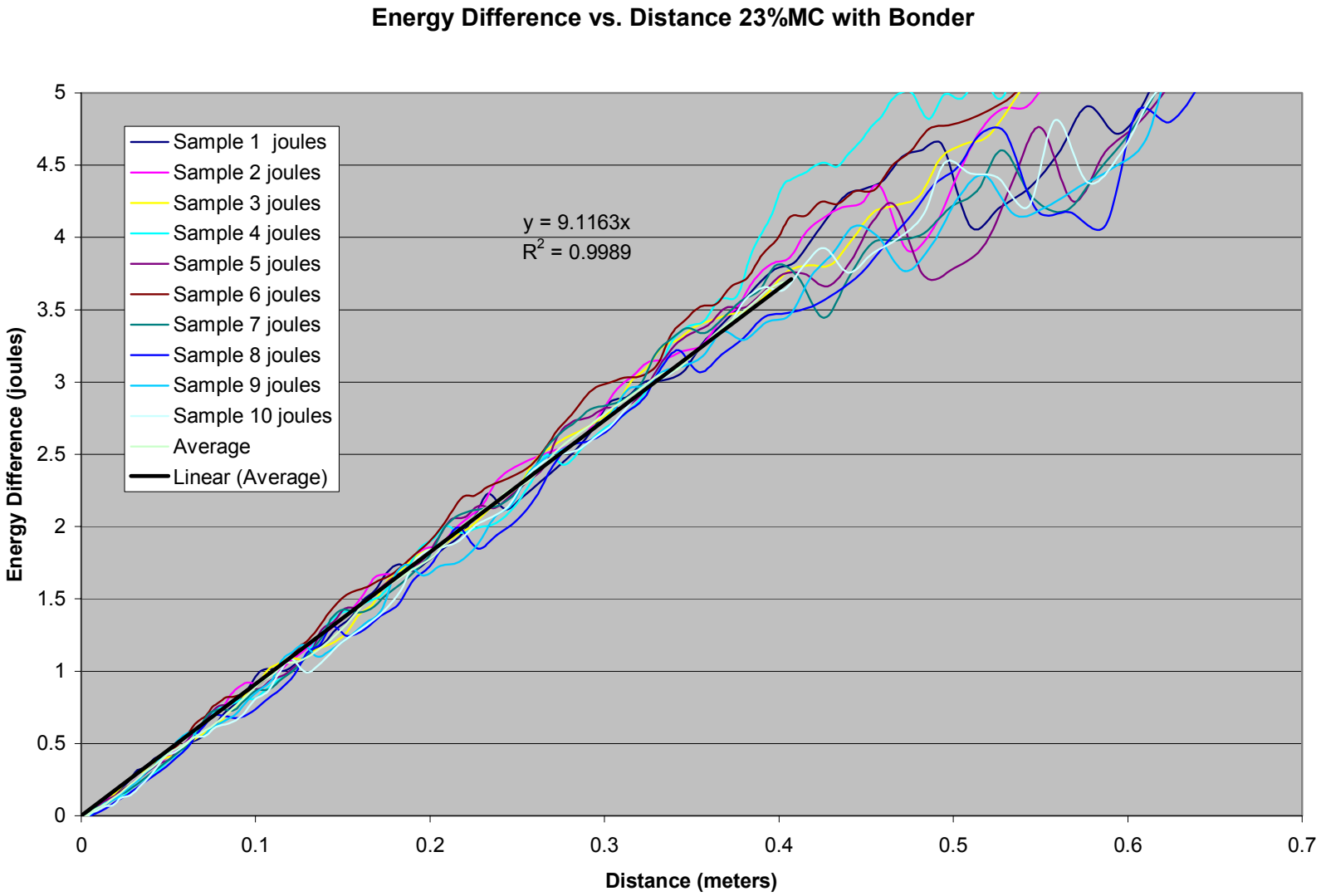
Energy Difference vs. Distance 23%MC with Bonder
Energy Difference (joules)
Distance (meters)
y = 9.1163x
R2 = 0.9989
Sample 1 joules
Sample 2 joules
Sample 3 joules
Sample 4 joules
Sample 5 joules
Sample 6 joules
Sample 7 joules
Sample 8 joules
Sample 9 joules
Sample 10 joules
Average
Linear (Average)
0
0.5
1
1.5
2
2.5
3
3.5
4
4.5
5
0
0.1
0.2
0.3
0.4
0.5
0.6
0.7

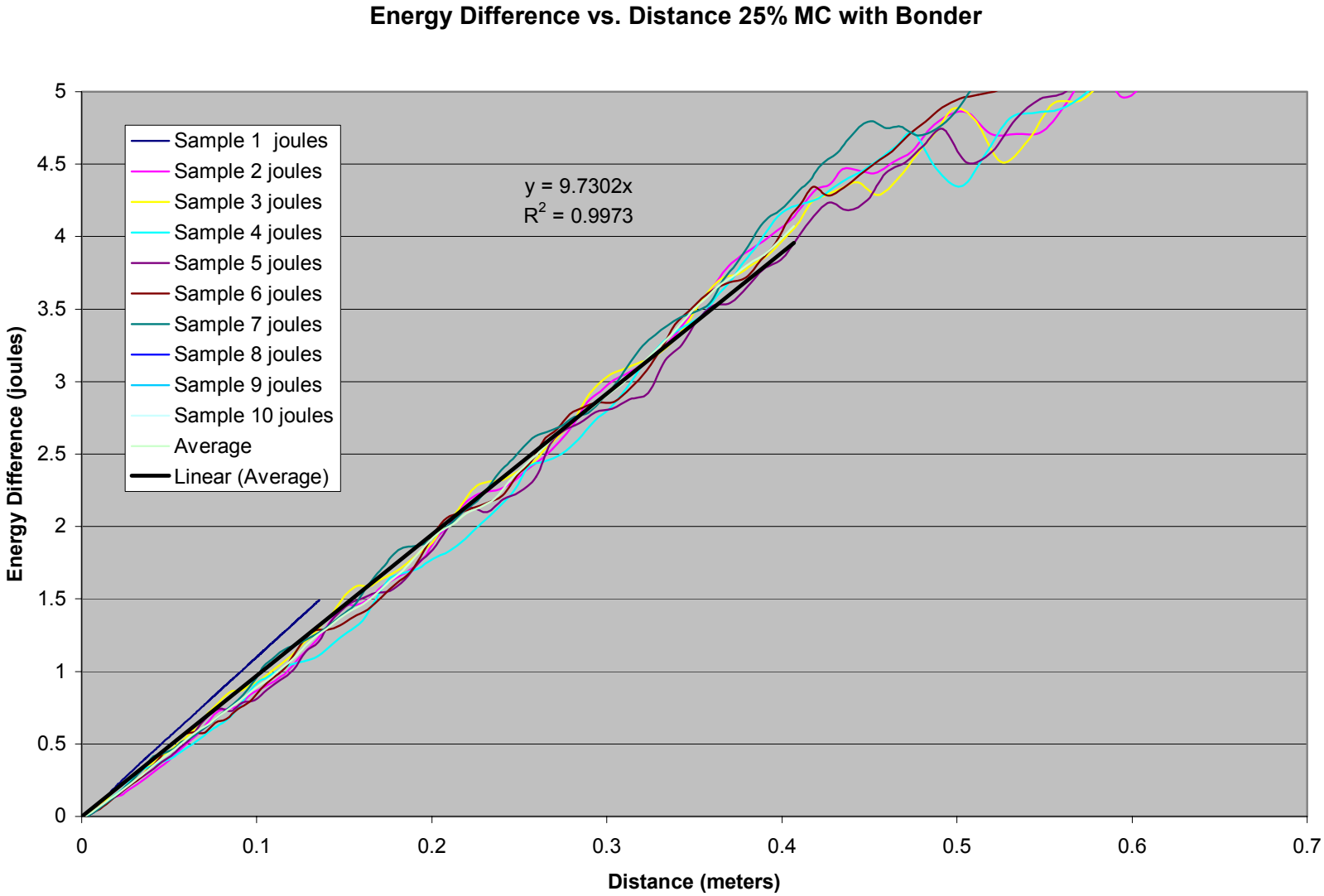
Energy Difference vs. Distance 25% MC with Bonder
Energy Difference (joules)
Distance (meters)
y = 9.7302x
R2 = 0.9973
Sample 1 joules
Sample 2 joules
Sample 3 joules
Sample 4 joules
Sample 5 joules
Sample 6 joules
Sample 7 joules
Sample 8 joules
Sample 9 joules
Sample 10 joules
Average
Linear (Average)
0
0.5
1
1.5
2
2.5
3
3.5
4
4.5
5
0
0.1
0.2
0.3
0.4
0.5
0.6
0.7

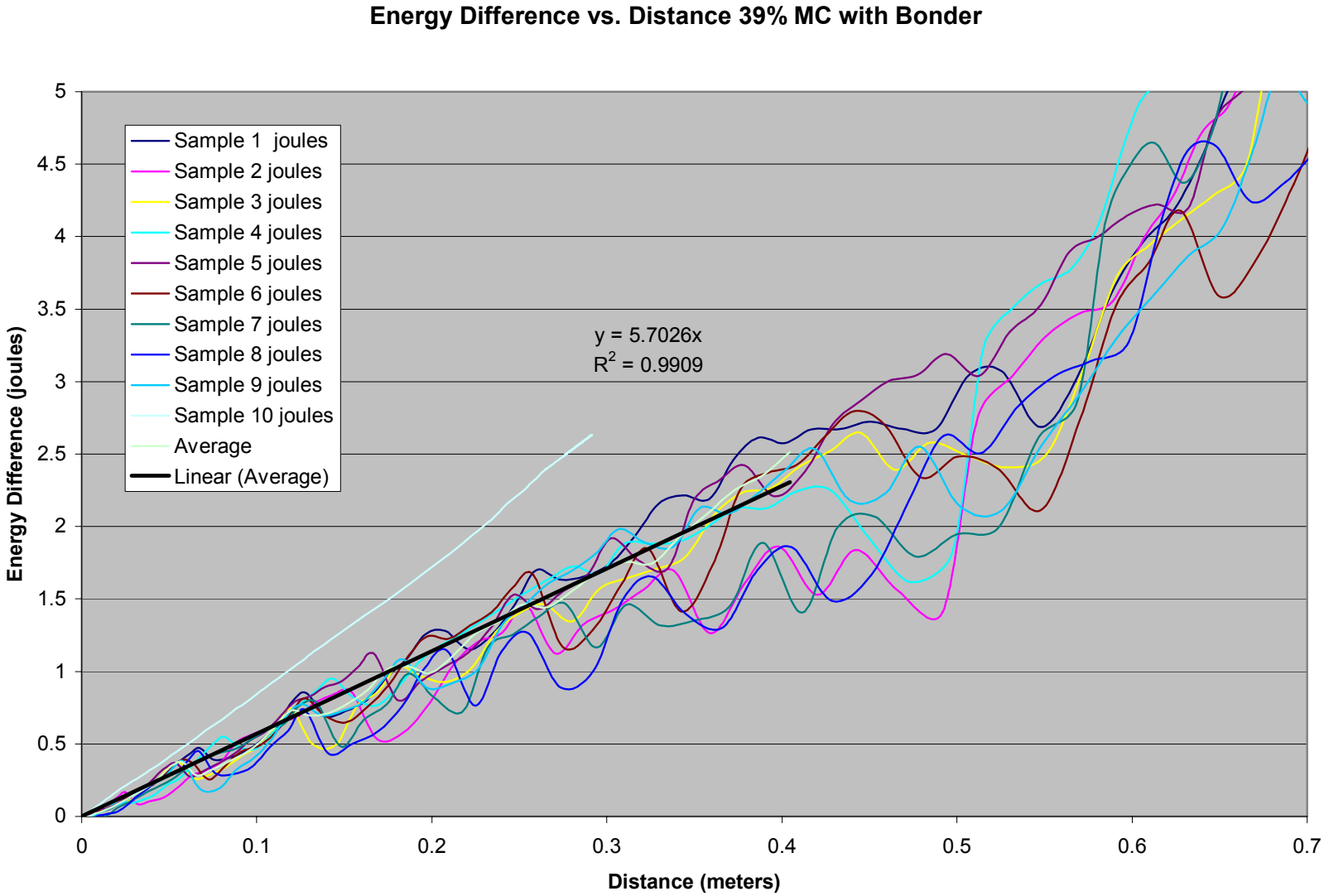
Energy Difference vs. Distance 39% MC with Bonder
Energy Difference (joules)
Distance (meters)
Sample 1 joules
Sample 2 joules
Sample 3 joules
Sample 4 joules
Sample 5 joules
Sample 6 joules
Sample 7 joules
Sample 8 joules
Sample 9 joules
Sample 10 joules
Average
Linear (Average)
y = 5.7026x
R2 = 0.9909
0
0.5
1
1.5
2
2.5
3
3.5
4
4.5
5
0
0.1
0.2
0.3
0.4
0.5
0.6
0.7

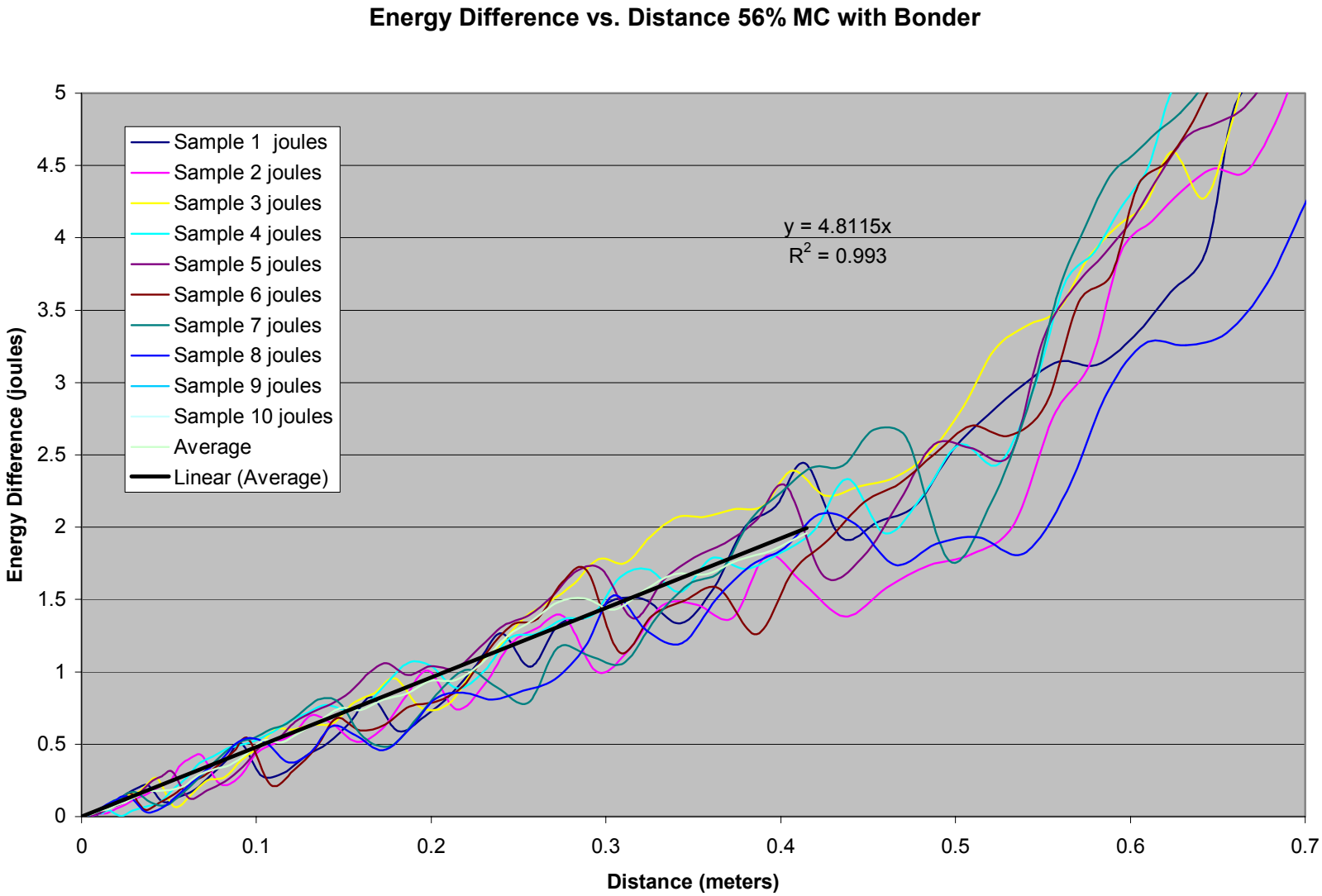
Energy Difference vs. Distance 56% MC with Bonder
Energy Difference (joules)
Distance (meters)
Sample 1 joules
Sample 2 joules
Sample 3 joules
Sample 4 joules
Sample 5 joules
Sample 6 joules
Sample 7 joules
Sample 8 joules
Sample 9 joules
Sample 10 joules
Average
Linear (Average)
y = 4.8115x
R2 = 0.993
0
0.5
1
1.5
2
2.5
3
3.5
4
4.5
5
0
0.1
0.2
0.3
0.4
0.5
0.6
0.7

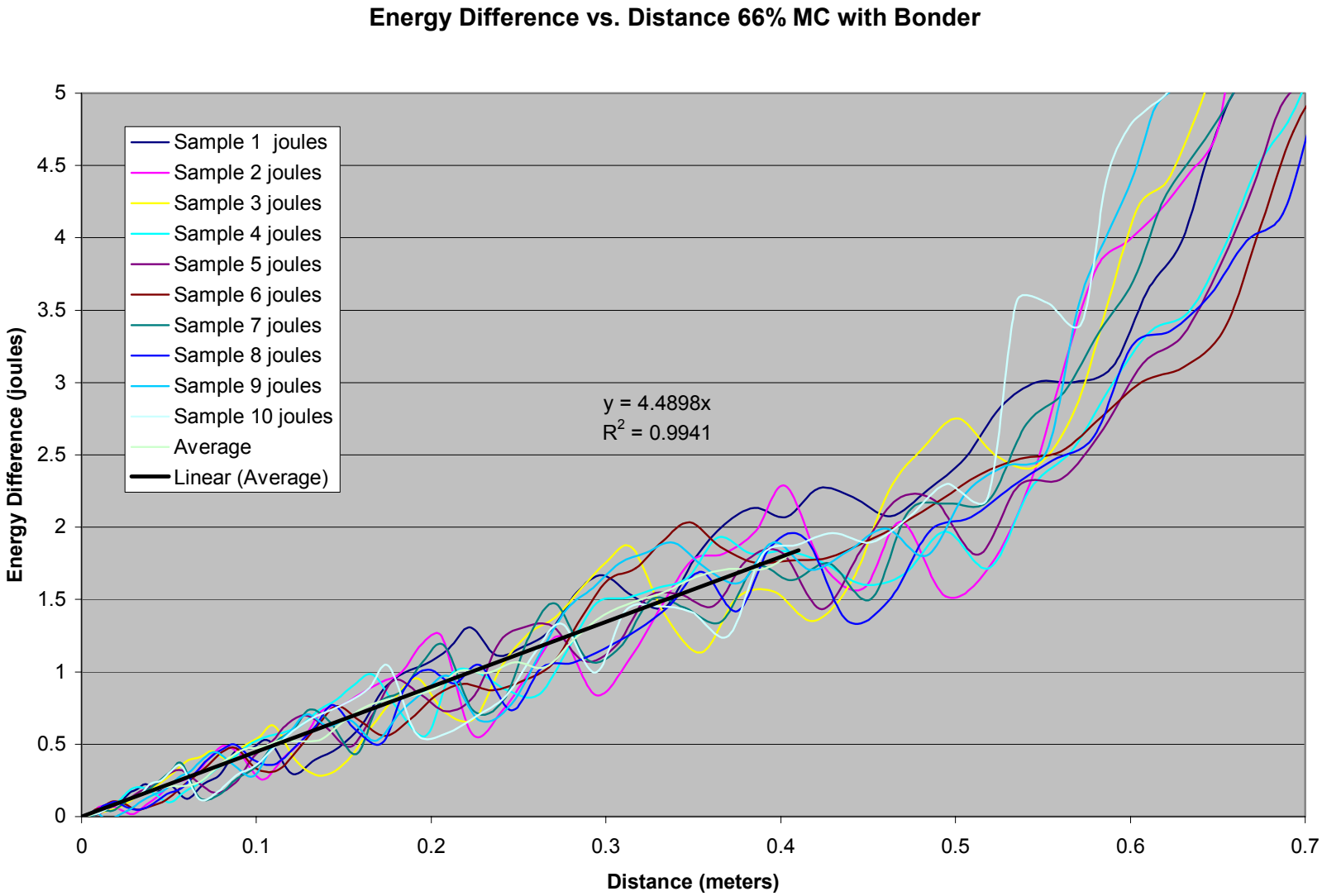
Energy Difference vs. Distance 66% MC with Bonder
Energy Difference (joules)
Distance (meters)
Sample 1 joules
Sample 2 joules
Sample 3 joules
Sample 4 joules
Sample 5 joules
Sample 6 joules
Sample 7 joules
Sample 8 joules
Sample 9 joules
Sample 10 joules
Average
Linear (Average)
y = 4.4898x
R2 = 0.9941
0
0.5
1
1.5
2
2.5
3
3.5
4
4.5
5
0
0.1
0.2
0.3
0.4
0.5
0.6
0.7

APPENDIX B: SPLITS

Split Results with No Additives

9.10% Moisture Content

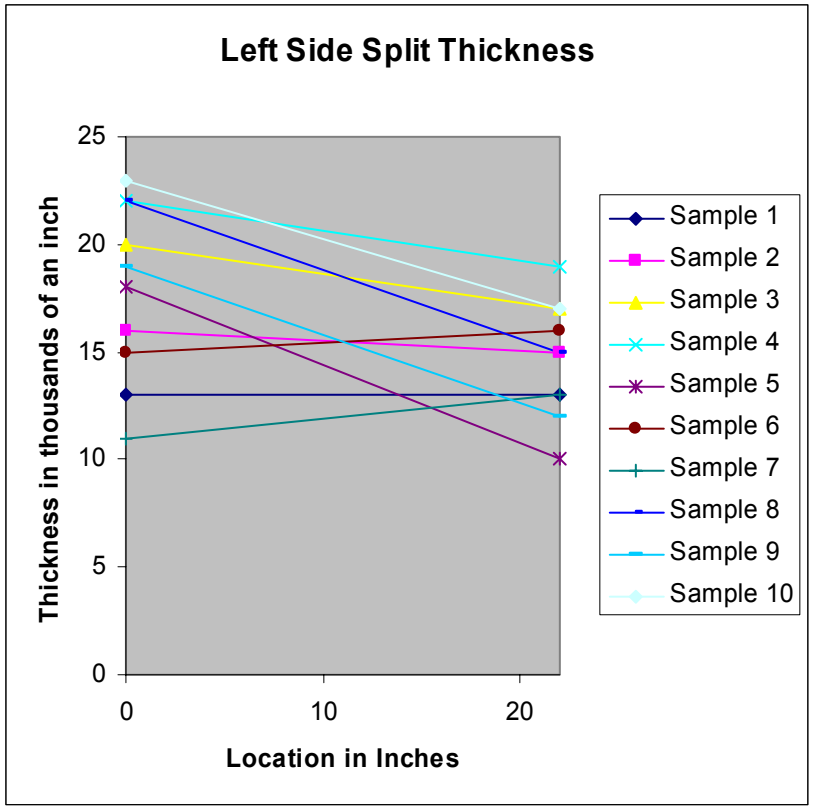

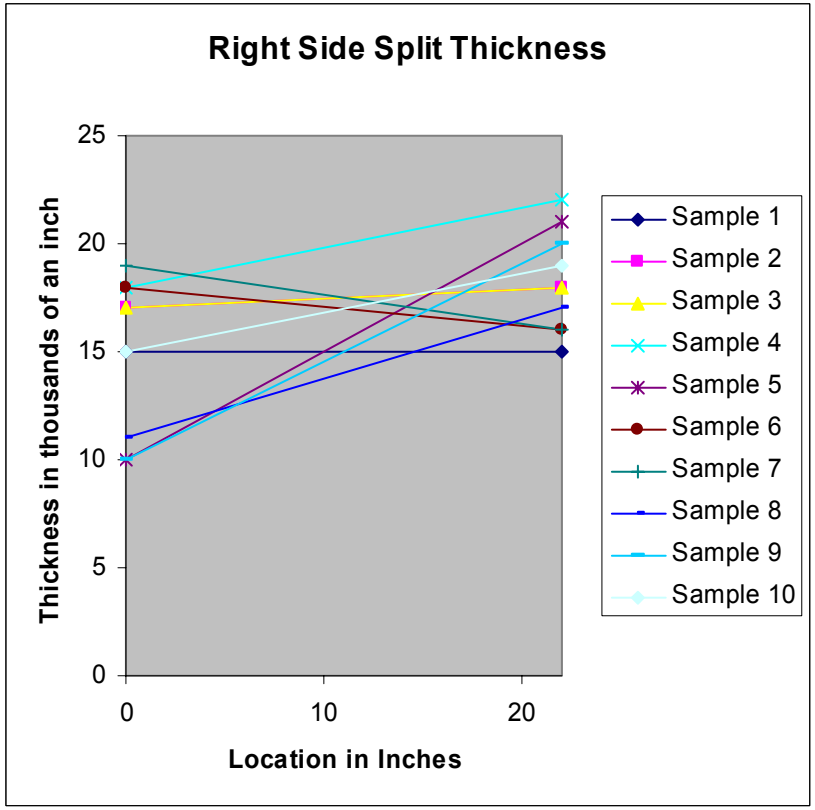

21.46% Moisture Content

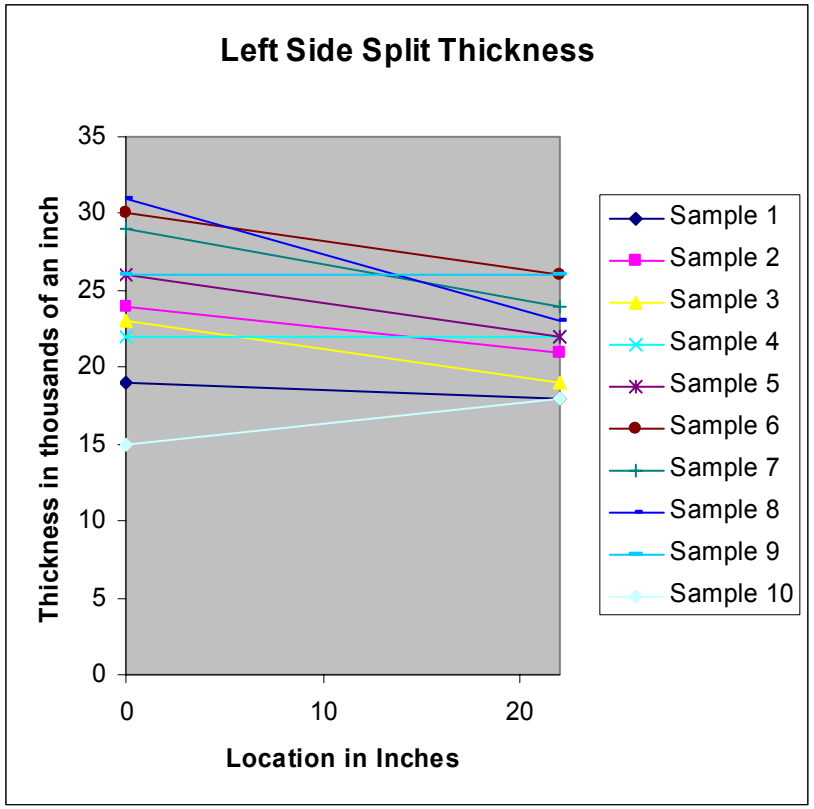

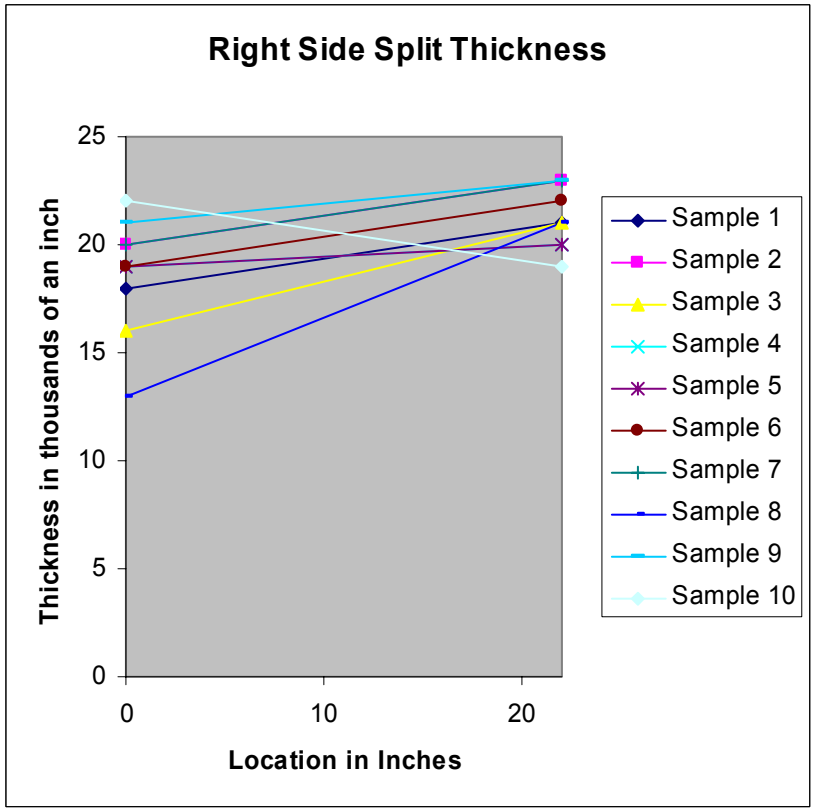

52.78% Moisture Content

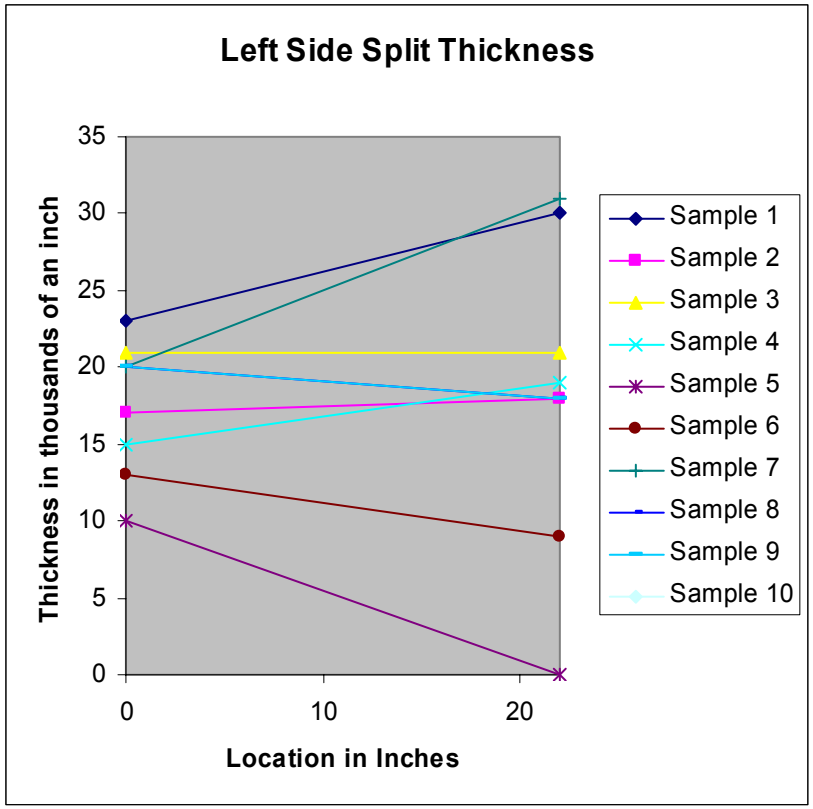

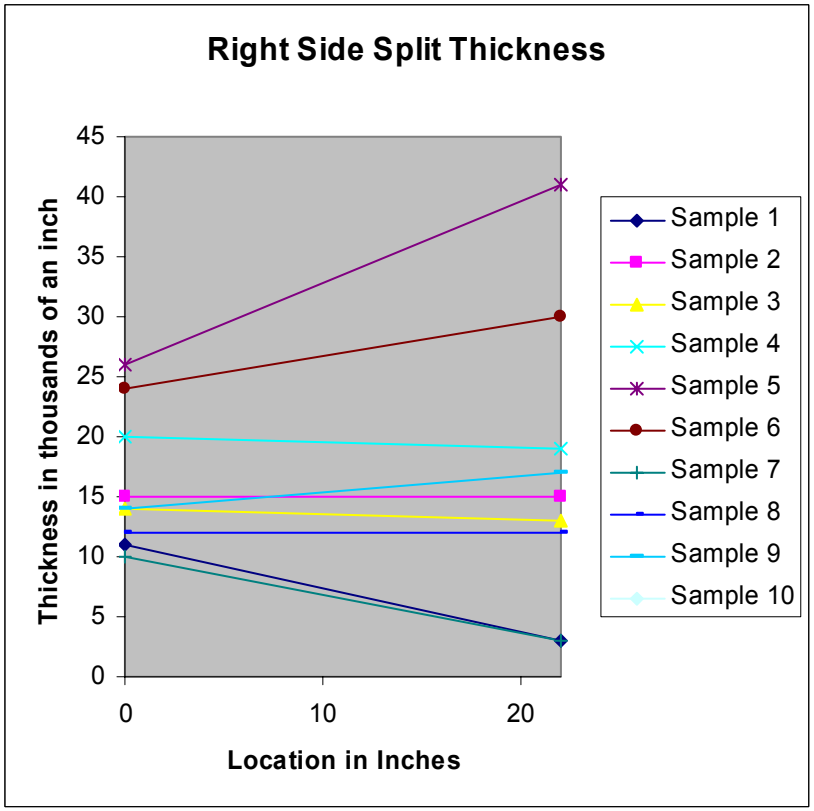

56.67% Moisture Content

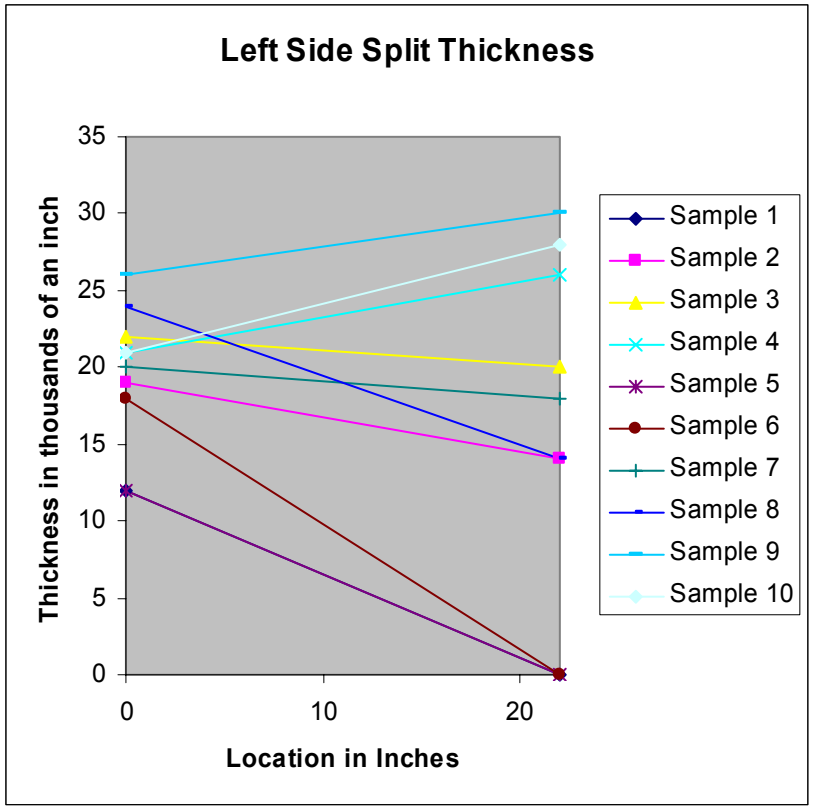

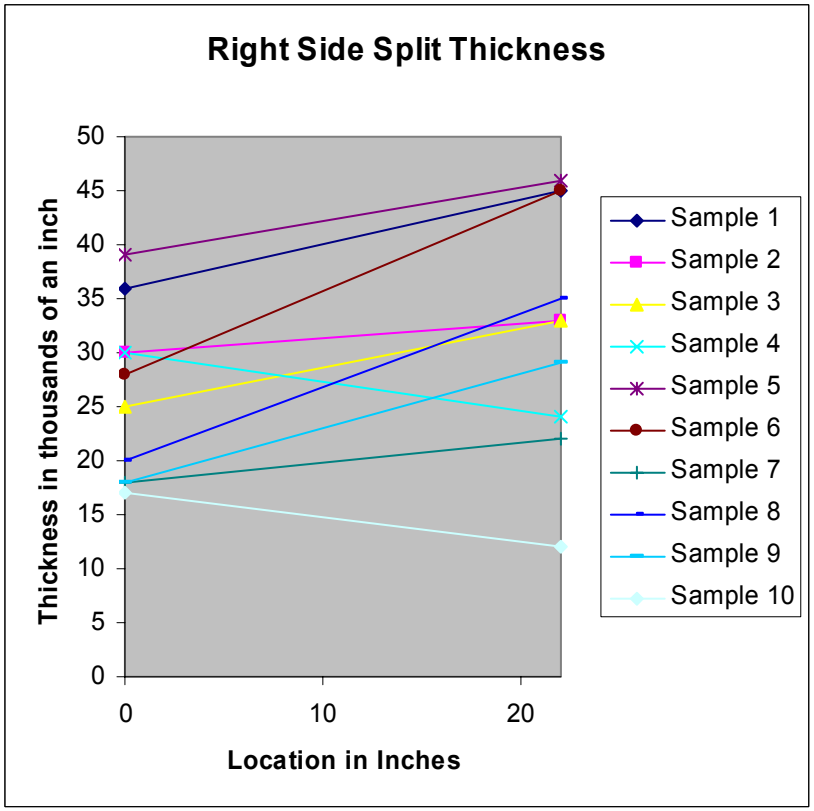

66.59% Moisture Content

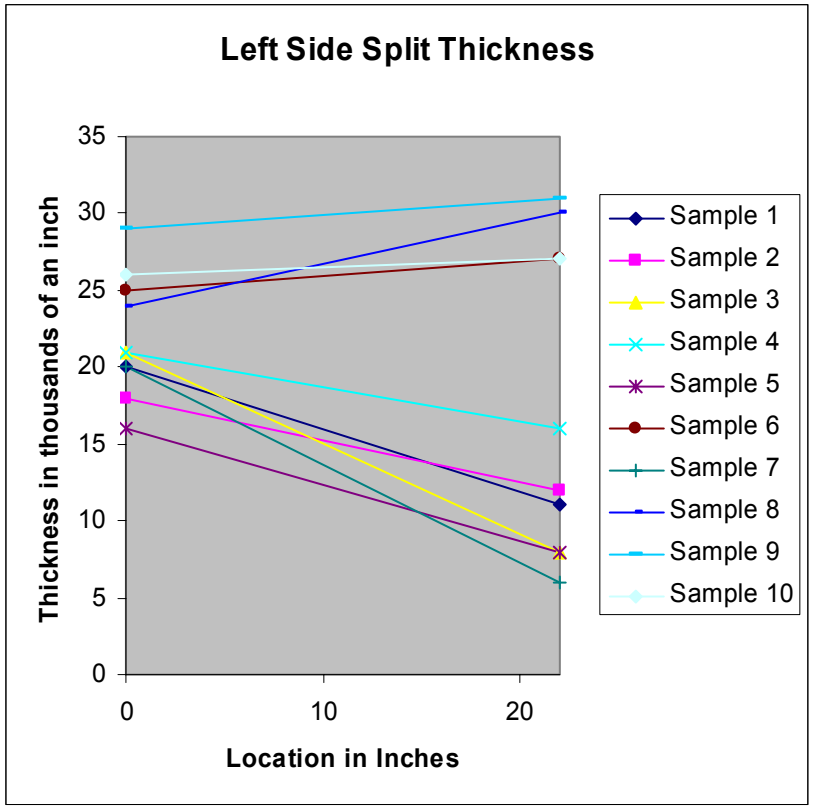

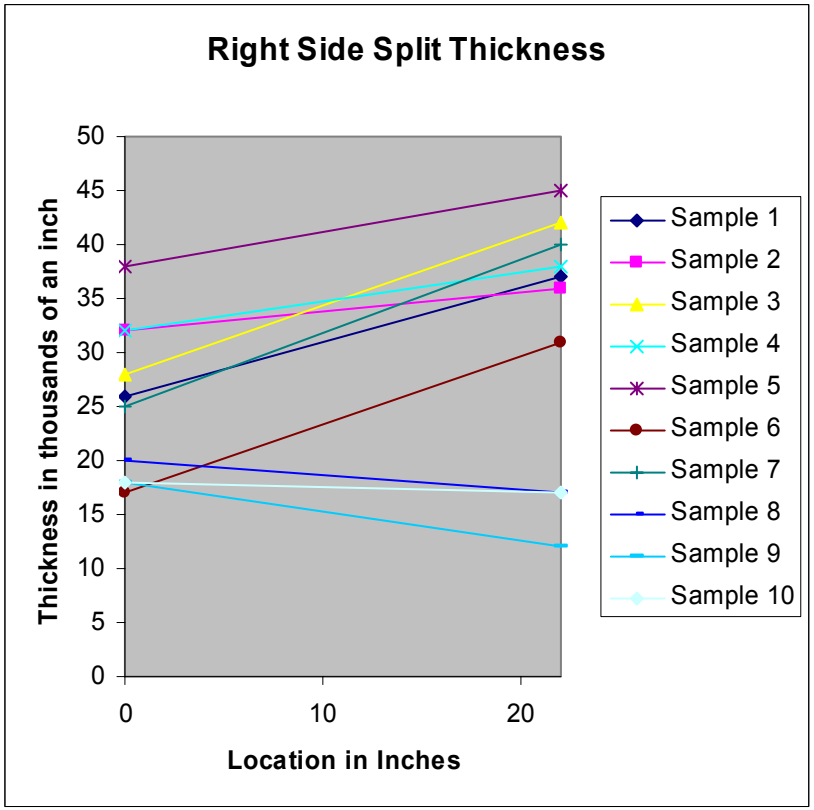

Split Results with Debonder

27.35% Moisture Content

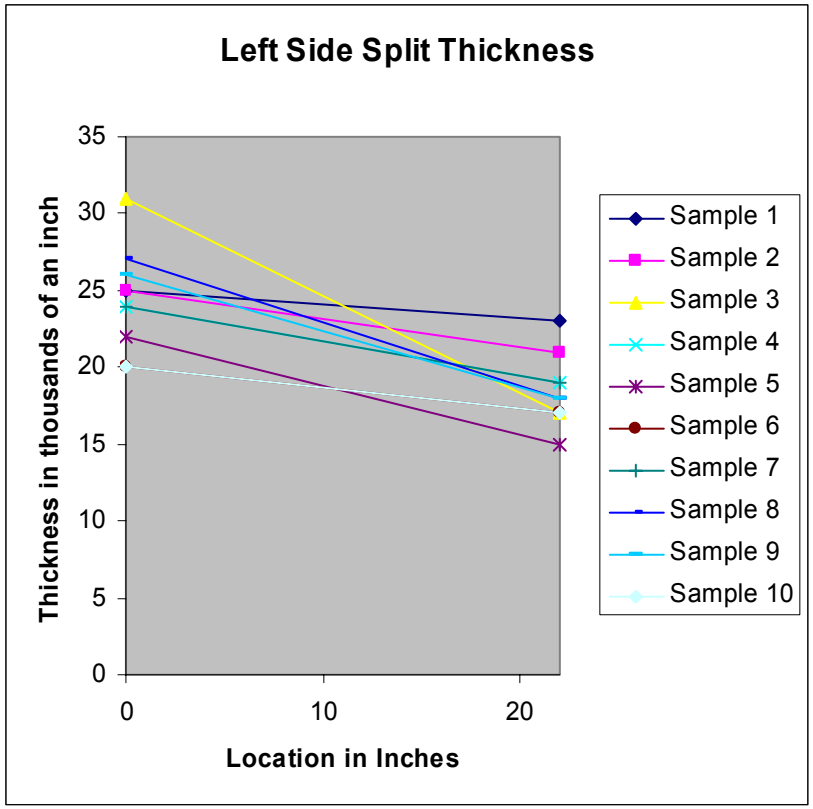

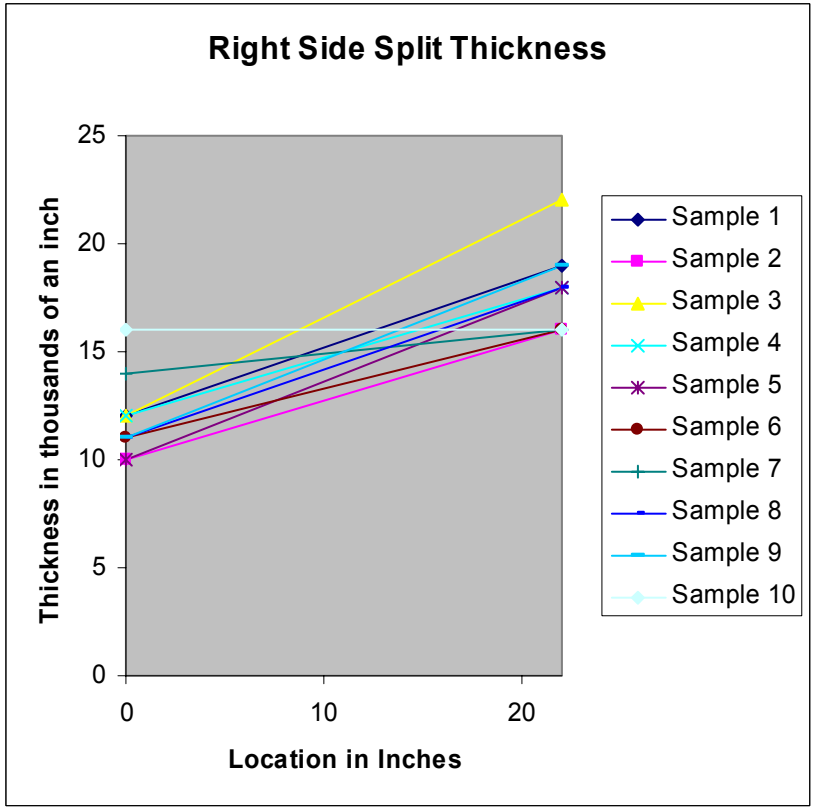

43.70% Moisture Content

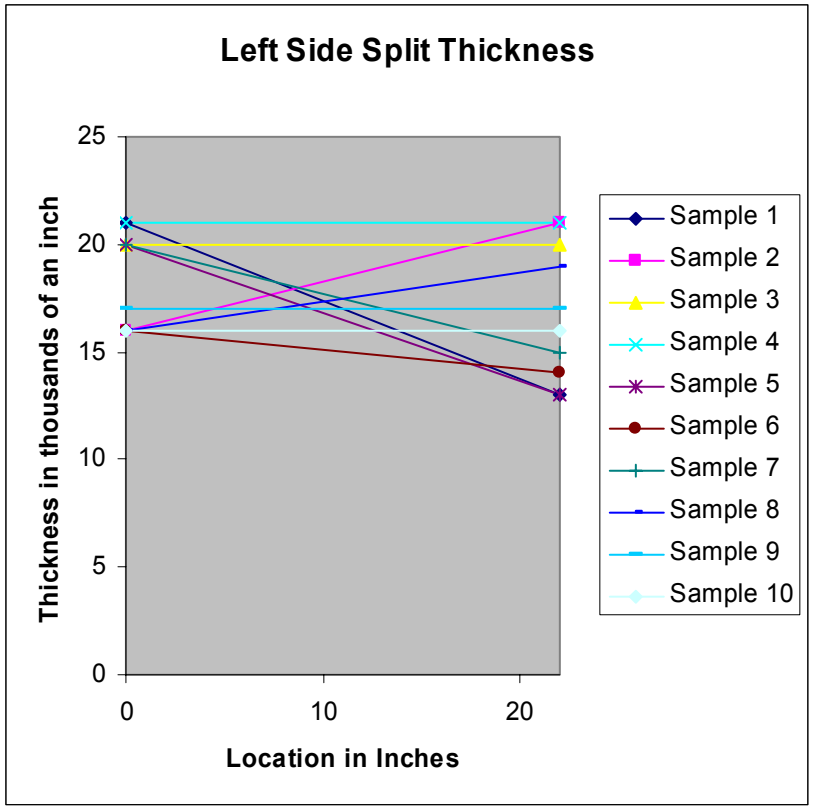

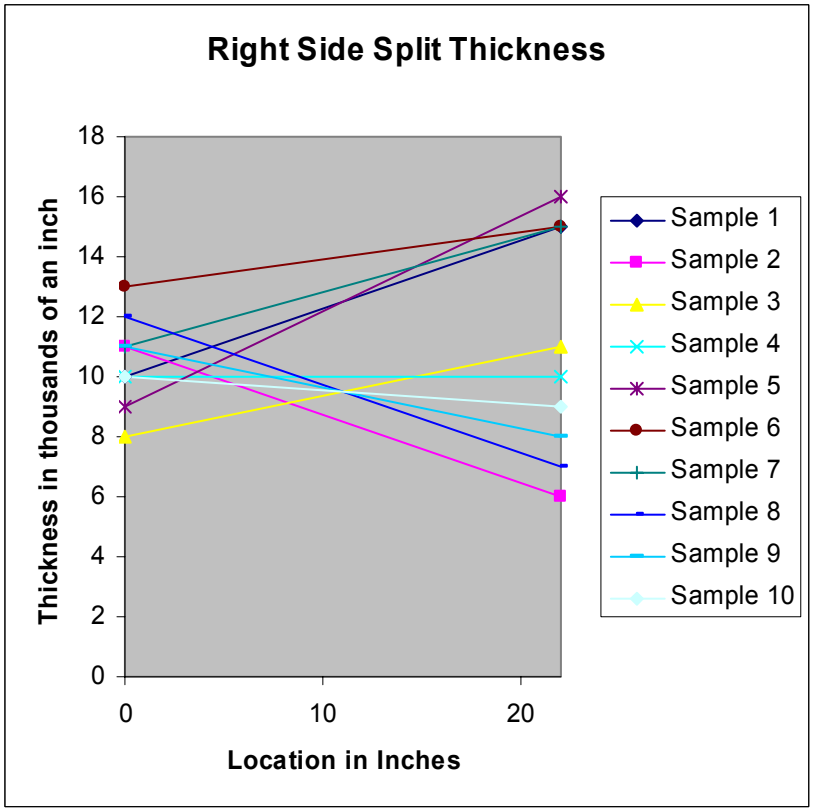

44.49% Moisture Content

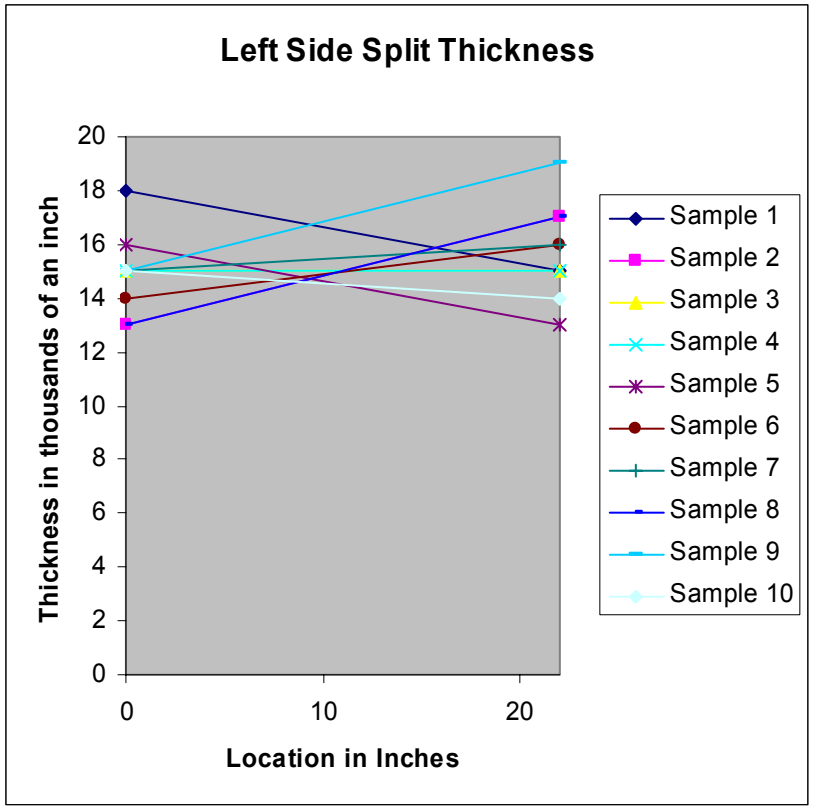

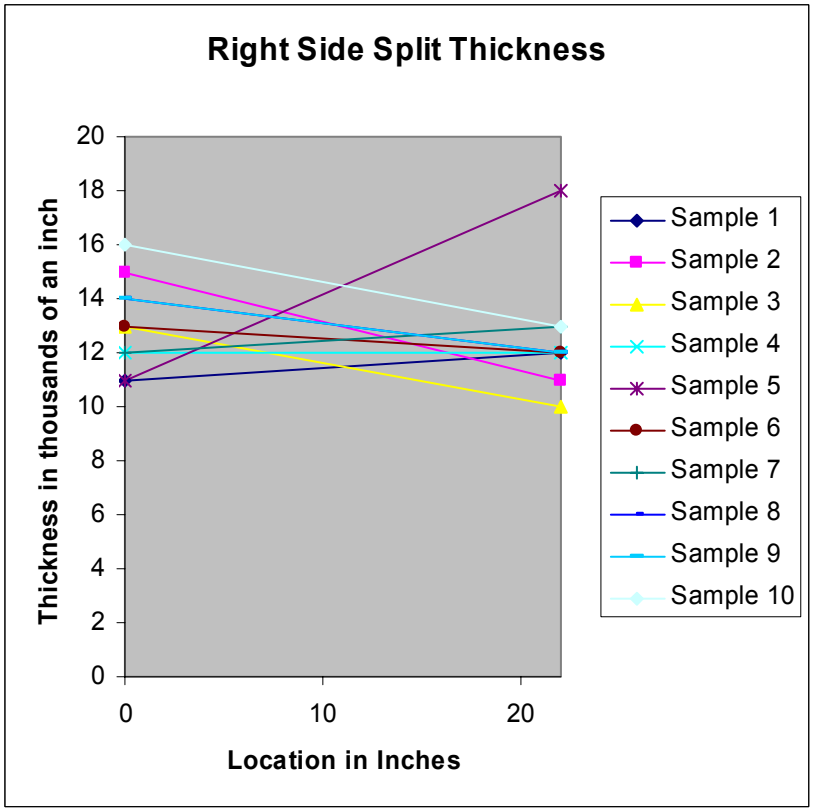

53.75% Moisture Content

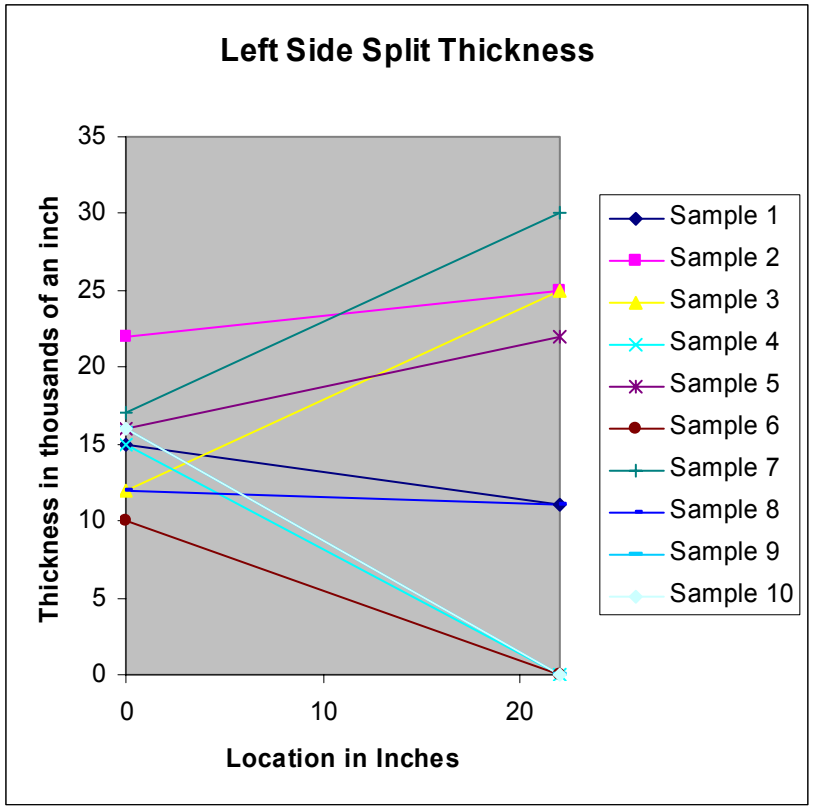

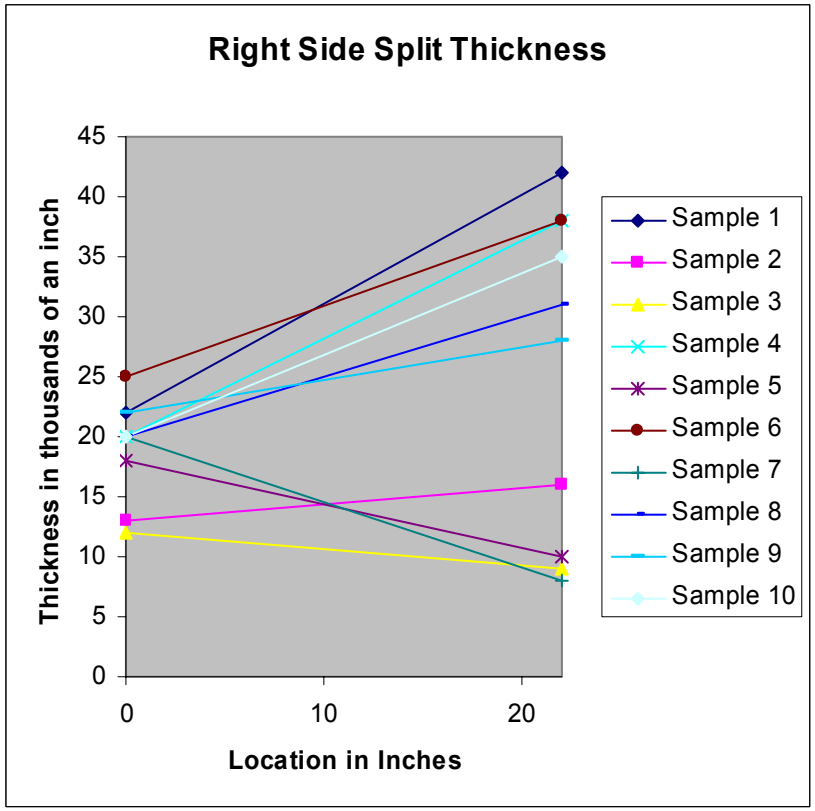

64.52% Moisture Content

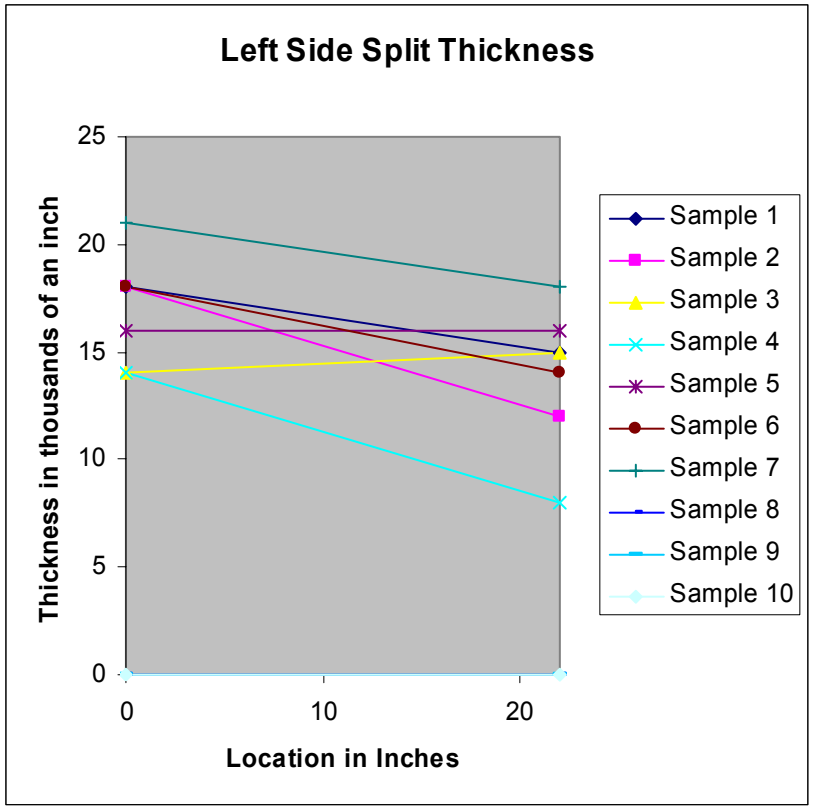

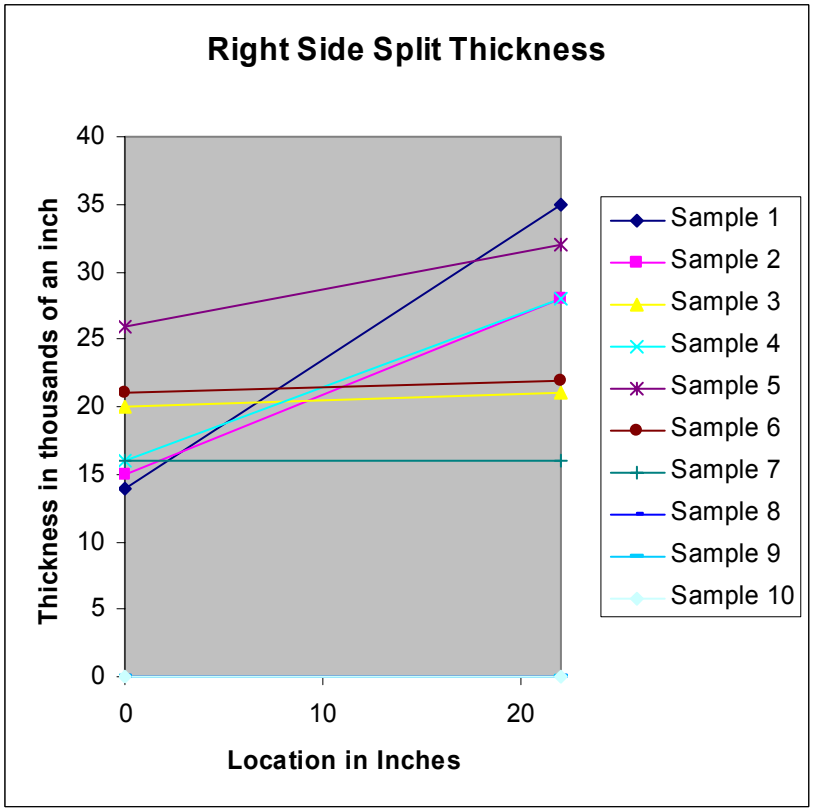

Split Results with Bonder

8.72% Moisture Content

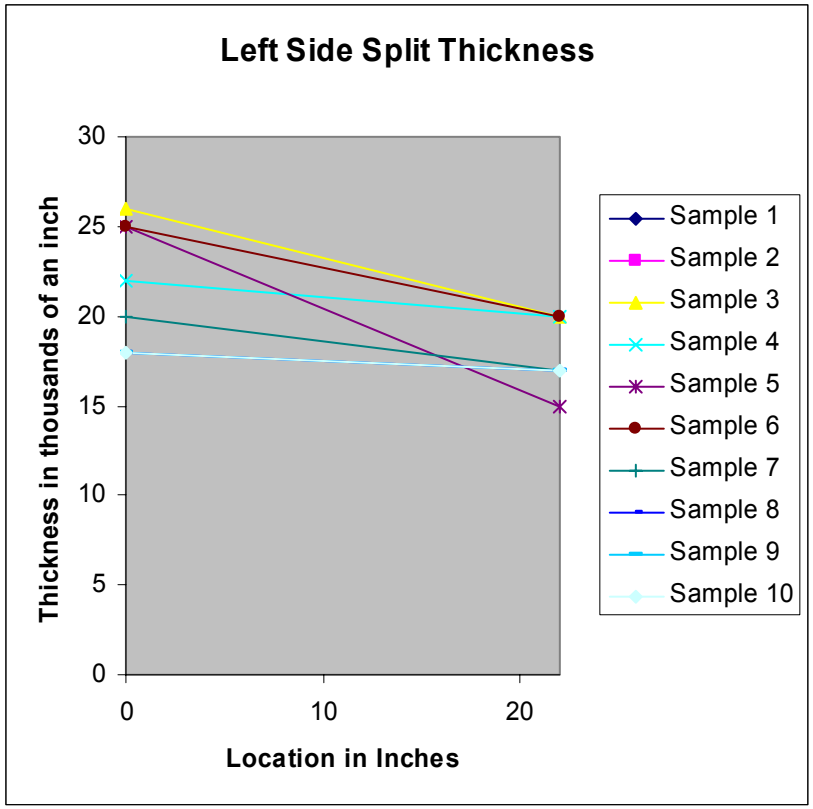

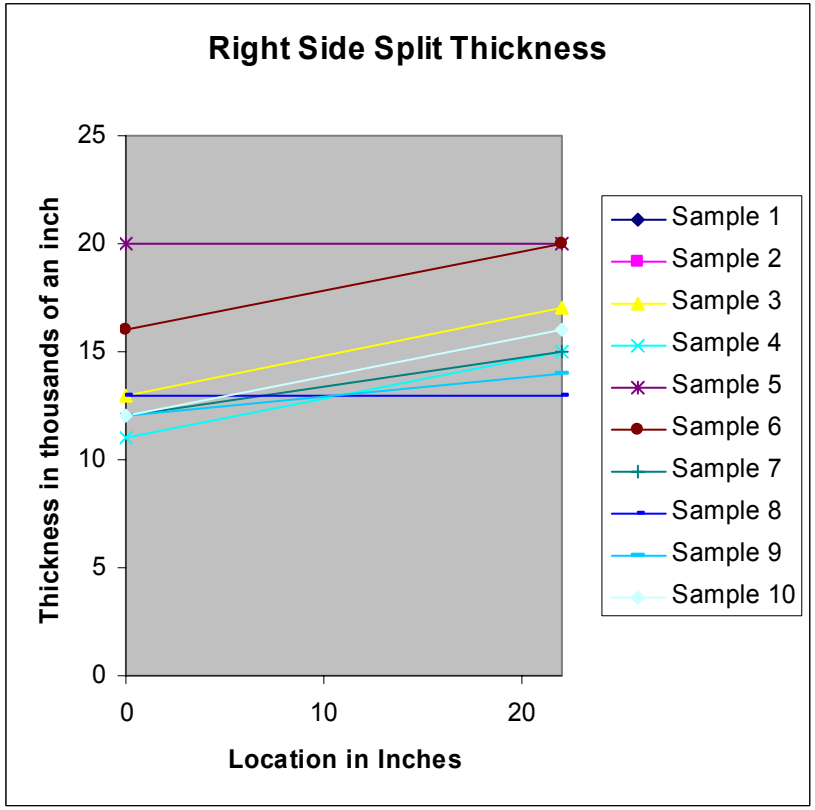

23.48% Moisture Content

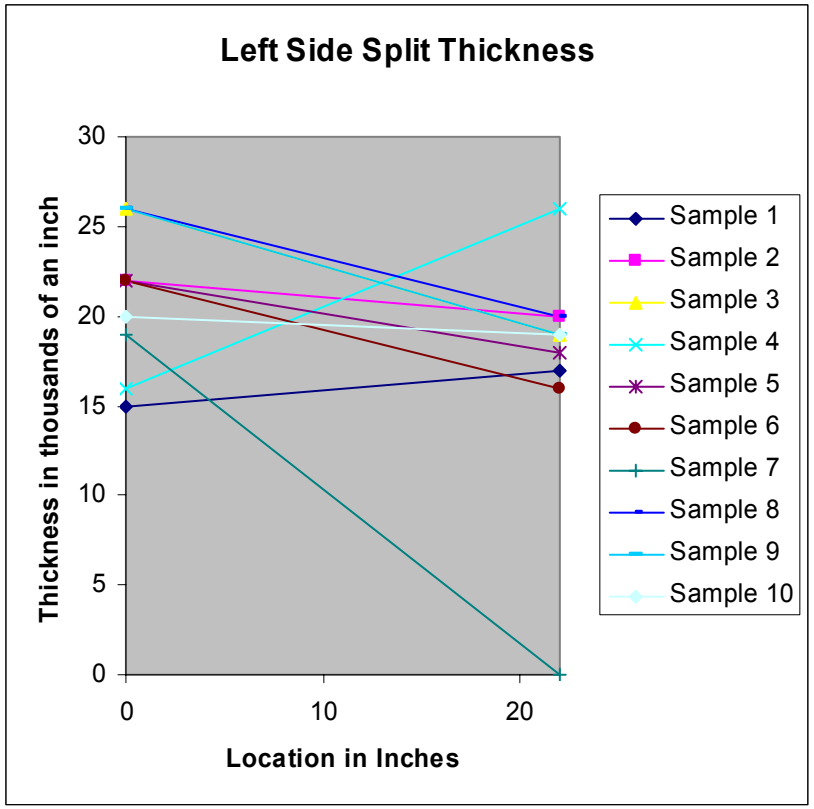

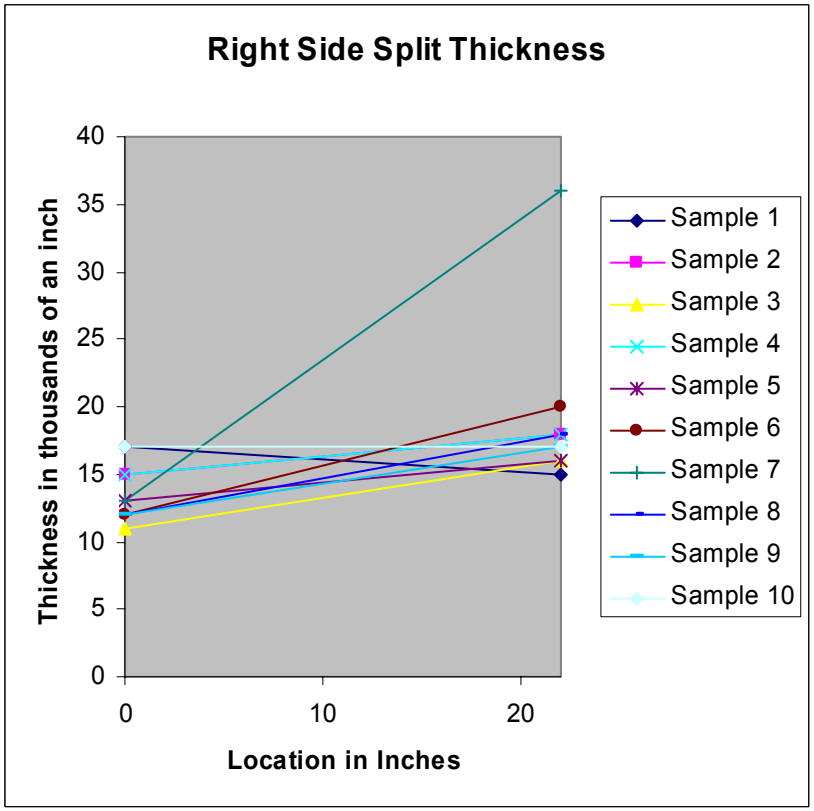

39.26% Moisture Content

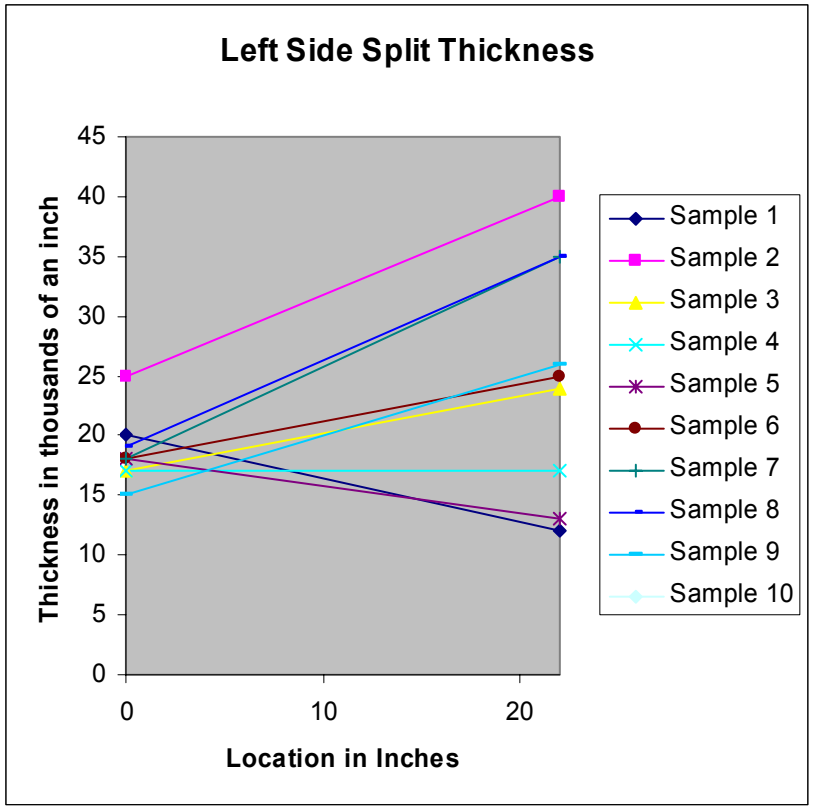

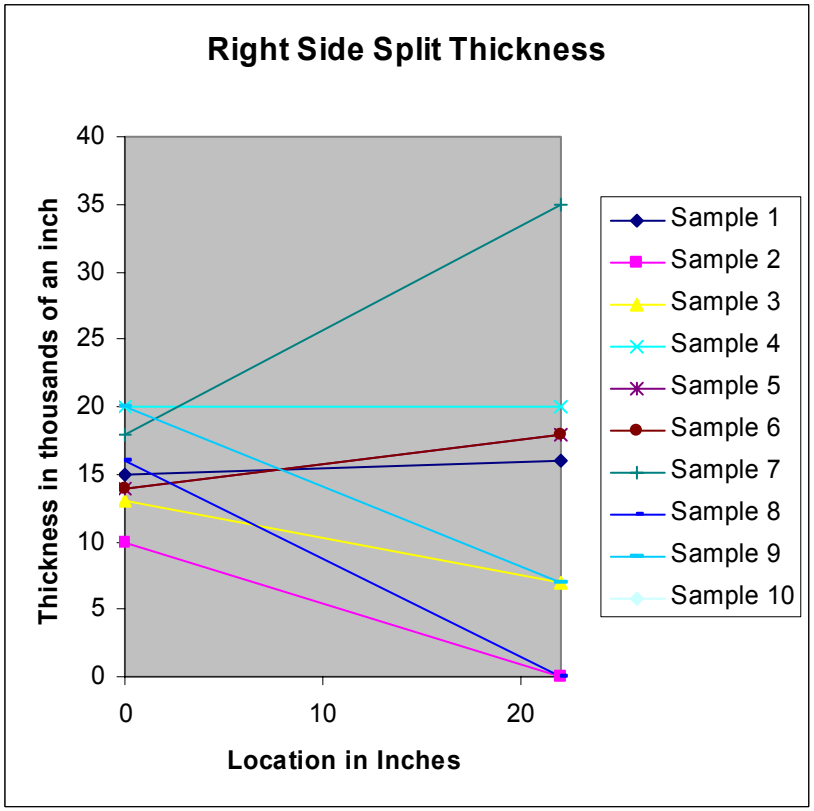

55.55% Moisture Content

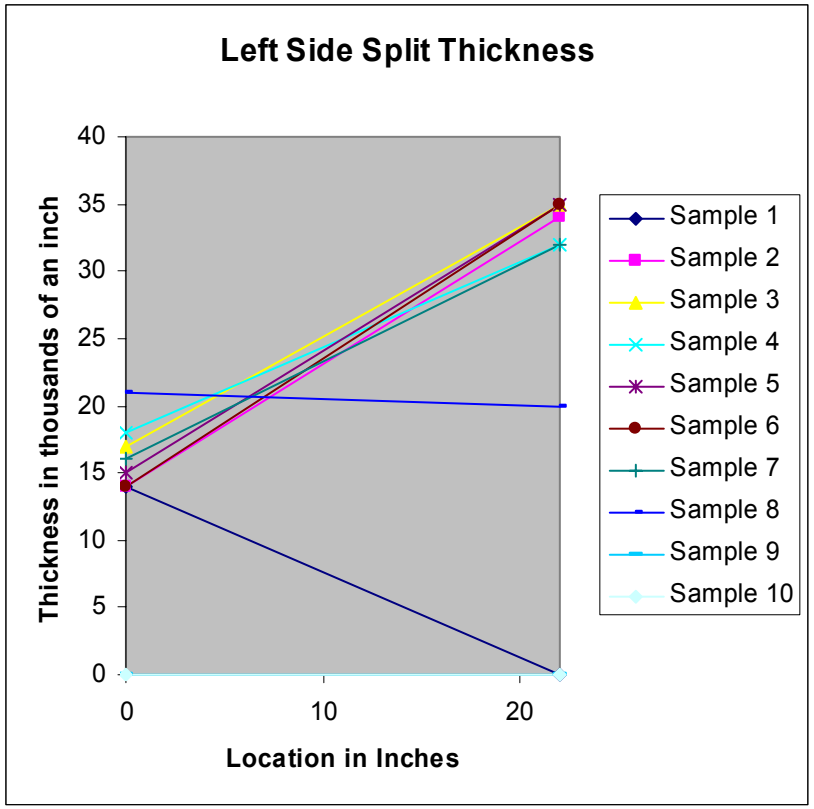

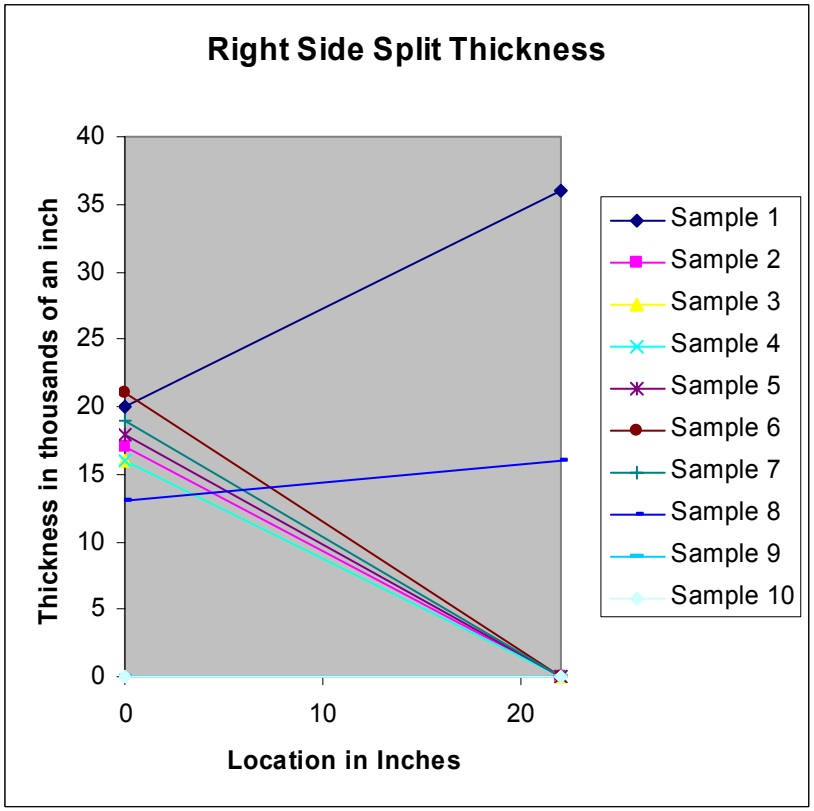

66.17% Moisture Content

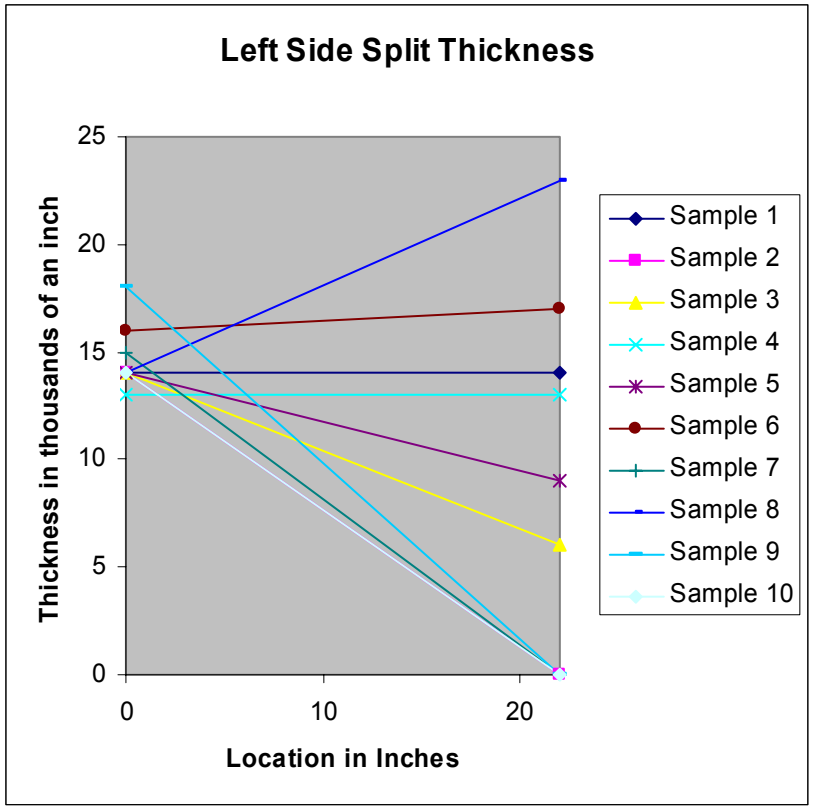

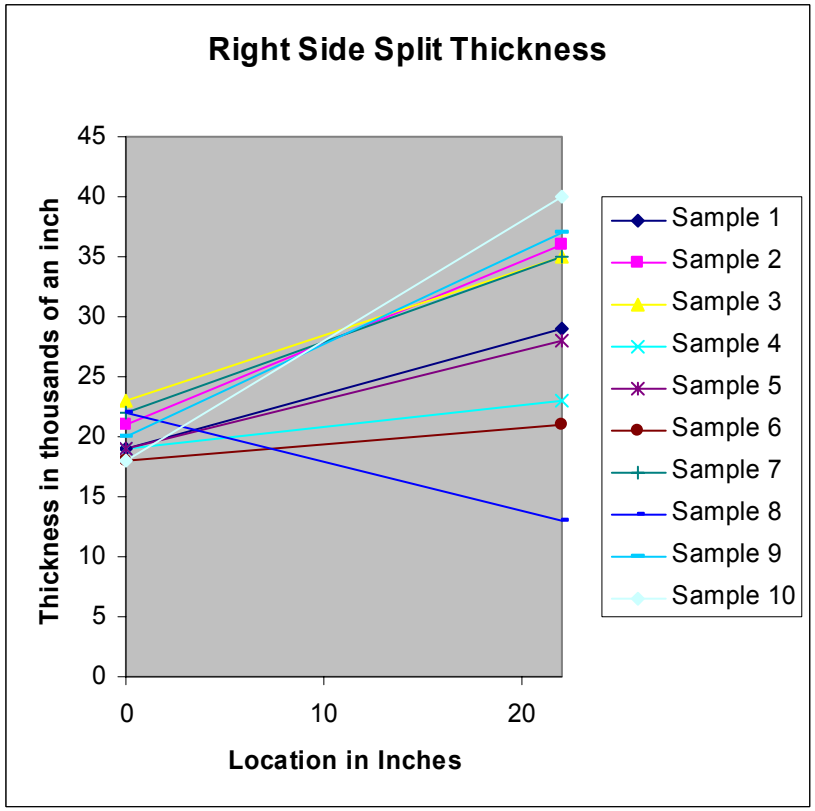

APPENDIX C: COMPUTED STRAINS

Computed Strains with No Additives

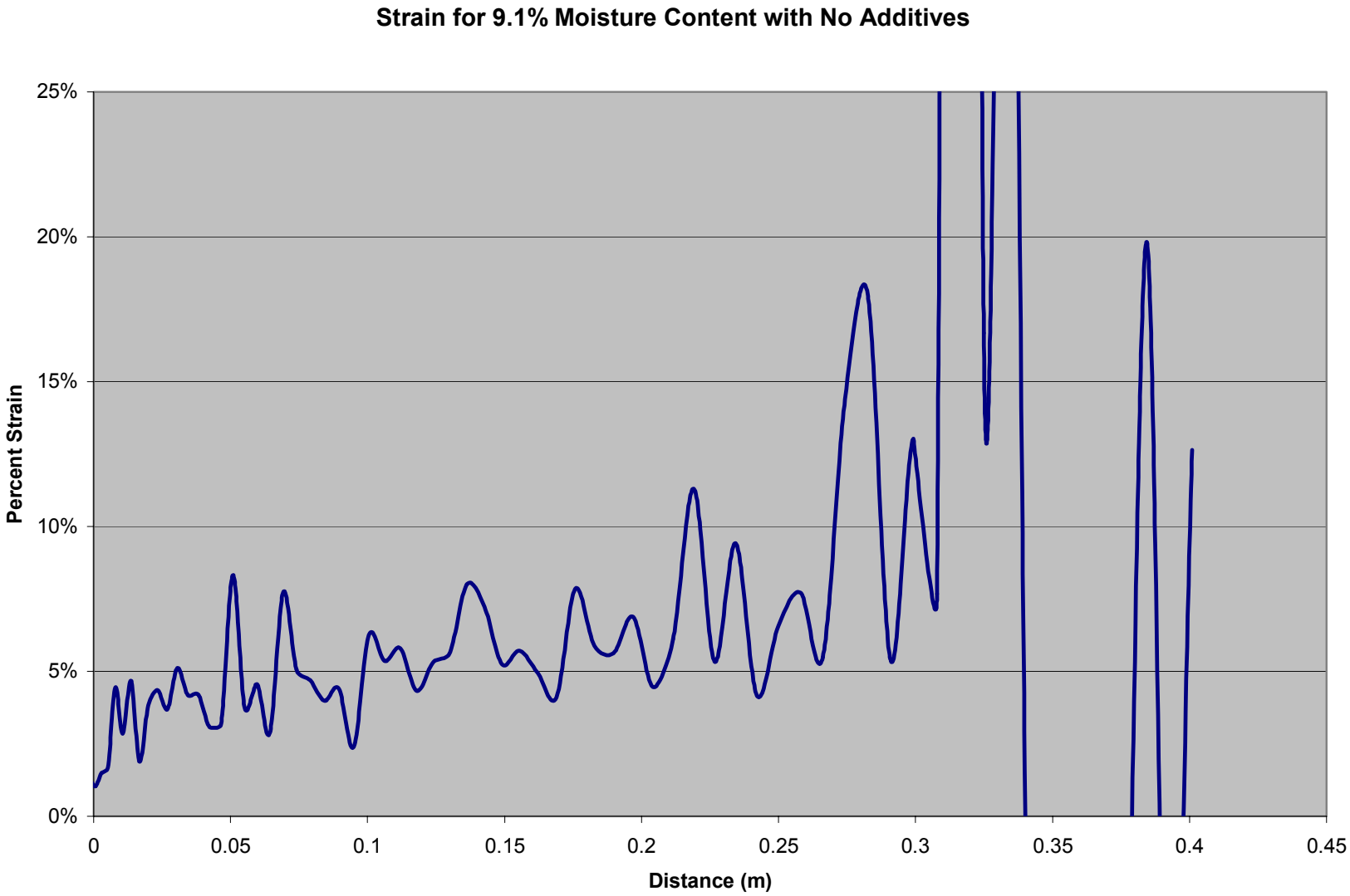
Strain for 9.1% Moisture Content with No Additives
Percent Strain
25%
20%
15%
10%
5%
0%
0
0.05
0.1
0.15
0.2
0.25
0.3
0.35
0.4
0.45
Distance (m)

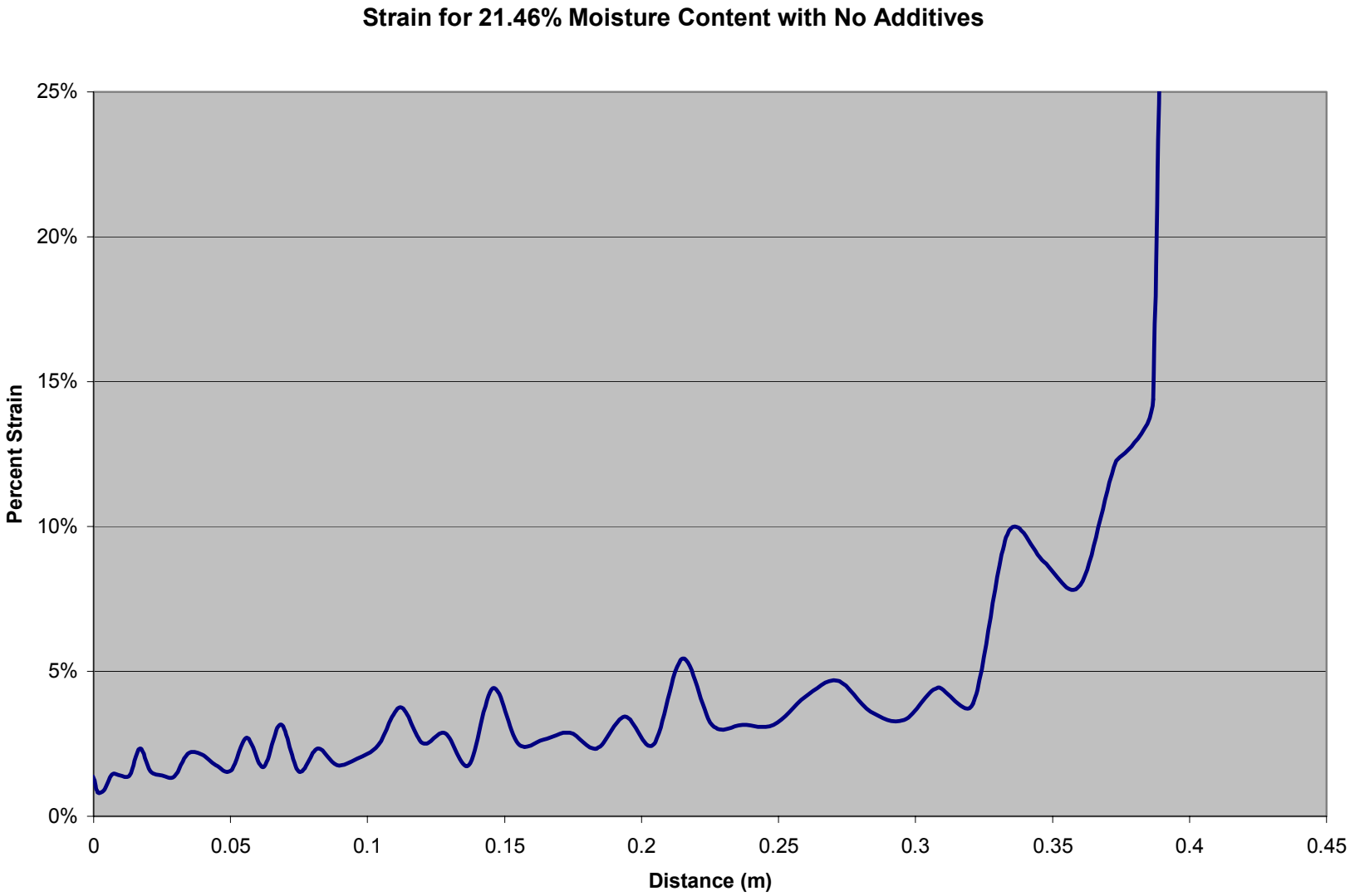
Strain for 21.46% Moisture Content with No Additives
Percent Strain
25%
20%
15%
10%
5%
0%
0
0.05
0.1
0.15
0.2
0.25
0.3
0.35
0.4
0.45
Distance (m)

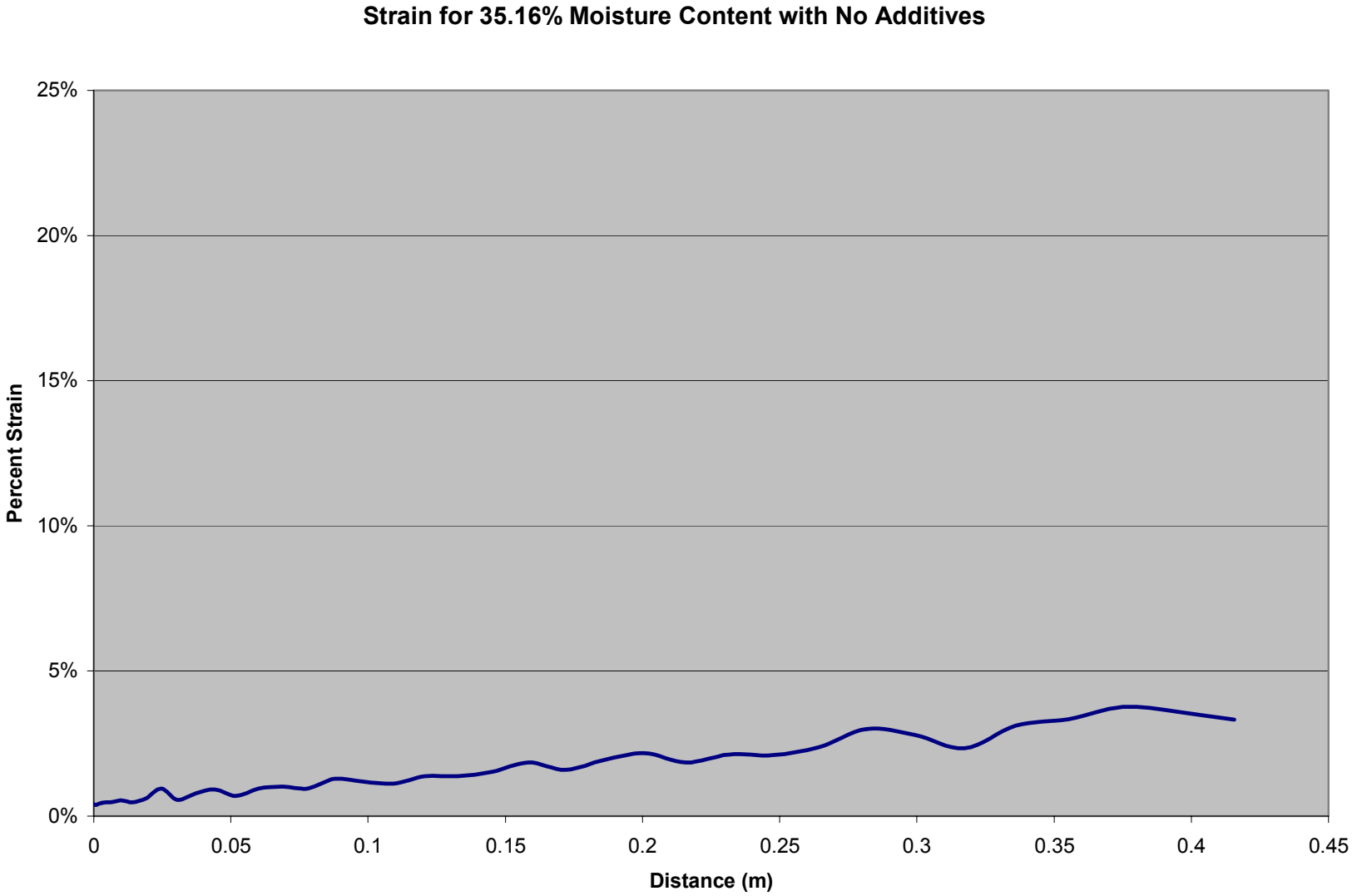
Strain for 35.16% Moisture Content with No Additives
Percent Strain
25%
20%
15%
10%
5%
0%
0
0.05
0.1
0.15
0.2
0.25
0.3
0.35
0.4
0.45
Distance (m)

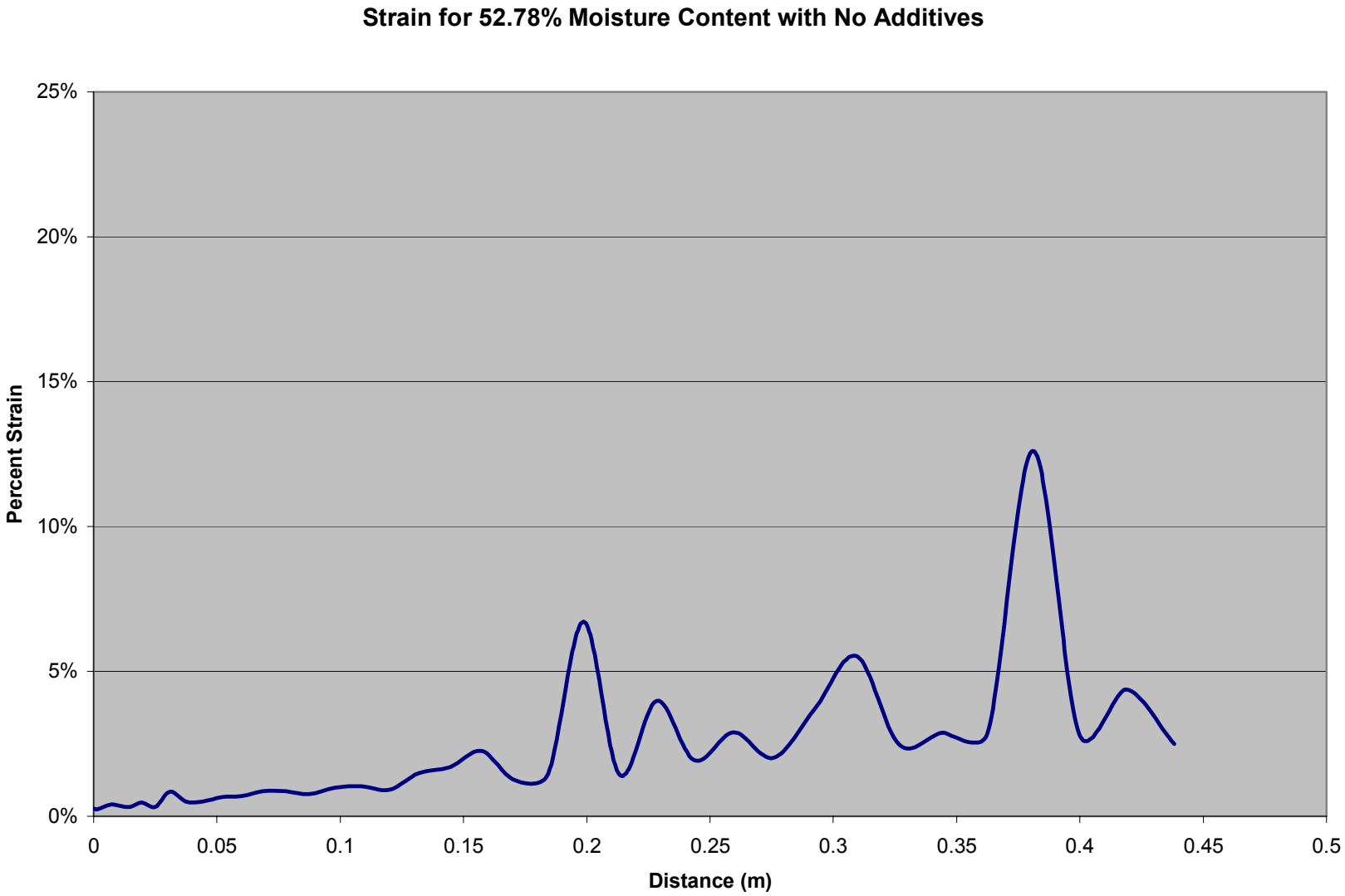
Strain for 52.78% Moisture Content with No Additives
Percent Strain
25%
20%
15%
10%
5%
0%
0
0.05
0.1
0.15
0.2
0.25
0.3
0.35
0.4
0.45
0.5
Distance (m)

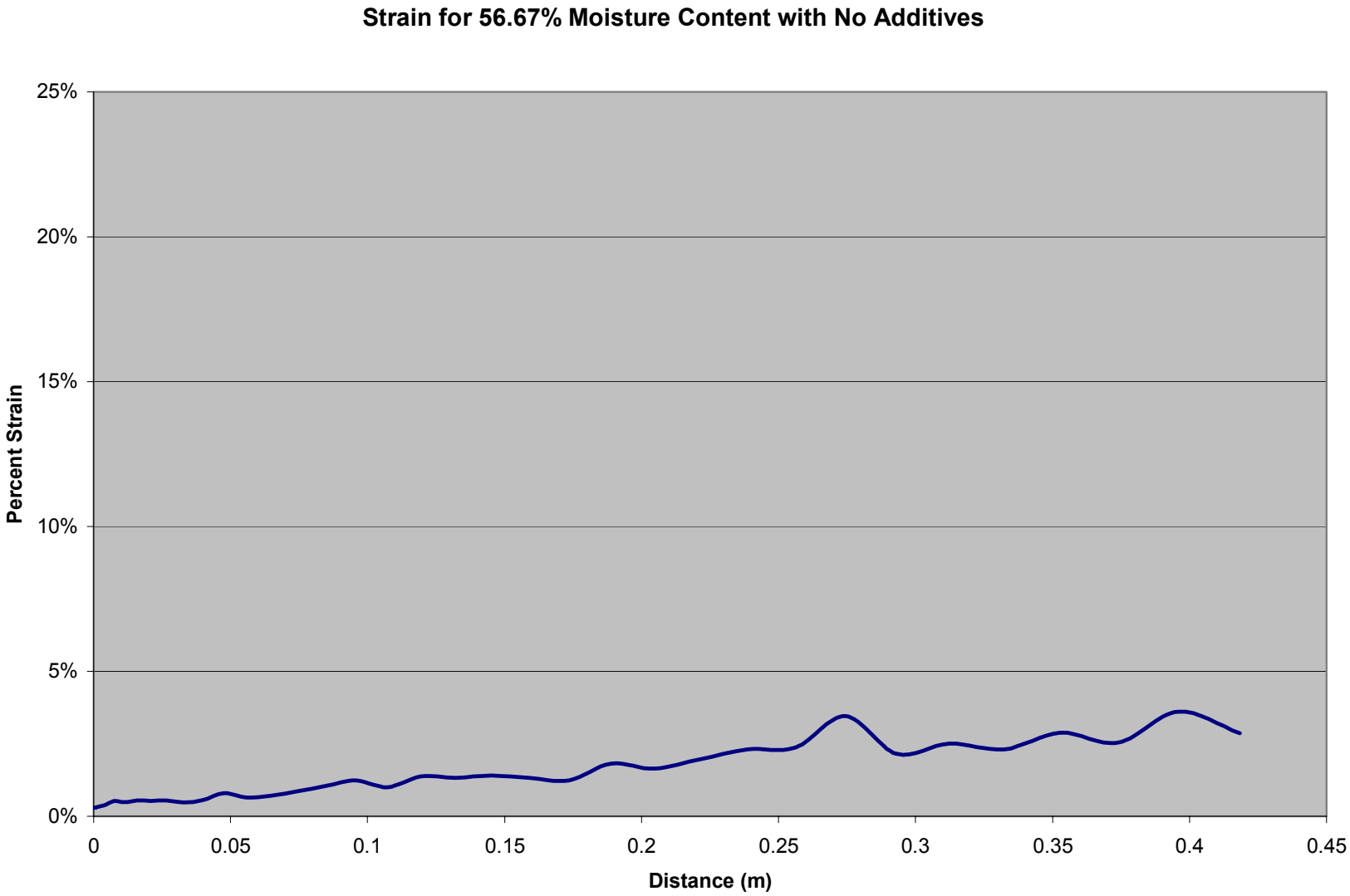
Strain for 56.67% Moisture Content with No Additives
25%
20%
15%
10%
5%
0%
Percent Strain
0
0.05
0.1
0.15
0.2
0.25
0.3
0.35
0.4
0.45
Distance (m)

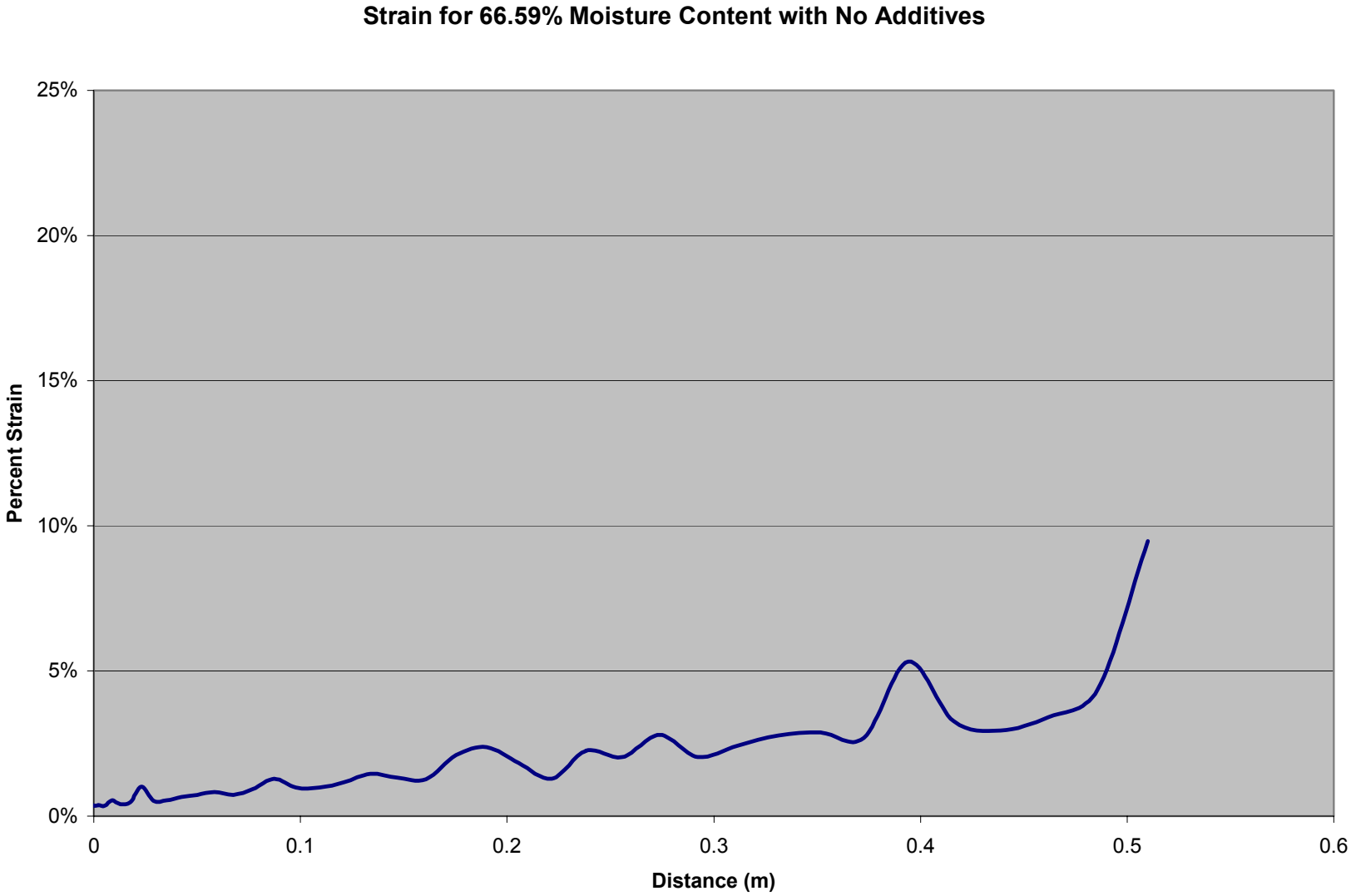
Strain for 66.59% Moisture Content with No Additives
25%
20%
15%
10%
5%
0%
Percent Strain
0
0.1
0.2
0.3
0.4
0.5
0.6
Distance (m)

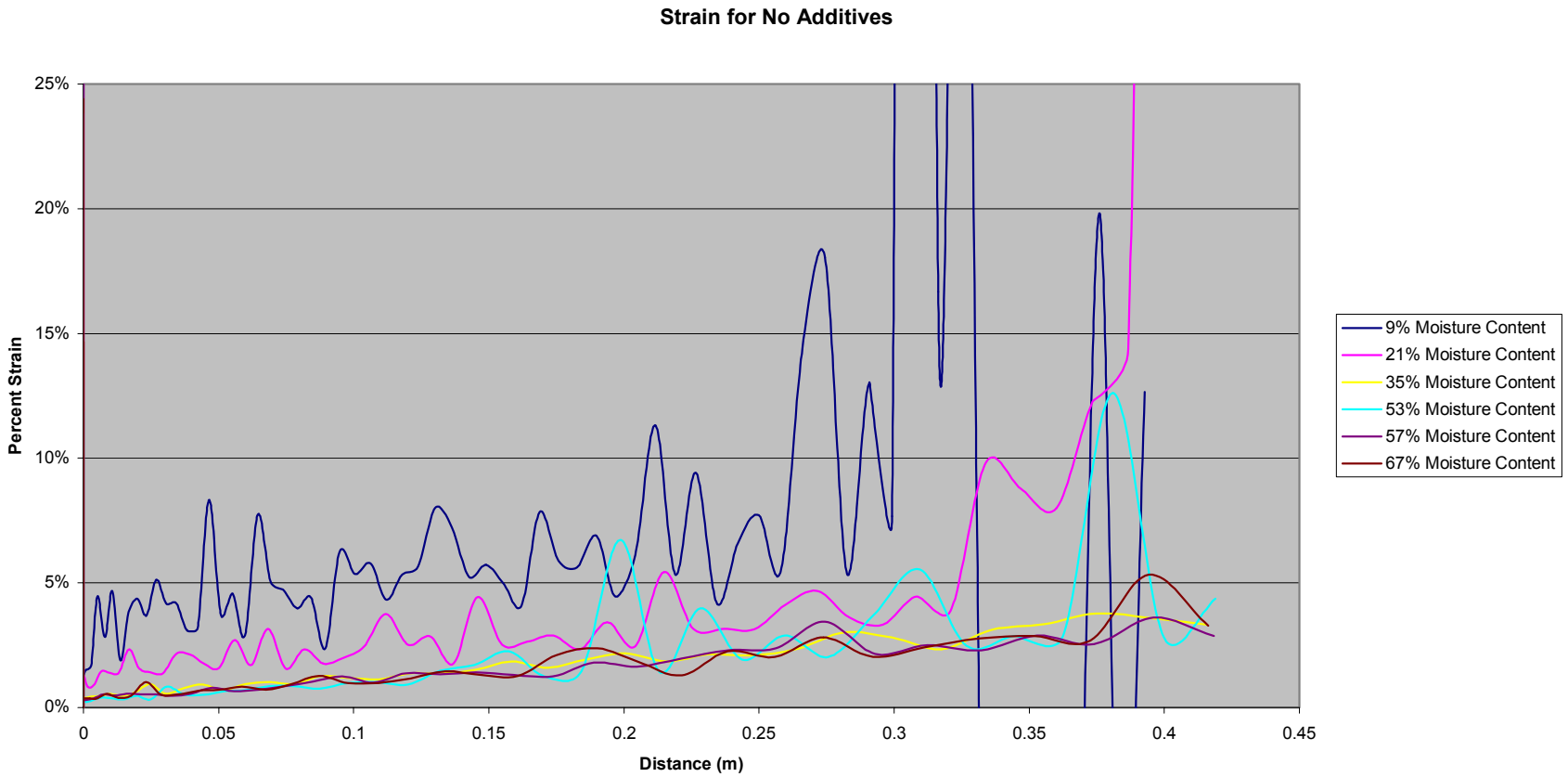
Strain for No Additives
25%
20%
15%
10%
5%
0%
Percent Strain
0
0.05
0.1
0.15
0.2
0.25
0.3
0.35
0.4
0.45
Distance (m)
9% Moisture Content
21% Moisture Content
35% Moisture Content
53% Moisture Content
57% Moisture Content
67% Moisture Content

Computed Strains with Debonder

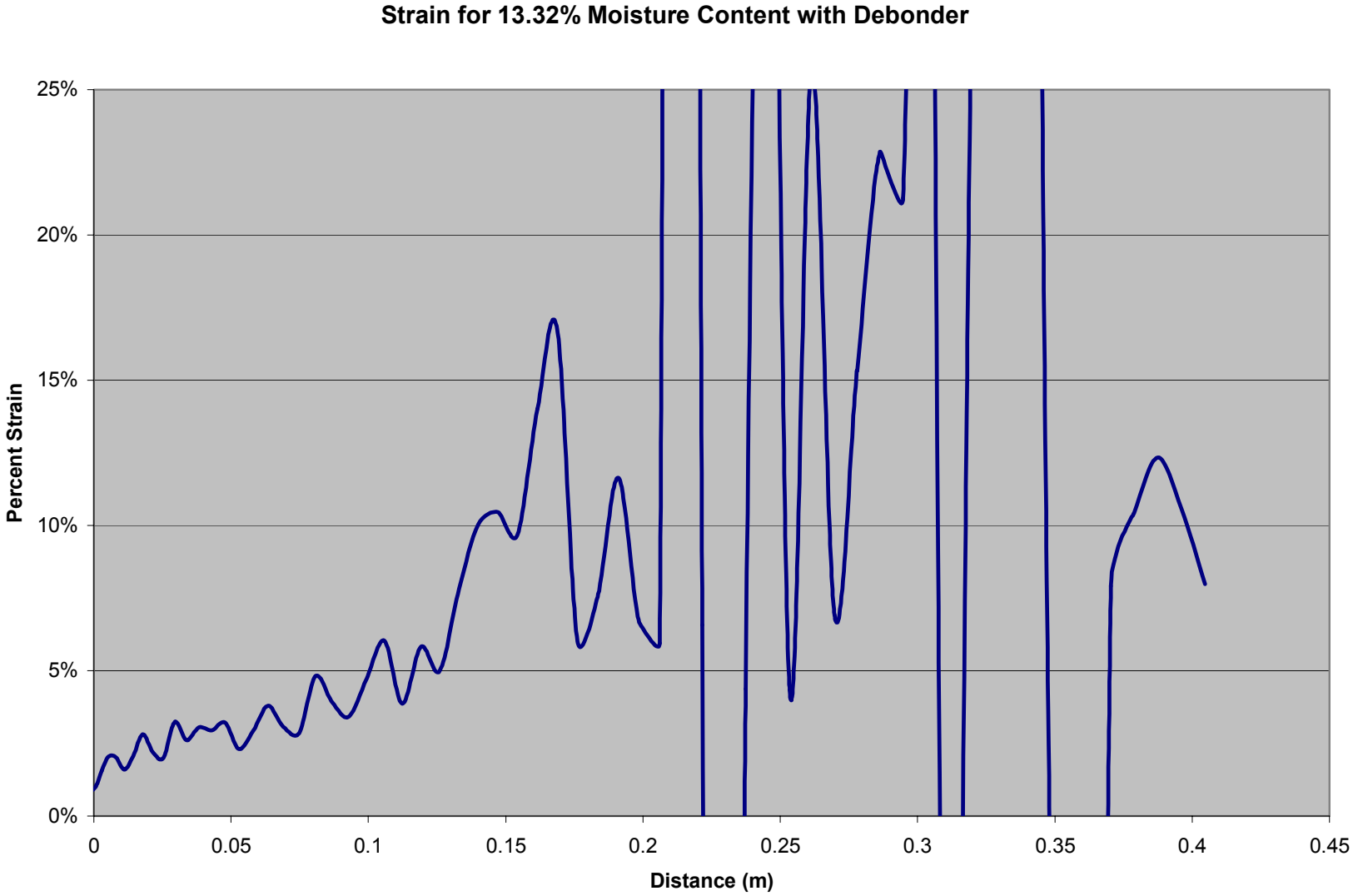
Strain for 13.32% Moisture Content with Debonder
Percent Strain
25%
20%
15%
10%
5%
0%
0
0.05
0.1
0.15
0.2
0.25
0.3
0.35
0.4
0.45
Distance (m)

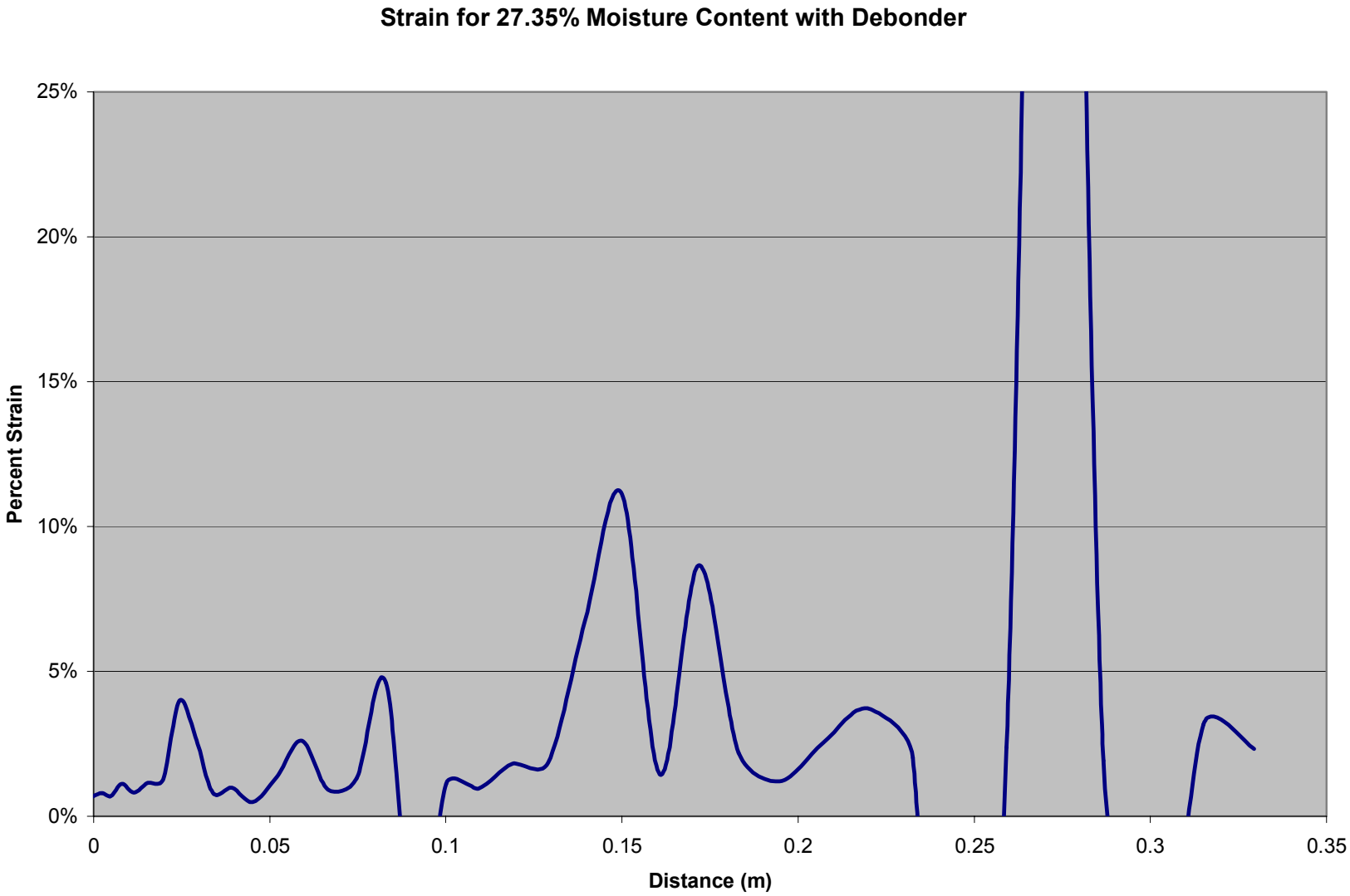
Strain for 27.35% Moisture Content with Debonder
Percent Strain
25%
20%
15%
10%
5%
0%
0
0.05
0.1
0.15
0.2
0.25
0.3
0.35
Distance (m)

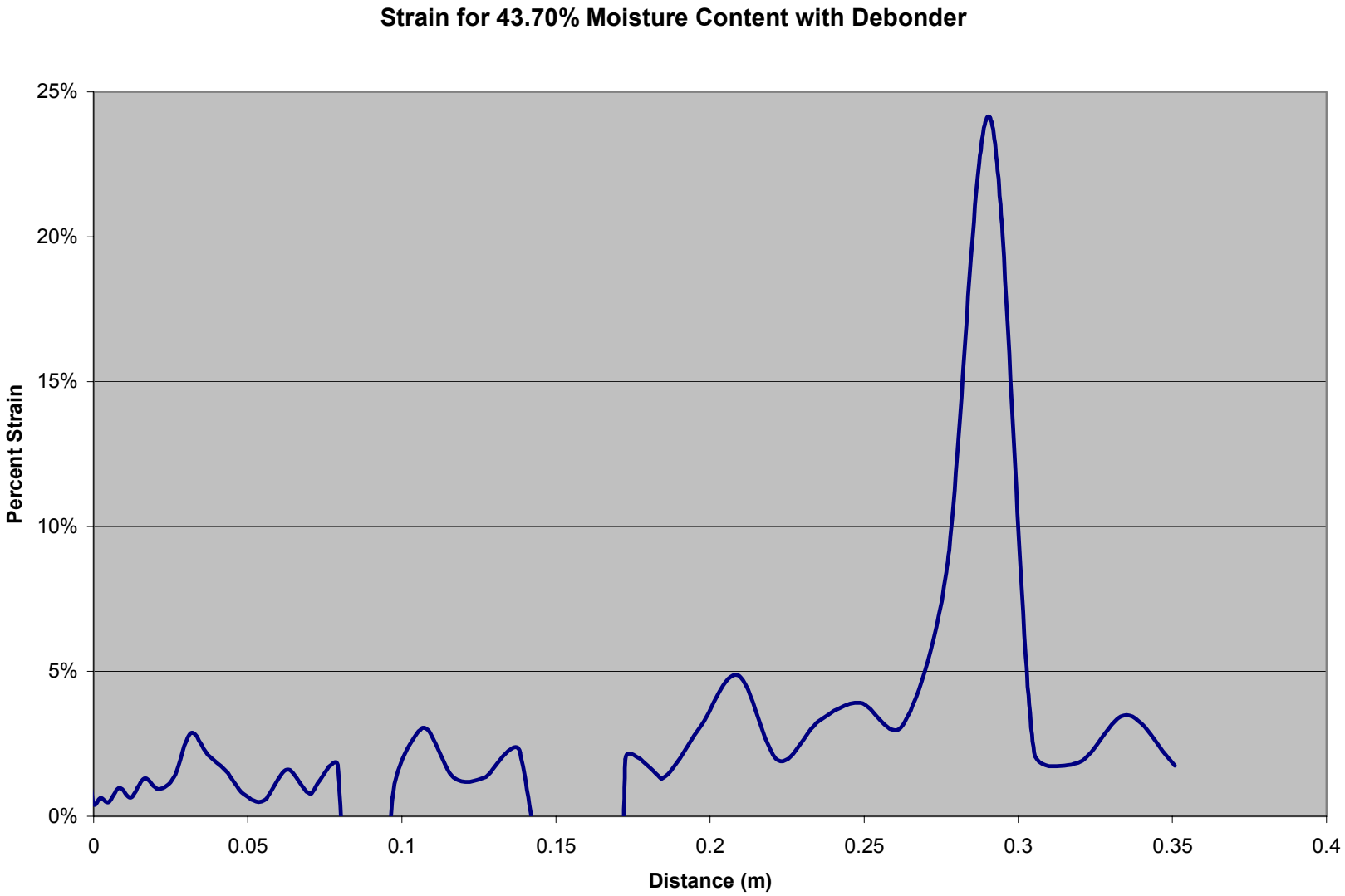
Strain for 43.70% Moisture Content with Debonder
25%
20%
15%
10%
5%
0%
Percent Strain
0
0.05
0.1
0.15
0.2
0.25
0.3
0.35
0.4
Distance (m)

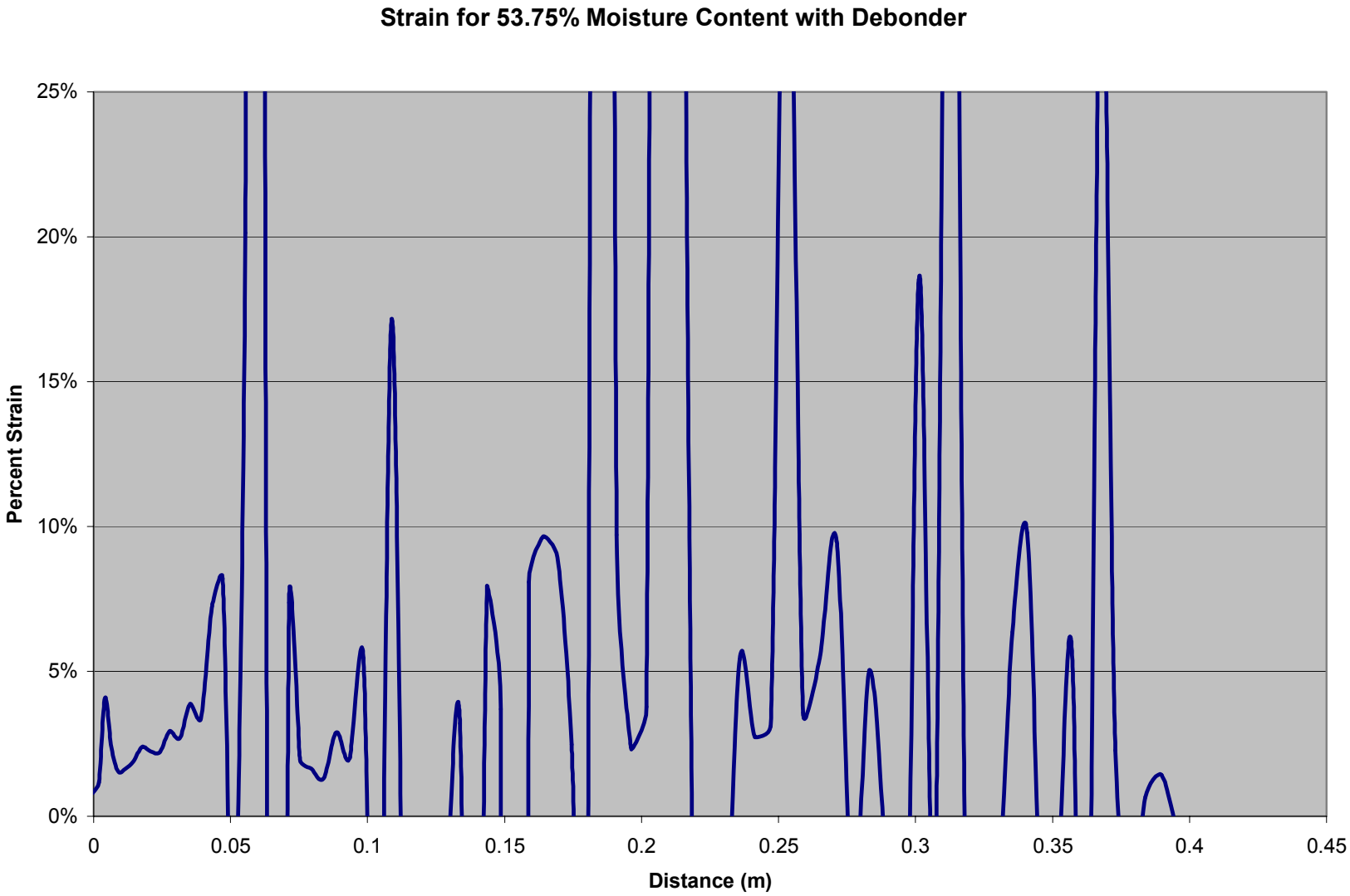
Strain for 53.75% Moisture Content with Debonder
Percent Strain
25%
20%
15%
10%
5%
0%
0
0.05
0.1
0.15
0.2
0.25
0.3
0.35
0.4
0.45
Distance (m)

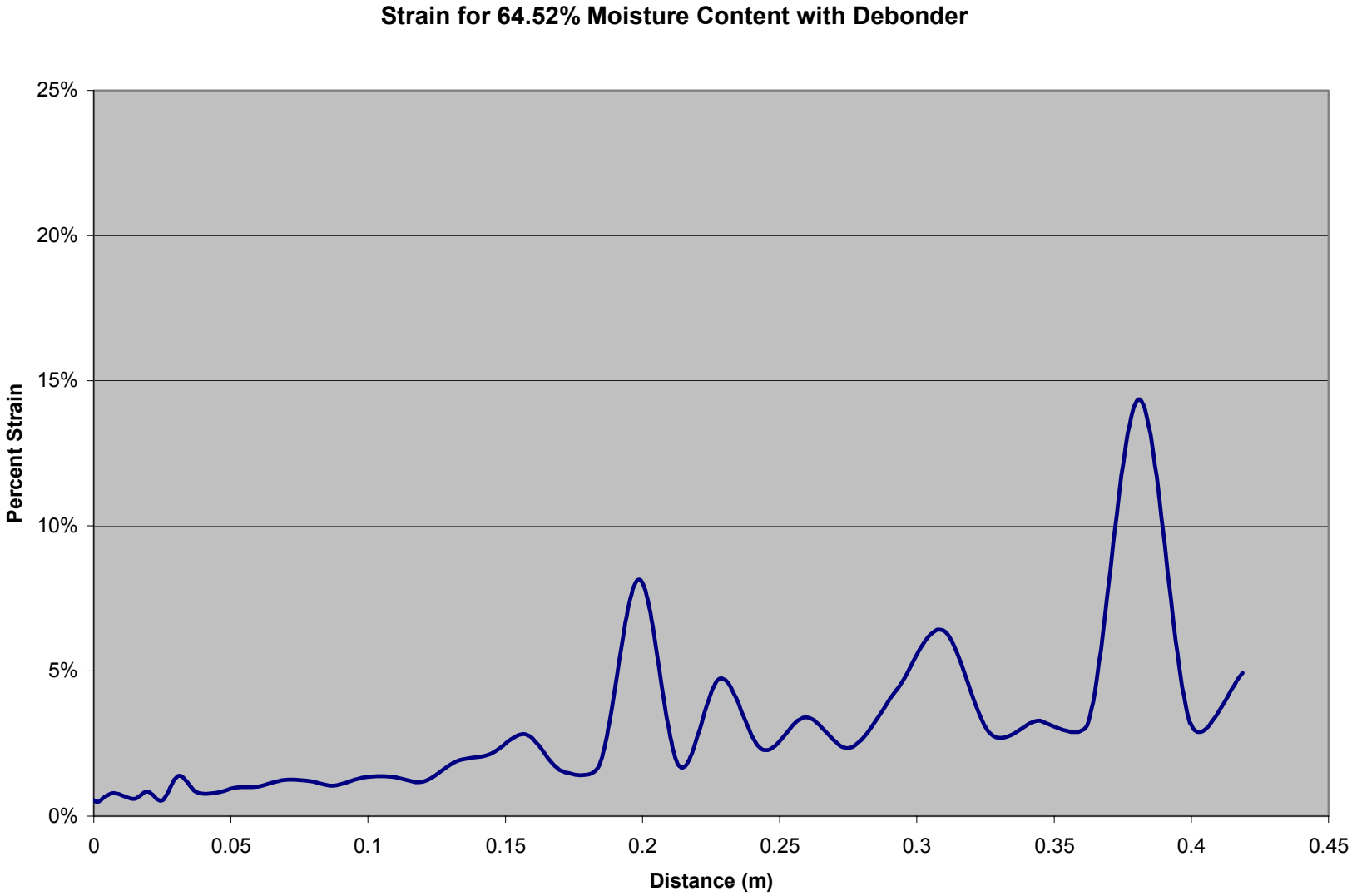
Strain for 64.52% Moisture Content with Debonder
Percent Strain
25%
20%
15%
10%
5%
0%
0
0.05
0.1
0.15
0.2
0.25
0.3
0.35
0.4
0.45
Distance (m)

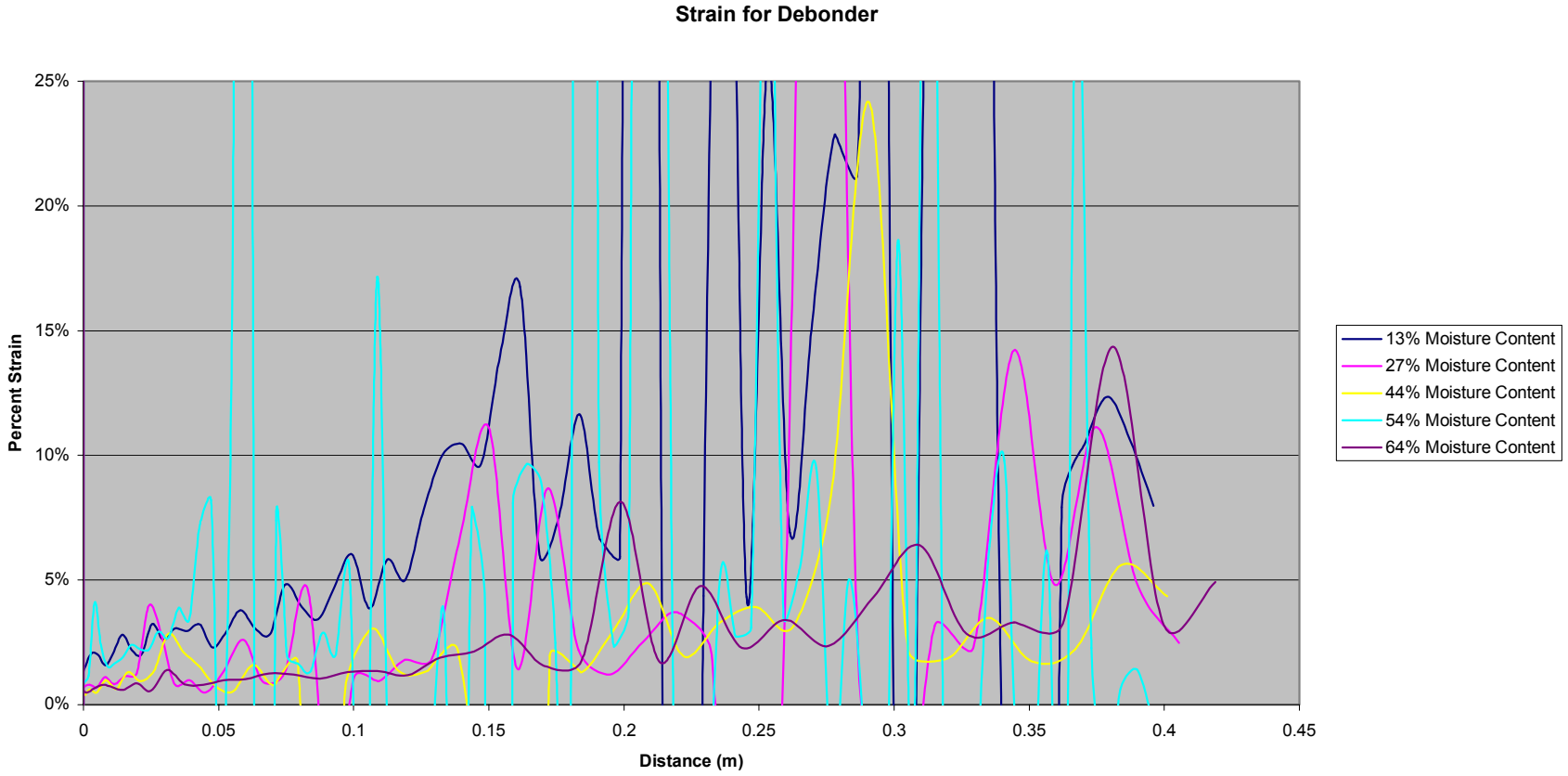
Strain for Debonder
25%
20%
15%
10%
5%
0%
Percent Strain
0
0.05
0.1
0.15
0.2
0.25
0.3
0.35
0.4
0.45
Distance (m)
13% Moisture Content
27% Moisture Content
44% Moisture Content
54% Moisture Content
64% Moisture Content

Computed Strains with Bonder

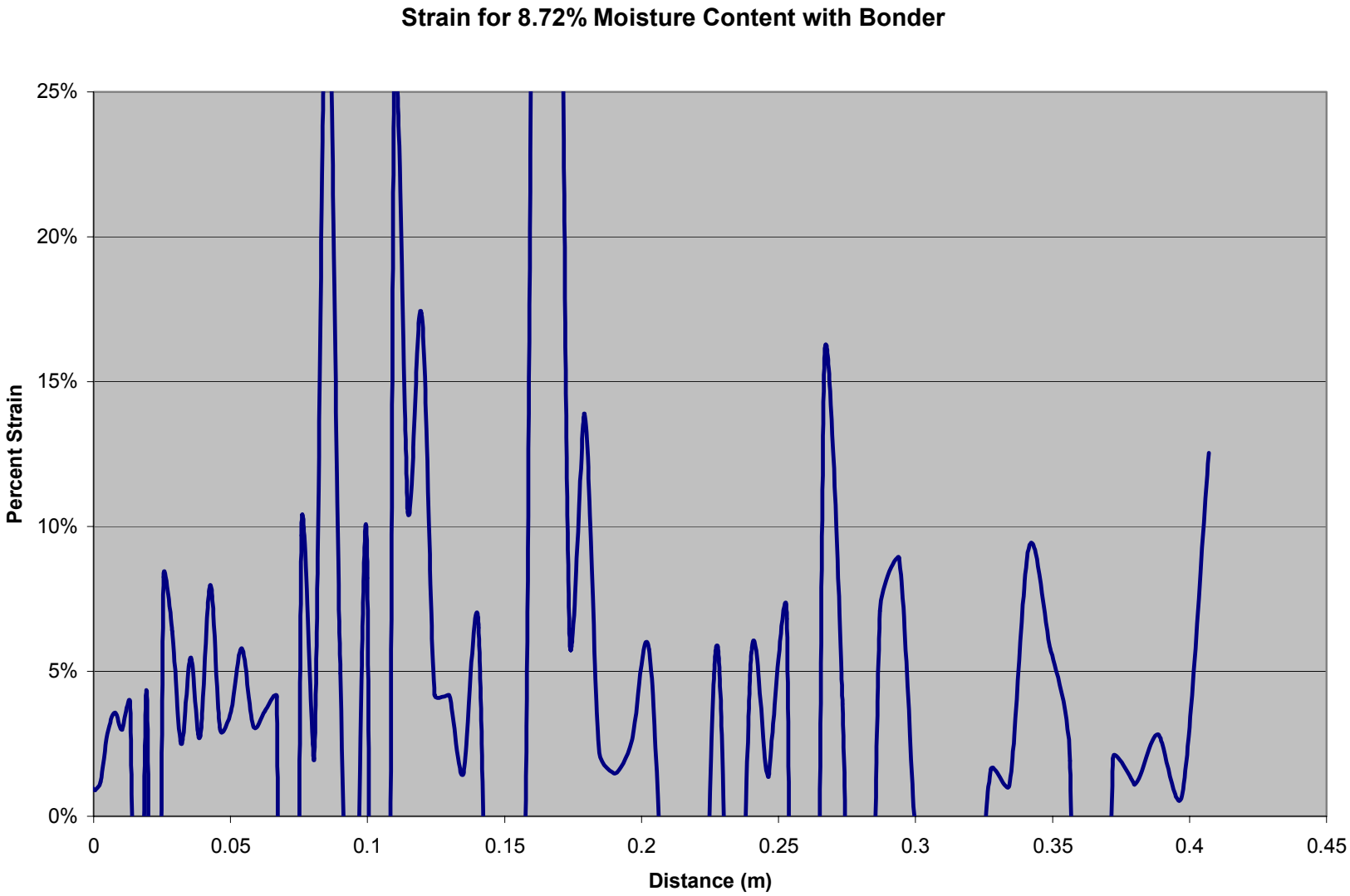
Strain for 8.72% Moisture Content with Bonder
Percent Strain
25%
20%
15%
10%
5%
0%
0
0.05
0.1
0.15
0.2
0.25
0.3
0.35
0.4
0.45
Distance (m)

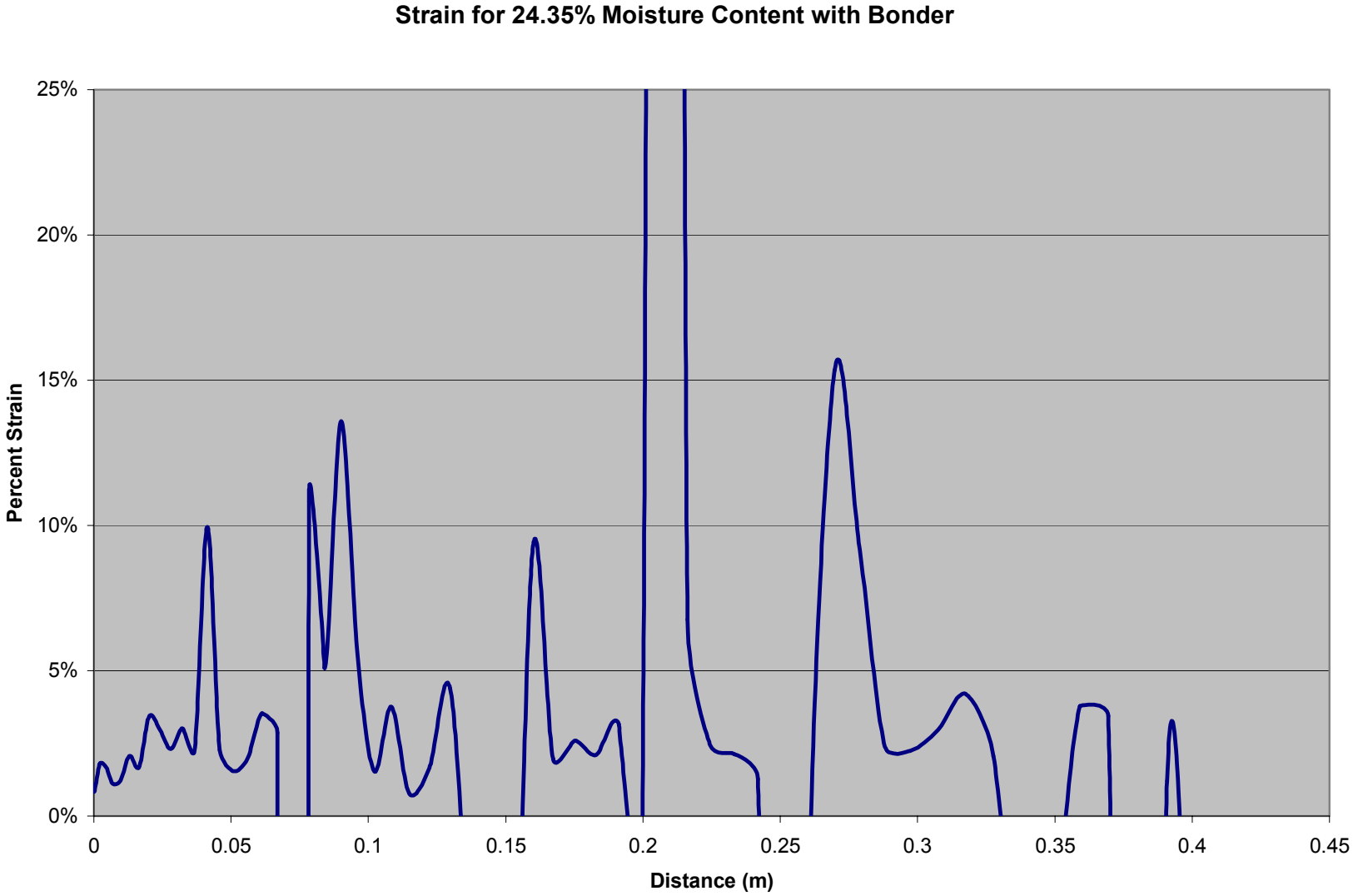
Strain for 24.35% Moisture Content with Bonder
Percent Strain
25%
20%
15%
10%
5%
0%
0
0.05
0.1
0.15
0.2
0.25
0.3
0.35
0.4
0.45
Distance (m)

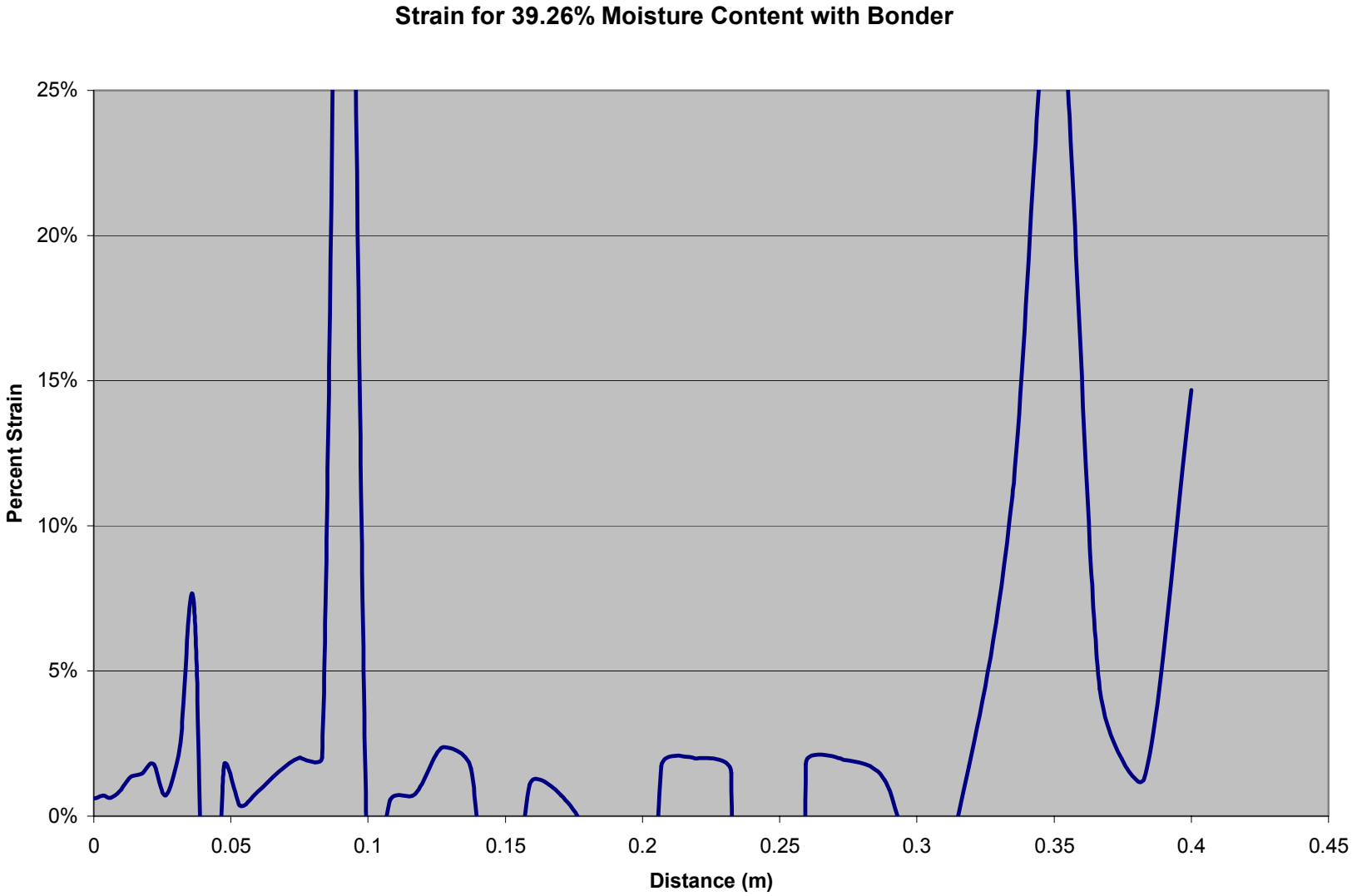
Strain for 39.26% Moisture Content with Bonder
Percent Strain
25%
20%
15%
10%
5%
0%
0
0.05
0.1
0.15
0.2
0.25
0.3
0.35
0.4
0.45
Distance (m)

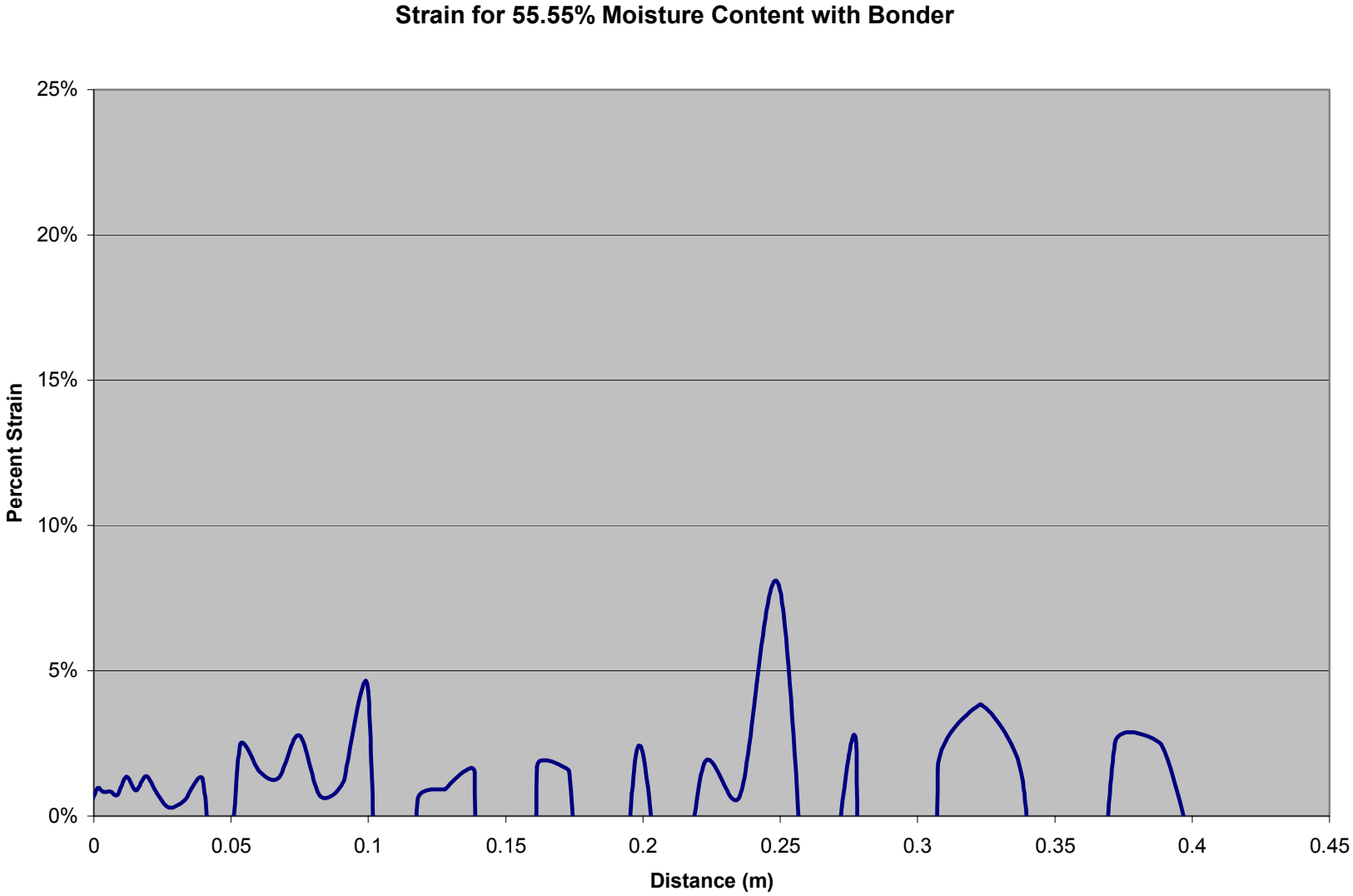
Strain for 55.55% Moisture Content with Bonder
25%
20%
15%
10%
5%
0%
Percent Strain
0
0.05
0.1
0.15
0.2
0.25
0.3
0.35
0.4
0.45
Distance (m)

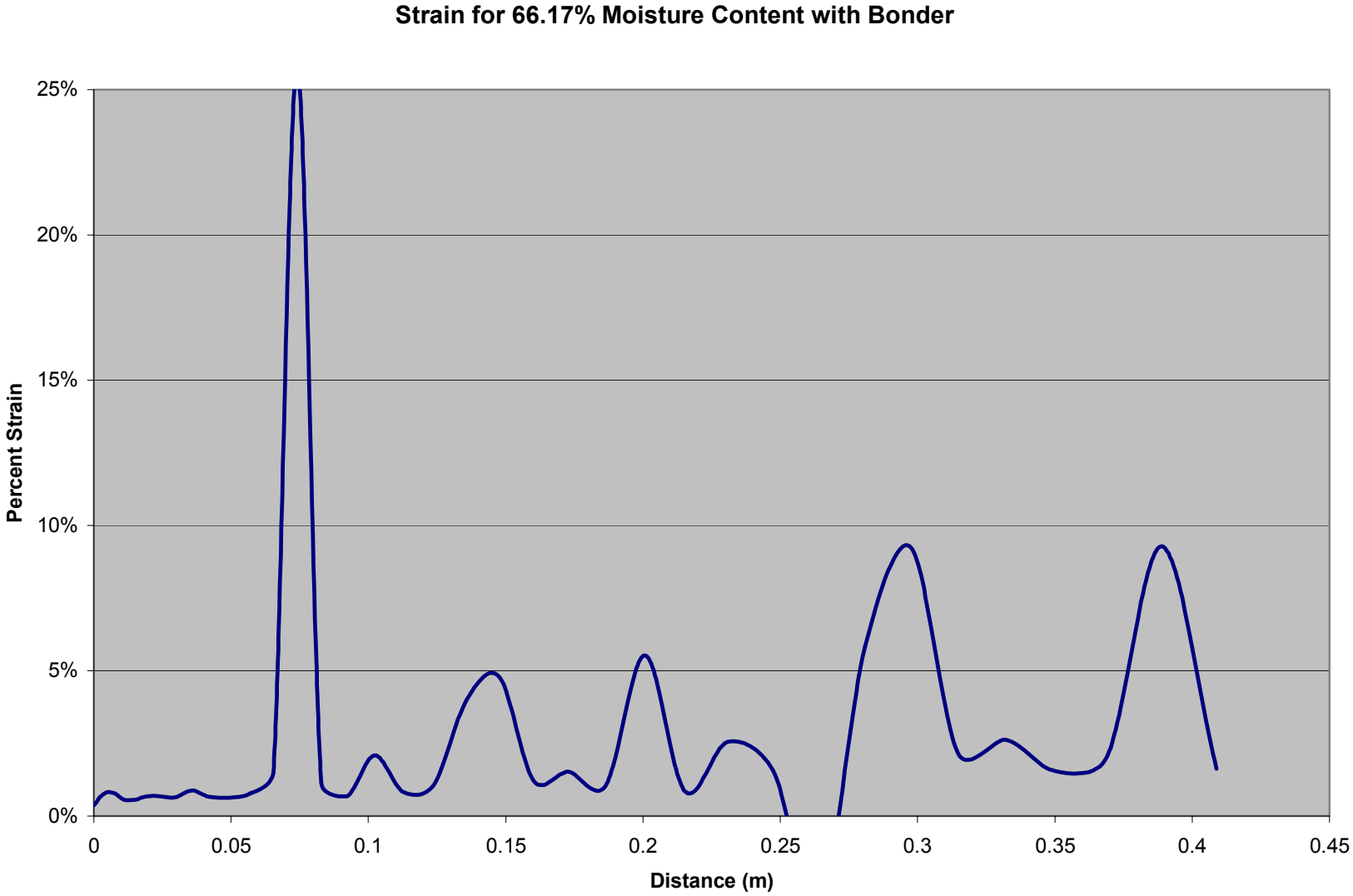
Strain for 66.17% Moisture Content with Bonder
Percent Strain
25%
20%
15%
10%
5%
0%
0
0.05
0.1
0.15
0.2
0.25
0.3
0.35
0.4
0.45
Distance (m)

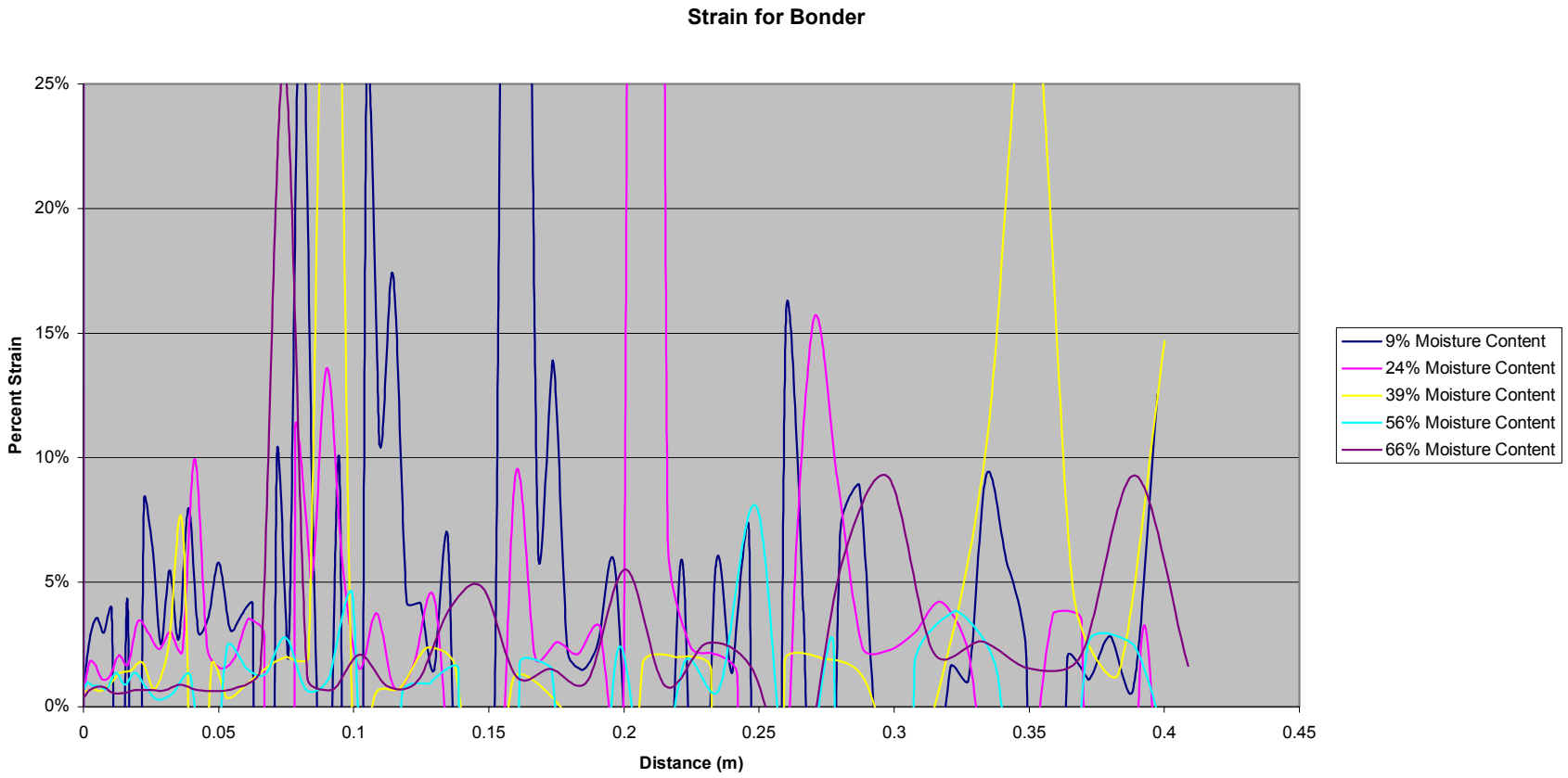
Strain for Bonder
25%
20%
15%
10%
5%
0%
Percent Strain
0
0.05
0.1
0.15
0.2
0.25
0.3
0.35
0.4
0.45
Distance (m)
9% Moisture Content
24% Moisture Content
39% Moisture Content
56% Moisture Content
66% Moisture Content

APPENDIX D: LOAD VERSUS DISPLACEMENT

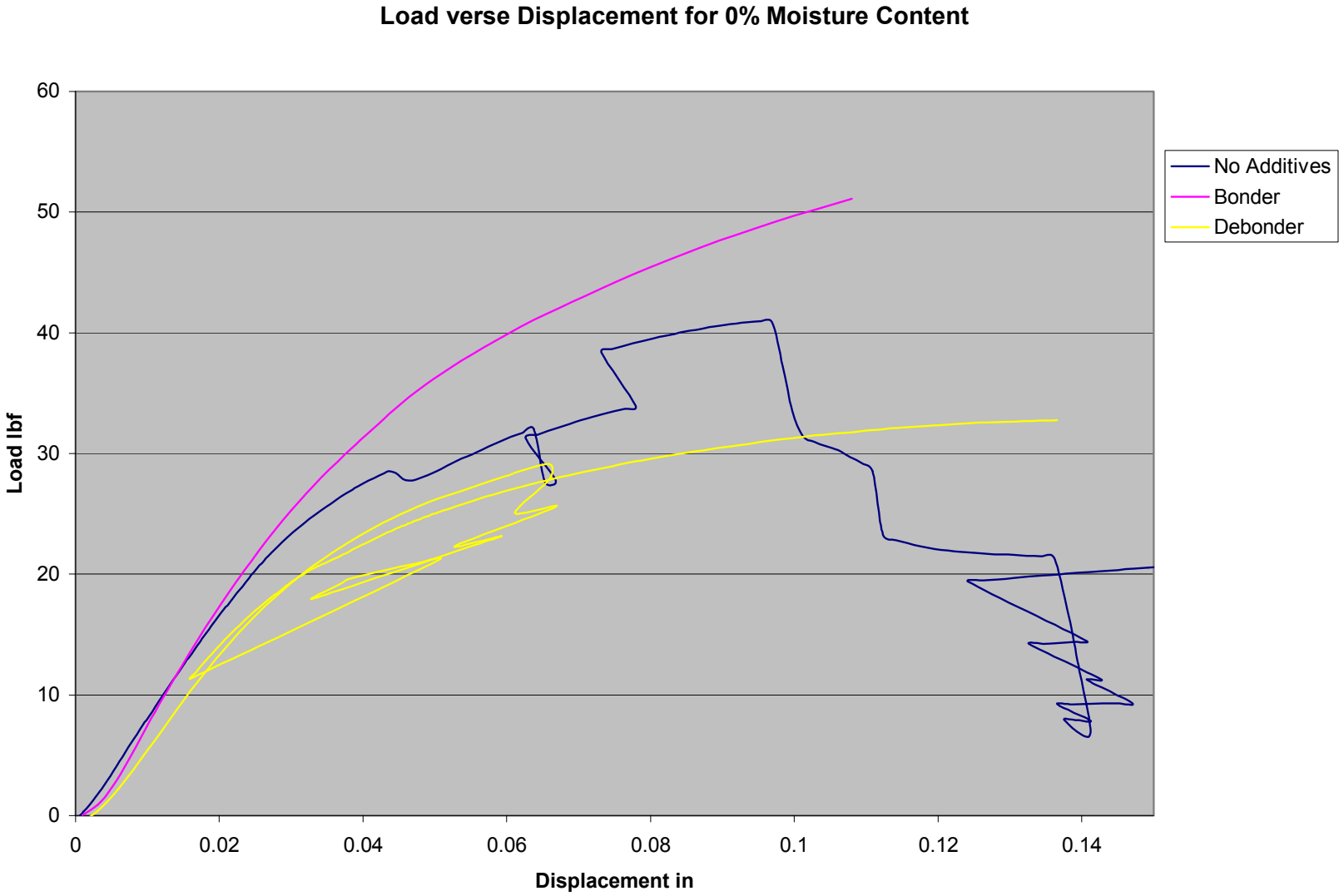
Load verse Displacement for 0% Moisture Content
Load lbf
60
50
40
30
20
10
0
0
0.02
0.04
0.06
0.08
0.1
0.12
0.14
Displacement in
No Additives
Bonder
Debonder

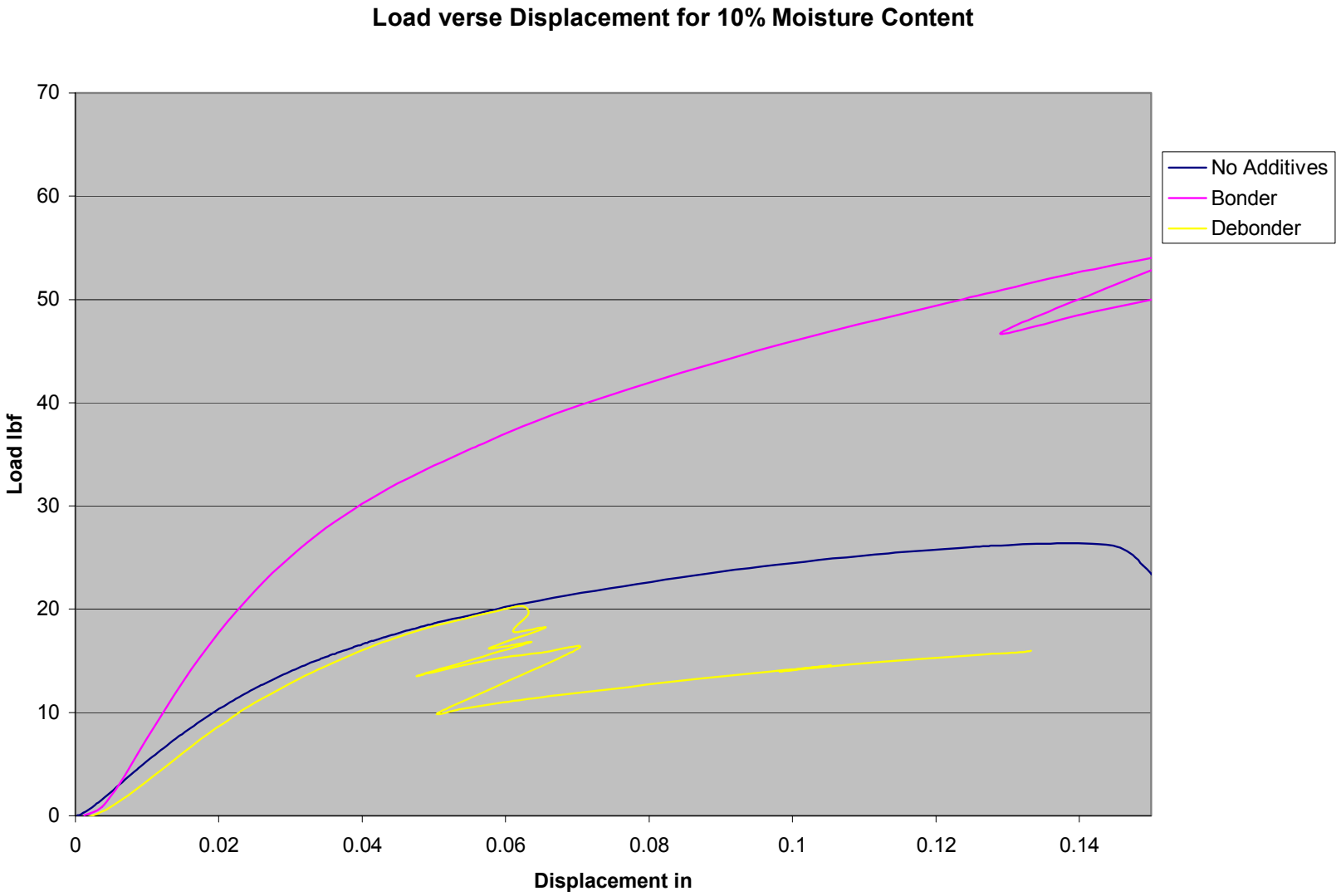
Load verse Displacement for 10% Moisture Content
70
60
50
40
30
20
10
0
Load lbf
0
0.02
0.04
0.06
0.08
0.1
0.12
0.14
Displacement in
No Additives
Bonder
Debonder

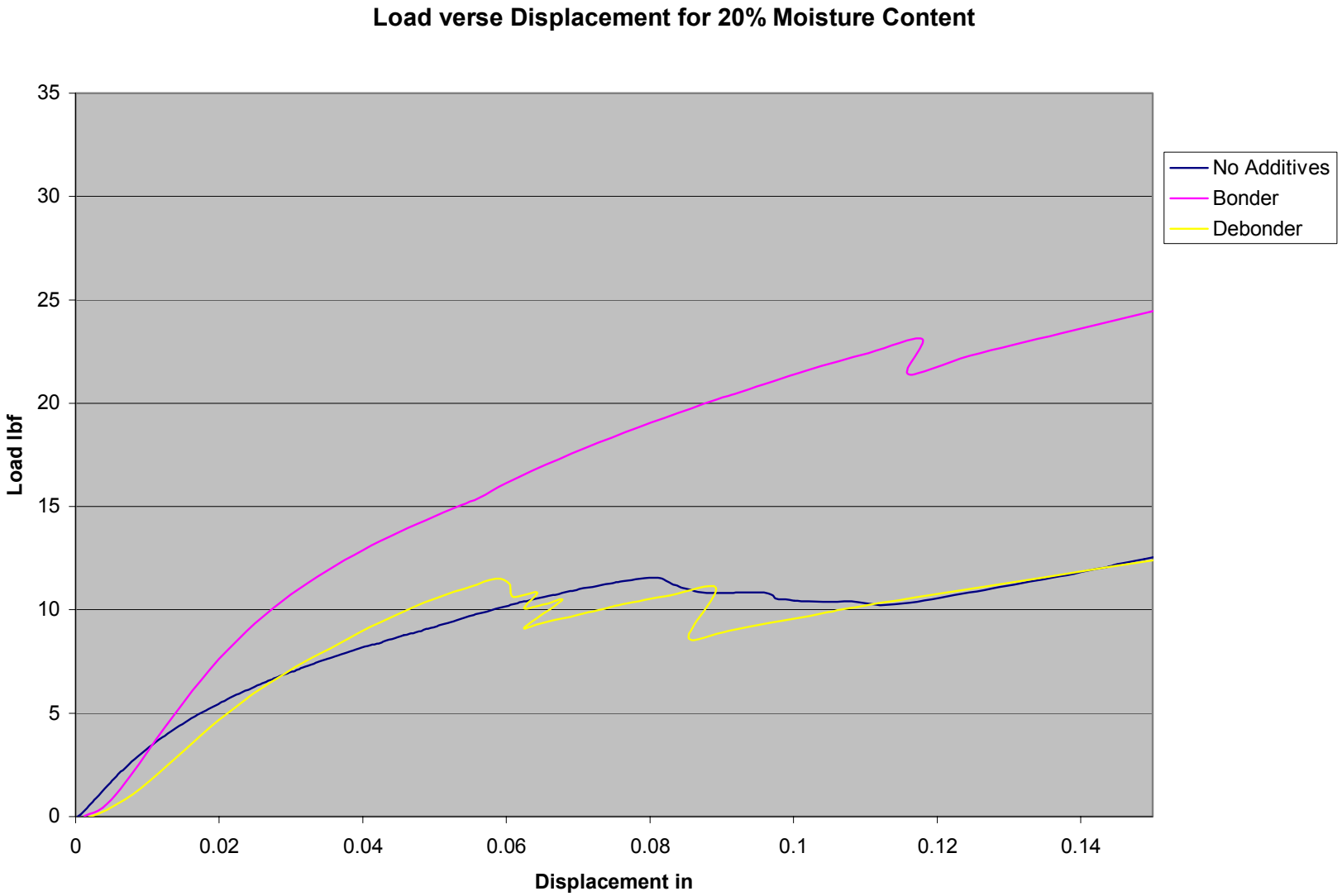
Load verse Displacement for 20% Moisture Content
Load lbf
35
30
25
20
15
10
5
0
0
0.02
0.04
0.06
0.08
0.1
0.12
0.14
Displacement in
No Additives
Bonder
Debonder

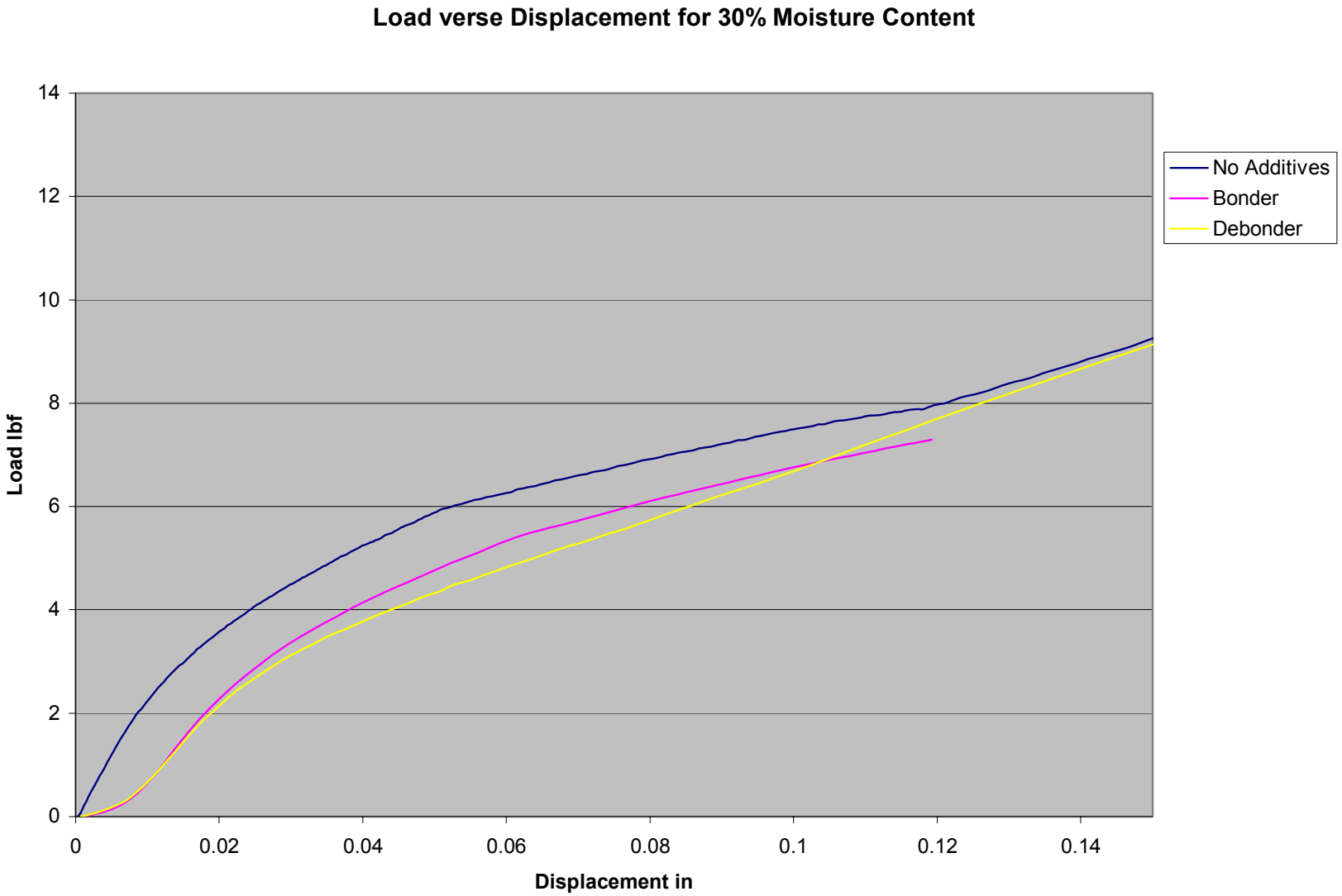
Load verse Displacement for 30% Moisture Content
Load lbf
Displacement in
0
2
4
6
8
10
12
14
0
0.02
0.04
0.06
0.08
0.1
0.12
0.14
No Additives
Bonder
Debonder

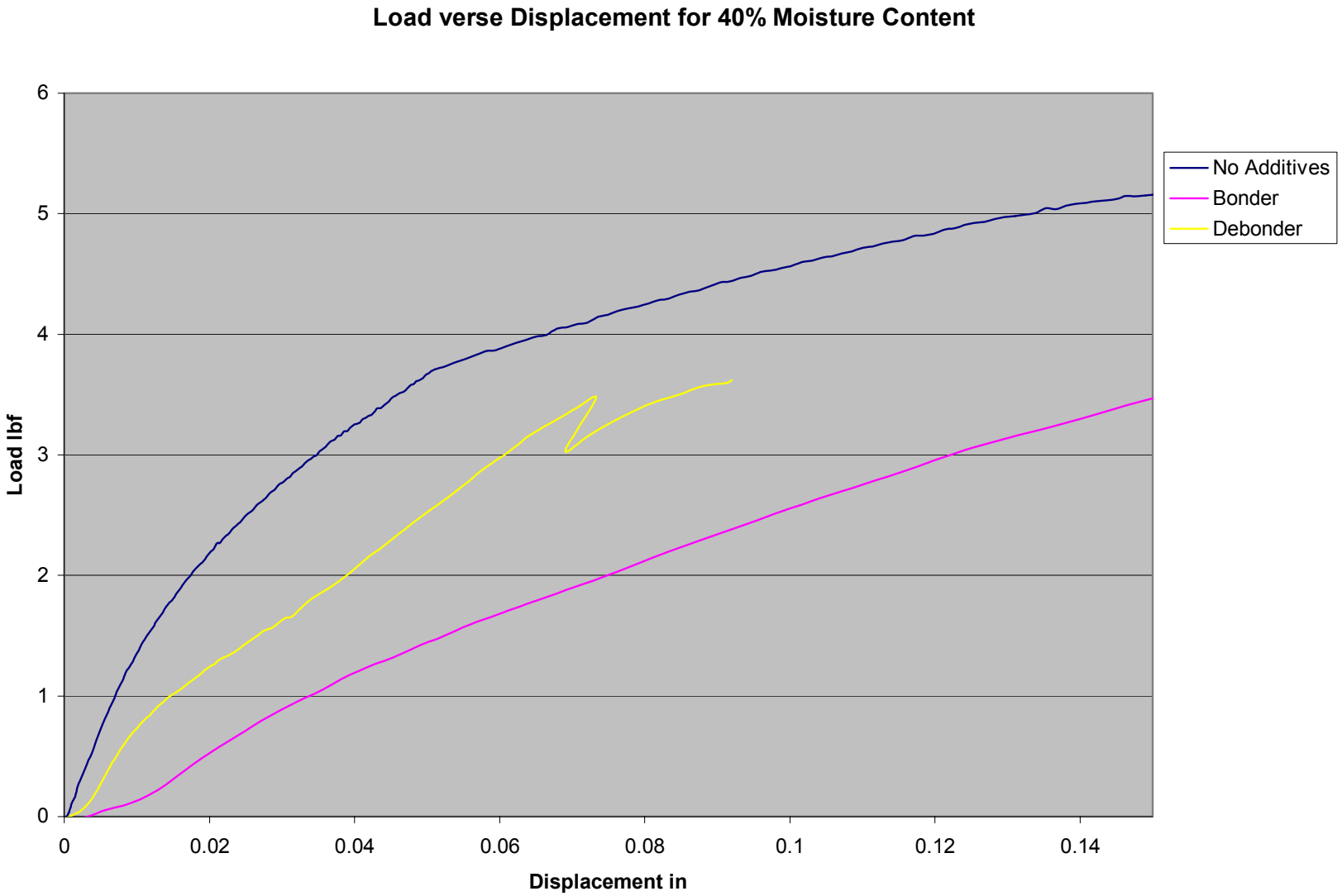
Load verse Displacement for 40% Moisture Content
Load lbf
Displacement in
0
1
2
3
4
5
6
0
0.02
0.04
0.06
0.08
0.1
0.12
0.14
No Additives
Bonder
Debonder

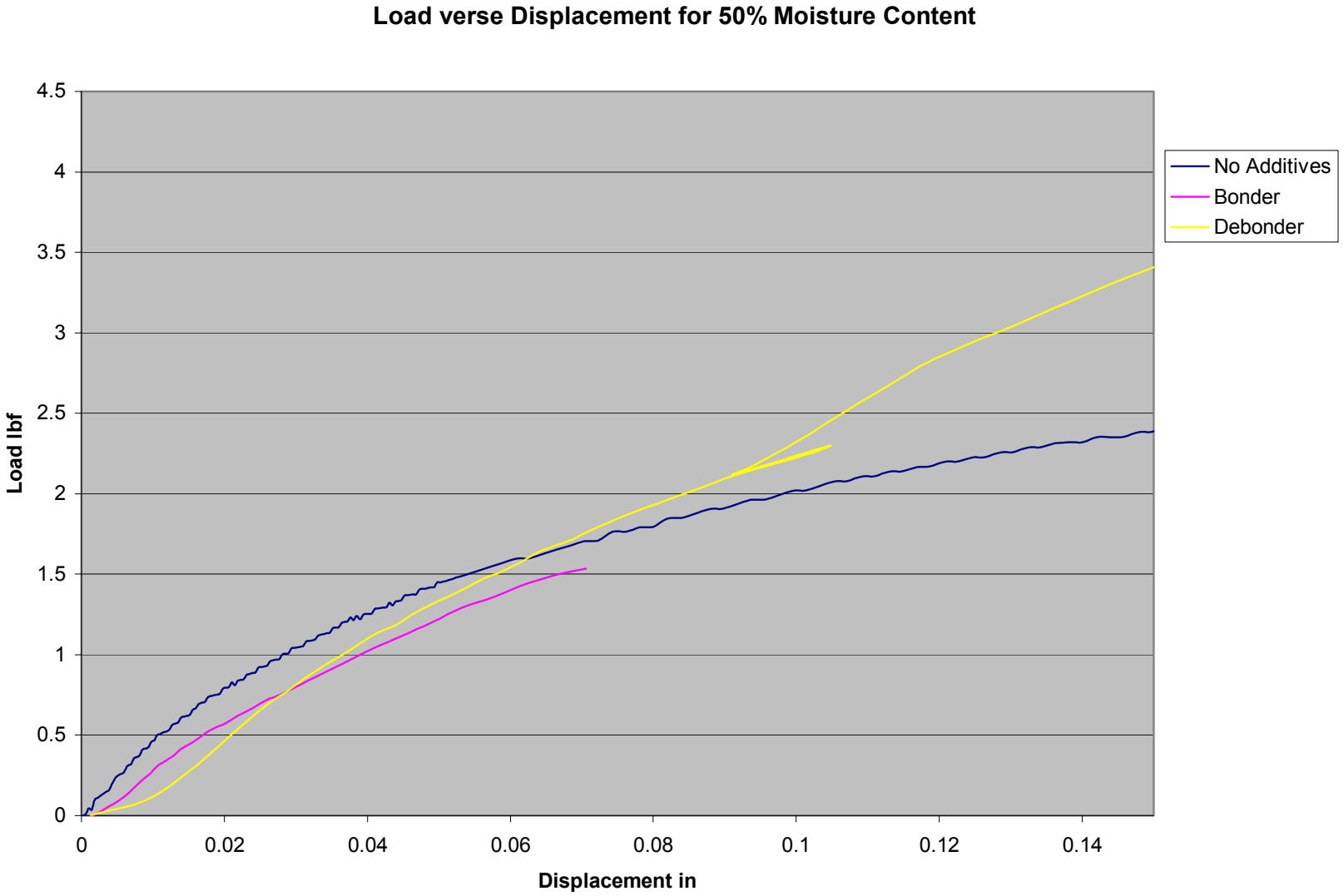
Load verse Displacement for 50% Moisture Content
Load lbf
4.5
4
3.5
3
2.5
2
1.5
1
0.5
0
0
0.02
0.04
0.06
0.08
0.1
0.12
0.14
Displacement in
No Additives
Bonder
Debonder

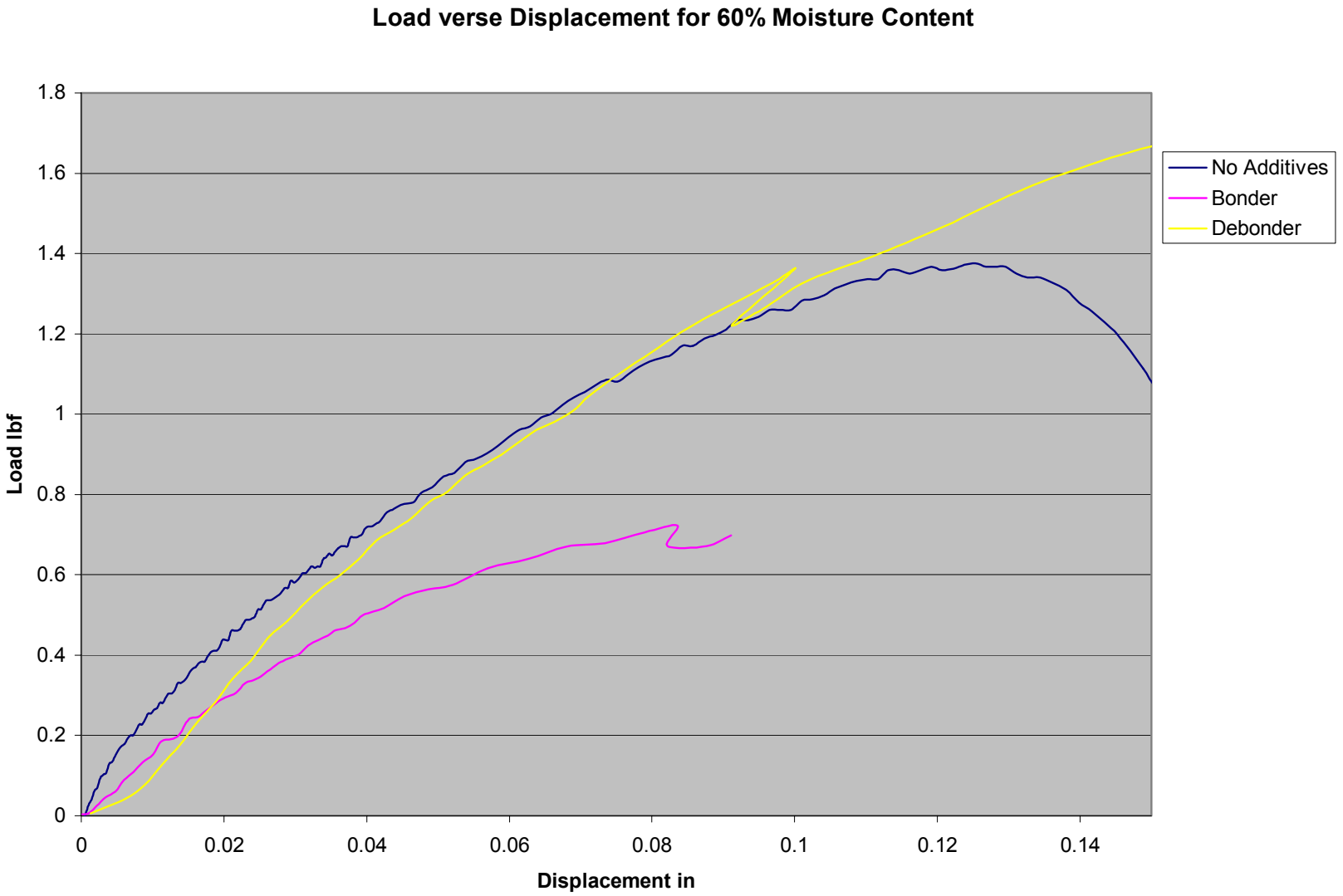
Load verse Displacement for 60% Moisture Content
Load lbf
Displacement in
0
0.2
0.4
0.6
0.8
1
1.2
1.4
1.6
1.8
0
0.02
0.04
0.06
0.08
0.1
0.12
0.14
No Additives
Bonder
Debonder

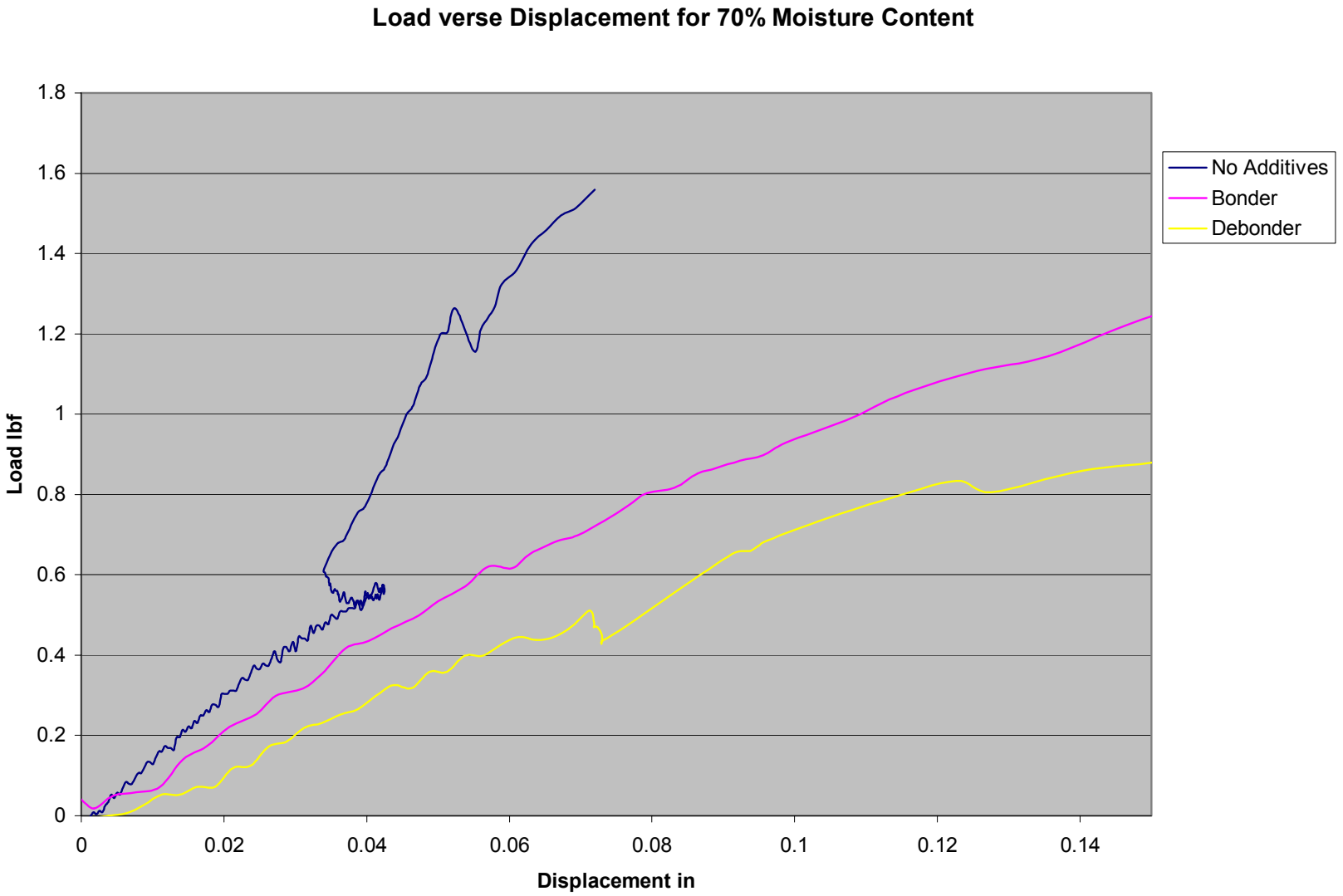
Load verse Displacement for 70% Moisture Content
Load lbf
Displacement in
0
0.2
0.4
0.6
0.8
1
1.2
1.4
1.6
1.8
0
0.02
0.04
0.06
0.08
0.1
0.12
0.14
No Additives
Bonder
Debonder

APPENDIX E: FINITE ELEMENT PROGRAM

```
%Paper Splitting Program

%Clears the Command Window
clc
clear all

% Set up all of the points that will be used in the program
% number of rows and columns of the nodes make the number
% of columns an even number
nrow = 10;
ncol = 10;
% Calculate the total number of nodes
n = nrow * ncol;

% Dis is the distance between nodes in meters
xdis = 0.001;
ydis = 0.001;

%Determine the diagonal distance between nodes
ddis = ((0.5*xdis)^2 + ydis^2)^(0.5);

% Count keeps track of what column and row is being written to
countx = 1;
county = 1;



% The origin of all the points is placed at node 1
% which is at the top left side of the nodal matrix
% 1 is even 0 is odd
for i = 1:n
        if mod(county,2) == 1 %This is an odd row top row
      x(i) = (countx-1)*xdis;
   end
   if mod(county,2) == 0 %This is an even row
      x(i) = 0.5*xdis + (countx-1)*xdis;
   end

        % Calculate all of the related nodes
   % The notation is upper right and clockwise around
   % relnode(related nodes, node of question)
```

```
% Calculate the top nodes
if county == 1 % left shift
        if countx == 1
        relnode(:,1) = [0;2;(i+ncol);0;0;0];
   elseif countx == ncol
                relnode(:,ncol) = [0;0;(i+ncol);(i+(ncol-1));(i-1);0];
   else
                relnode(:,i) = [0;(i+1);(i+ncol);(i+(ncol-1));(i-1);0];
   end
end

% Calculate the bottom nodes
if county == (nrow)
   if mod(county,2) == 1 %This is an even row and shorter in length top row
           if countx == 1
                   relnode(:,(n-(ncol-1))) = [(i-ncol);(i+1);0;0;0;0];
      elseif countx == ncol
                   relnode(:,n) = [(i-ncol);0;0;0;(i-1);(i-(ncol+1))];
      else
                   relnode(:,i) = [(i-ncol);(i+1);0;0;(i-1);(i-(ncol+1))];
      end
   end

   if mod(county,2) == 0 %This is an odd row and full length
           if countx == 1
                     relnode(:,(n-(ncol-1))) = [(i-(ncol-1));(i+1);0;0;0;(i-ncol)];
      elseif countx == ncol
                   relnode(:,n) = [0;0;0;0;(i-1);(i-ncol)];
      else
                   relnode(:,i) = [(i-(ncol-1));(i+1);0;0;(i-1);(i-ncol)];
      end
   end
end

% Calculate all of the other nodes
if mod(county,2) == 1 % This means that it is an even row top row
   if county ~= 1
           if county ~= (nrow)
        % If the node is located along either edge
                   if countx == 1
                           relnode(:,i) = [(i-ncol);(i+1);(i+ncol);0;0;0];
        elseif countx == ncol
                           relnode(:,i) = [(i-ncol);0;(i+ncol);(i+(ncol-1));(i-1);(i-
(ncol+1))];
        else
```

```
                                relnode(:,i) = [(i-ncol);(i+1);(i+ncol);(i+(ncol-1));(i-1);(i-
(ncol+1))];
            end
         end
      end
   end

   if mod(county,2) == 0 % This means that it is an odd row full
      if county ~= 1
            if county ~= (nrow)
         % If the node is located along either edge
                  if countx == 1
                        relnode(:,i) = [(i-(ncol-1));(i+1);(i+(ncol+1));(i+ncol);0;(i-
ncol)];
         elseif countx == ncol
                        relnode(:,i) = [0;0;0;(i+ncol);(i-1);(i-ncol)];
         else
                        relnode(:,i) = [(i-(ncol-1));(i+1);(i+(ncol+1));(i+ncol);(i-1);(i-
ncol)];
         end
         end
      end
   end

         y(i) = -(county - 1)*ydis;

         if countx == ncol
            countx = 1;
                  county = county + 1;
         else
                  countx = countx + 1;
         end

end

% Plot the initial Shape
hold on
   for i = 1:n
      for j = 1:6
         if relnode(j,i) ~= 0
            plot([x(i) x(relnode(j,i))],[y(i) y(relnode(j,i))],'k')
         end
      end
   end
drawnow
```

```
% Store the initial x and y coordinates of all of the nodes
xint = x;
yint = y;

%%%%%%%%%%%%%%%%%%%%%%%%%%%%%%%%%%%%%%%%%%%%
%%%%%%%%%%%%%%%%%%%%%%%%%%%%%%%%%%%%%%%%%%%%
%%%%%%%%%%%%%%%%%%%%%%%%%%%
% Now that all of the initial node locations have been
% determined the looping time variable part of the
% program begins
%%%%%%%%%%%%%%%%%%%%%%%%%%%%%%%%%%%%%%%%%%%%
%%%%%%%%%%%%%%%%%%%%%%%%%%%%%%%%%%%%%%%%%%%%
%%%%%%%%%%%%%%%%%%%%%%%%%%%

% Time step in seconds
deltat = .000001;

% Time stop set in seconds
tstop = 1.0;

% Time for replot
replotinterval = .0001;
replottime = replotinterval;

% Reset initial time
time = 0;

% All of the initial forces need to be set to zero

forcex = 0*x;
forcey = 0*y;

% k1 is the spring constant for the bonding
% k2 is the spring constant for the entanglement
% k3 is the damping constant for the entanglement

k1 = 25000;     % Spring Constant N/m
k2 = 210000;    % Damping Spring Constant N/m
k3 = 400000;     % Damping Constant N/(m/s)

% For all of the dymanics parts of the program the node is
% given a theoretical mass that equates to 300 grams per meter square
% The split mass is the mass of an individual splitting weight

mass = 0.3*xdis*ydis;
splitmass = 0; %460.45 grams was used as splitting weight on both sides
```

```
maxforce = 10000000000;
maxstretch = 1.5; %Value is multiplyed by distance so is a percentage

% The initial velocities and accelerations of the nodes are zero
xvelocity = 0*x;
yvelocity = 0*y;
xaccel = 0*x;
yaccel = 0*y;

%%%%%%%%%%%%%%%%%%%%%%%%%%%%%%%%%%%%%%%%%%%%%%%%%%%%%%%%%%%%%%%%%%%%%%%%
%%%%%%%%%%%%%%%%%%%%%%%%%%%%%%%%%%%%%%%%%%%%%%%%%%%%%%%%%%%%%%%%%%%%%%%%
% End of constants and begining of loop
%%%%%%%%%%%%%%%%%%%%%%%%%%%%%%%%%%%%%%%%%%%%%%%%%%%%%%%%%%%%%%%%%%%%%%%%
%%%%%%%%%%%%%%%%%%%%%%%%%%%%%%%%%%%%%%%%%%%%%%%%%%%%%%%%%%%%%%%%%%%%%%%%

while time < tstop

% Create random numbers for whether the nodes are
% considered bonds or pullout
nodetype = rand(6,n);

% Calculate new x forces based on the x position
% as well as the position of the surrounding nodes
for i = 1:n
        % Determine the forces for each of the surrounding nodes
        for j = 1:6
      if relnode(j,i) ~= 0
        % Determine the angle for the calculations
        if x(i) ~= x(relnode(j,i))
                        length(j,i) = ((y(relnode(j,i))-y(i))^2 + (x(relnode(j,i))-x(i))^2)^0.5;
          angle(j,i) = atan((y(relnode(j,i))-y(i))/(x(relnode(j,i))-x(i)));

          if x(relnode(j,i)) < x(i)
            angle(j,i) = angle (j,i) + pi;
          end

        else
          length(j,i) = abs(y(relnode(j,i))-y(i));
          if y(i) > y(relnode(j,i))
            angle(j,i) = -pi/2;
          else
            angle(j,i) = pi/2;
          end
        end

        % Enable the nodes to split off that are beyond the defined length
```

```
if rem(xint(i),xdis) == 0 %top row and all left shifted rows
   if j == 1
      if length(j,i) >= maxstretch*ddis
         relnode(j,i) = 0;
         relnode(4,(i-ncol)) = 0;
      end
   end
   if j == 2
      if length(j,i) >= maxstretch*xdis
         relnode(j,i) = 0;
         relnode(5,(i+1)) = 0;
      end
   end
   if j == 3
      if length(j,i) >= maxstretch*ddis
         relnode(j,i) = 0;
         relnode(6,(i+ncol)) = 0;
      end
   end
   if j == 4
      if length(j,i) >= maxstretch*ddis
         relnode(j,i) = 0;
         relnode(1,(i+(ncol-1))) = 0;
      end
   end
   if j == 5
      if length(j,i) >= maxstretch*xdis
         relnode(j,i) = 0;
         relnode(2,(i-1)) = 0;
      end
   end
   if j == 6
      if length(j,i) >= maxstretch*ddis
         relnode(j,i) = 0;
         relnode(3,(i-(ncol+1))) = 0;
      end
   end
end
if rem(xint(i),xdis) ~= 0 %top row and all left shifted rows
   if j == 1
      if length(j,i) >= maxstretch*ddis
         relnode(j,i) = 0;
         relnode(4,(i-(ncol-1))) = 0;
      end
   end
   if j == 2
```

```
      if length(j,i) >= maxstretch*xdis
         relnode(j,i) = 0;
         relnode(5,(i+1)) = 0;
      end
   end
   if j == 3
      if length(j,i) >= maxstretch*ddis
         relnode(j,i) = 0;
         relnode(6,(i+(ncol+1))) = 0;
      end
   end
   if j == 4
      if length(j,i) >= maxstretch*ddis
         relnode(j,i) = 0;
         relnode(1,(i+ncol)) = 0;
      end
   end
   if j == 5
      if length(j,i) >= maxstretch*xdis
         relnode(j,i) = 0;
         relnode(2,(i-1)) = 0;
      end
   end
   if j == 6
      if length(j,i) >= maxstretch*ddis
         relnode(j,i) = 0;
         relnode(3,(i-ncol)) = 0;
      end
   end
end

% Enable the nodes to split off that are greater than the defined force
if rem(xint(i),xdis) == 0 %top row and all other odd rows
   if j == 1
      if ((length(j,i) - ddis) * k1) >= maxforce
         relnode(j,i) = 0;
         relnode(4,(i-ncol)) = 0;
      end
   end
   if j == 2
      if ((length(j,i) - xdis) * k1) >= maxforce
         relnode(j,i) = 0;
         relnode(5,(i+1)) = 0;
      end
   end
   if j == 3
```

```
      if ((length(j,i) - ddis) * k1) >= maxforce
         relnode(j,i) = 0;
         relnode(6,(i+ncol)) = 0;
      end
   end
   if j == 4
      if ((length(j,i) - ddis) * k1) >= maxforce
         relnode(j,i) = 0;
         relnode(1,(i+(ncol-1))) = 0;
      end
   end
   if j == 5
      if ((length(j,i) - xdis) * k1) >= maxforce
         relnode(j,i) = 0;
         relnode(2,(i-1)) = 0;
      end
   end
   if j == 6
      if ((length(j,i) - ddis) * k1) >= maxforce
         relnode(j,i) = 0;
         relnode(3,(i-(ncol+1))) = 0;
      end
   end
end
if rem(xint(i),xdis) ~= 0 %top row and all left shifted rows
   if j == 1
      if ((length(j,i) - ddis) * k1) >= maxforce
         relnode(j,i) = 0;
         relnode(4,(i-(ncol-1))) = 0;
      end
   end
   if j == 2
      if ((length(j,i) - xdis) * k1) >= maxforce
         relnode(j,i) = 0;
         relnode(5,(i+1)) = 0;
      end
   end
   if j == 3
      if ((length(j,i) - ddis) * k1) >= maxforce
         relnode(j,i) = 0;
         relnode(6,(i+(ncol+1))) = 0;
      end
   end
   if j == 4
      if ((length(j,i) - ddis) * k1) >= maxforce
         relnode(j,i) = 0;
```

```
            relnode(1,(i+ncol)) = 0;
        end
    end
    if j == 5
        if ((length(j,i) - xdis) * k1) >= maxforce
            relnode(j,i) = 0;
            relnode(2,(i-1)) = 0;
        end
    end
    if j == 6
        if ((length(j,i) - ddis) * k1) >= maxforce
            relnode(j,i) = 0;
            relnode(3,(i-ncol)) = 0;
        end
    end
end

% Determine if the node is bonding
if nodetype(j,i) > 0.5
    if j == 1
        forcex(i) = forcex(i) + (length(j,i) - ddis) * k1 * cos(angle(j,i));
        forcey(i) = forcey(i) + (length(j,i) - ddis) * k1 * sin(angle(j,i));
    end
    if j == 2
        forcex(i) = forcex(i) + (length(j,i) - xdis) * k1 * cos(angle(j,i));
        forcey(i) = forcey(i) + (length(j,i) - xdis) * k1 * sin(angle(j,i));
    end
    if j == 3
        forcex(i) = forcex(i) + (length(j,i) - ddis) * k1 * cos(angle(j,i));
        forcey(i) = forcey(i) + (length(j,i) - ddis) * k1 * sin(angle(j,i));
    end
    if j == 4
        forcex(i) = forcex(i) + (length(j,i) - ddis) * k1 * cos(angle(j,i));
        forcey(i) = forcey(i) + (length(j,i) - ddis) * k1 * sin(angle(j,i));
    end
    if j == 5
        forcex(i) = forcex(i) + (length(j,i) - xdis) * k1 * cos(angle(j,i));
        forcey(i) = forcey(i) + (length(j,i) - xdis) * k1 * sin(angle(j,i));
    end
    if j == 6
        forcex(i) = forcex(i) + (length(j,i) - ddis) * k1 * cos(angle(j,i));
        forcey(i) = forcey(i) + (length(j,i) - ddis) * k1 * sin(angle(j,i));
    end
end
% Determine if the node is fiber entanglement
if nodetype(j,i) <= 0.5
```

```
            if j == 1
               forcex(i) = forcex(i) + (length(j,i) - ddis) * k2 * cos(angle(j,i)) -
k3*xvelocity(i);
               forcey(i) = forcey(i) + (length(j,i) - ddis) * k2 * sin(angle(j,i)) -
k3*yvelocity(i);
            end
            if j == 2
               forcex(i) = forcex(i) + (length(j,i) - xdis) * k2 * cos(angle(j,i)) -
k3*xvelocity(i);
               forcey(i) = forcey(i) + (length(j,i) - xdis) * k2 * sin(angle(j,i)) -
k3*yvelocity(i);
            end
            if j == 3
               forcex(i) = forcex(i) + (length(j,i) - ddis) * k2 * cos(angle(j,i)) -
k3*xvelocity(i);
               forcey(i) = forcey(i) + (length(j,i) - ddis) * k2 * sin(angle(j,i)) -
k3*yvelocity(i);
            end
            if j == 4
               forcex(i) = forcex(i) + (length(j,i) - ddis) * k2 * cos(angle(j,i)) -
k3*xvelocity(i);
               forcey(i) = forcey(i) + (length(j,i) - ddis) * k2 * sin(angle(j,i)) -
k3*yvelocity(i);
            end
            if j == 5
               forcex(i) = forcex(i) + (length(j,i) - xdis) * k2 * cos(angle(j,i)) -
k3*xvelocity(i);
               forcey(i) = forcey(i) + (length(j,i) - xdis) * k2 * sin(angle(j,i)) -
k3*yvelocity(i);
            end
            if j == 6
               forcex(i) = forcex(i) + (length(j,i) - ddis) * k2 * cos(angle(j,i)) -
k3*xvelocity(i);
               forcey(i) = forcey(i) + (length(j,i) - ddis) * k2 * sin(angle(j,i)) -
k3*yvelocity(i);
            end
         end
      end
   end

%     % Determine if the node is on either of the top corners and add in the splitting force
%     if i == 1
%        forcex(1) = forcex(1) - splitmass*9.81;
%     end
%     if i == ncol
%        forcex(ncol) = forcex(ncol) + splitmass*9.81;
```

```
%     end

    %drive the top nodes of the matrix at a given velocity
    if i <= ncol
       if i < ncol/2
          x(i) = x(i) - 1*deltat;
       end
       if i >= ncol
          x(i) = x(i) + 1*deltat;
       end
    end

    % Dynamics Computations
    xaccel(i) = forcex(i)/mass;
    yaccel(i) = forcey(i)/mass;

    xvelocity(i) = xvelocity(i) + xaccel(i)*deltat;
    yvelocity(i) = yvelocity(i) + yaccel(i)*deltat;

    xnew(i) = x(i) + xvelocity(i)*deltat + 0.5 * xaccel(i) * deltat^2;
    ynew(i) = y(i) + yvelocity(i)*deltat + 0.5 * yaccel(i) * deltat^2;

    plot(x(i),y(i))

end

    if time >= replottime
       for i = 1:n
          for j = 1:6
             if relnode(j,i) ~= 0
                plot([x(i) x(relnode(j,i))],[y(i) y(relnode(j,i))],'r');

             end
          end
       end
       drawnow
       replottime = replottime + replotinterval;
    end


time = time + deltat;


x = xnew;
y = ynew;
```

```
% %This will reset the position of the top nodes so that they stay along the top
% %Also will reset the x position of the top nodes
% for i = 1:ncol
%     y(i) = 0;
%     if i <= (ncol/2)
%         x(i) = x(1) + (i-1)*xdis;
%     else
%         x(i) = x(ncol) - (ncol-i)*xdis;
%     end
% end


% Set the x and y forces back to zero for the next calculation
forcex = forcex * 0;
forcey = forcey * 0;

end


% Plot the final shape of the paper

for i = 1:n
   for j = 1:6
      if relnode(j,i) ~= 0
         plot([x(i) x(relnode(j,i))],[y(i) y(relnode(j,i))],'r')

      end
   end
end
drawnow
hold off
```

LITERATURE CITED

1. Ahrens, F. et.al., forthcoming (2005).

2. Baum, G. A., Institute of Paper Chemistry. A257 – Fibrous Structures.

3. Campbell, W. B., *Paper Trade Journal* 95, No. 8:29-32 (1932).

4. Cox, H. L., *British Journal of Applied Physics* 3: 72 (1952).

5. How watercolor papers are made. (January 6, 2005). Retrieved October 24, 2005, from http://www.handprint.com/HP/WCL/paper1.html

6. Kallmes, O. J. and Bernier, G., *Tappi* 45(11):867 (1962).

7. Lehtonen, L. Phd Thesis, IPST (2004).

8. Lyne, L. M. and Gallay, W., *Tappi* 37(12):581 (1954).

9. Mardon, J., *Papper och Trä* 11:797 (1976).

10. Nordman, L. S., Bonding in Paper Sheets. Fundamentals Properties of Papermaking Fibres. Transactions of the Fundamental Research Symposium – Cambridge, 1957. pp. 333-347.

11. Nordman, L. S., Gustafsson, C., and Olofsson, G. Strength of bonding in paper II. Paperi Puu 36(8):315(1954).

12. Osterberg, L., Svensk Papperstid. 65 (6):222 (1962).

13. Page, D. H., *Tappi J*. 77(3):201(1994)

14. Page, D. H., *Tappi* 52(4): 674 (1969).

15. Page, D. H. The beating of chemical pulps – the action and the effect. 12H. pp. 1-38.

16. Page, D.H., Seth, R. S., *The Role of Fundamental Research on Papermaking* Vol.1., Mechancial Engineering Publication Series, London, 1983. pp. 421-452.

17. Page, D.H., Seth, R. S., and De Grace, J. H., *Tappi* 62 (9): 99 (1979).

18. Page, D. H. and Tydeman, P. A., *Paper Technol*. 1:T207 (1960).

19. Parsons, S. R., *Paper Trade J.* 115(25):34 (1942).

20. Rance, H.F., ed. Handbook of Paper Science. 2 vol., Elsevier Scientific Publishing Co., New York, 1980. pp. 12-25.

21. Rance, H.F., *Tappi*, 1956, 39(2), 104-115.

22. Retulainen, E., Moss, P., and Nieminen, K.,Tenth Fundamental Research Symposium Proceedings, Mechanical Engineering Publications Ltd., London, 1993, p.727.

23. Retulainen, E., Nieminen, K., and Nurminen, I., *Appita* 46(1):33(1993).

24. Robertson, A. A., *Tappi* 42(12):969 (1959).

25. Smith, J. C., and Graminski, E. L. Characterizing the interfiber bond strength of paper pulps in terms of breaking energy. NBSIR 76-1148, October 15, 1976.

26. Smith, W. E., *Tappi* 48(8):476 (1965).

27. Wahren, D., *Tappi* 64(3):89 (1981).